Statistical Methods for Integrating Multiple CO$_2$ Leak Detection Techniques at Geologic Sequestration Sites

Submitted in partial fulfillment of the requirements for

the degree of

Doctor of Philosophy

in

Civil and Environmental Engineering

Ya-Mei Yang

B.S. in Civil Engineering, National Taiwan University, Taipei, Taiwan
M.S. in Environmental Planning and Management,
National Taiwan University, Taipei, Taiwan
M.S. in Environmental Engineering, Science and Management,
Carnegie Mellon University, Pittsburgh, PA

Carnegie Mellon University
Pittsburgh, PA

May, 2011

ABSTRACT

Near-surface monitoring is an essential component of leak detection at geologic CO_2 sequestration sites. With different strengths and weaknesses for every monitoring technique, an integrated system of leak detection monitoring methods is needed to combine the information provided by different techniques deployed at a site, and no current methodology exists that allows one to quantitatively combine the results from different monitoring technologies and optimize their design. More importantly, an evaluation that is able to provide the assessment of possible size of a leak based on the multiple monitoring results further helps the managers and decision makers to know whether the unexpected leakage event is smaller than the required annual seepage rate for effective long-term storage. The proposed methodology for this application is the development and use of a Bayesian belief network (BBN) for combining measurements from multiple leak detection technologies at a site.

The Bayesian Belief Network for CO_2 leak detection is built through an integrated application of a subsurface model for CO_2 migration under different site conditions; field-generated background information on several monitoring techniques; and statistical methods for processing the field background data to infer the leak detection threshold for each monitoring technique and the conditional probability values used in the BBN. Several statistical methods are applied to estimate the detection thresholds and the conditional probabilities, including (1) Bayesian methods for characterizing the natural background (pre-injection) conditions of the techniques for leak detection, (2) the combination of the characterization of the background monitoring results and the

simulated CO_2 migration for estimating the probability of leak detection for each monitoring technique given the size of leak, (3) a probabilistic design of CO_2 leak detection for estimating the detection probability of a monitoring technique under different site conditions and monitoring densities, (4) a Bayesian belief network for combining measurements from multiple leak detection technologies at an actual test site, with the site conditions and the probability distributions of leak detection and leakage rate estimated for the site.

The BBN model is built for the Zero Emissions Research and Technology (ZERT) test site in Montana. The monitoring techniques considered in this dissertation include soil CO_2 flux measurement and PFC tracer monitoring. The possible near-surface CO_2 and PFC tracer flux rates as a function of distance from a leakage point are simulated by TOUGH2, given different leakage rates and permeabilities. The natural near-surface CO_2 flux and background PFC tracer concentration measured at the ZERT site are used to determine critical values for leak inference and to calculate the probabilities of leak detection given a monitoring network. A BBN of leak detection is established by combing the TOUGH2 simulations and the background characterization of near-surface CO_2 flux and PFC tracer at the sequestration site. The BBN model can be used as an integrated leak detection tool at a geologic sequestration site, increasing the predicted precision and inferring the possible leak distribution by combining the information from multiple leak detection techniques. Moreover, the BBN model can also be used for evaluating each monitoring technique deployed at a site and for determining the performance of a proposed monitoring network design by a single or multiple techniques.

This Work Is Dedicated To

My Parents

Yu-Hao Yang and Ting-Lan Chung

The CMU-WVU-NETL research team

Prof. Mitchell J. Small,

Dr. Egemen O. Ogretim,

Prof. Donald D. Gray,

Dr. Grant S. Bromhal,

Dr. Brian R. Strazisar and

Dr. Arthur W. Wells.

Acknowledgements

I would like to express my sincere gratitude to my advisor, Prof. Mitchell Small. Mitch has been a great mentor, generously sharing his knowledge, experiences and ideas with me and educating me to be a good scientific researcher as best as he can. He's also an excellent joke-teller, bringing joy, encouragement and wisdom to people around him. I am very lucky to have Mitch as my advisor and truly appreciate his guidance and help at work and in life. Next, I would like to thank Prof. David Dzombak for his teachings, patience and encouragement over the past years. Working with Dave, I learned how to get organized at work and how to take care of the details in scientific research. And, I want to thank Prof. Brian Junker for his guidance on my learning of Statistics and my research. Brian's rich knowledge, creative thinking and constructive advice have always been a resource for me whenever I faced the challenges of framing and solving research problems. Also, I would like to thank Prof. Greg Lowry for his constant support and valuable advice on this work, and his patience in teaching me organic chemistry. Finally, great thanks to Professor Paul Fischbeck and Dr. David Gerald. They are great mentors in

Table of Contents

List of Tables

List of Figures

Chapter 1:   Introduction

Geologic carbon sequestration is regarded as a promising technique for reducing the anthropogenic CO_2 emission into the atmosphere because of the technical feasibility and the potential storage capacity (*1, 2*). Since injecting CO_2 into the subsurface has been applied to enhance oil and gas recovery in petroleum industry, plus existing CO_2 contained gas fields as a natural analogue, geologic sequestration has been considered as the major sequestration method to mitigate atmospheric CO_2 levels. Moreover, the storage capacity from oil and gas reservoir, unmineable coal seams, and saline formations are estimated at 1,157 billion metric tons in North America (*3*). Compared to the emission of greenhouse gases, which is around 7 billion metric tons per year (*2*), the storage capacity can provide quite a long time for us to adjust our living style and to develop new energy technologies in order to cope with the impacts of climate change.

With geologic sequestration of CO_2 now planned in a number of nations as a short- to medium-term strategy for reducing carbon emissions, there is a need for CO_2 leak detection monitoring to ensure that the sequestered CO_2 at a site does not return to the atmosphere, yielding the mitigation strategy ineffective. Leakage from the CO_2 storage reservoir can make all the effort against climate change in vain and possibly pose surface ecosystem danger if the leakage rate is not small enough (*4*) or the seepage can lead to high concentrations on the spot (*5*).

A number of methods have been proposed for detecting CO_2 leakage at sequestration and storage sites, including: seismic profiling, pressure measurement, and other geophysical methods for detecting changes at the deep reservoir level; groundwater

sampling for changes in water chemistry in observation wells; analysis of natural, injected and recovered carbon isotopes; near-surface monitoring of soil CO_2 fluxes; soil gas measurement for the presence of tracers added to the injected CO_2; and measurement of CO_2, tracers or other indicator gases in the air above the sequestration site (*6-10*). These alternatives for site monitoring target different locations at the site at different stages of the geologic sequestration process, and it is generally recognized that a combination of some methods will provide for the most effective coverage for leak detection.

With different strengths and weaknesses for every monitoring technique, an integrated system of leak detection monitoring methods is needed to combine the information provided by different techniques deployed at a site, and no current methodology exists that allows one to quantitatively combine the results from different monitoring technologies and optimize their design. The proposed methodology for this application is the development and use of a Bayesian Belief Network (BBN) for combining measurements from multiple leak detection technologies at a site.

The Bayesian Belief Network for CO_2 leak detection is built through an integrated application of a subsurface model for CO_2 migration under different site conditions; field-generated background information on several monitoring techniques; and statistical methods for processing the field background data and the simulation results and for inferring the leak detection threshold for each monitoring technique and the conditional probability values used in the BBN. Several statistical methods are applied to estimate the detection thresholds and the conditional probabilities, including (1) Bayesian methods for characterizing the natural background (pre-injection) conditions of the techniques for leak

detection, (2) the combination of the characterization of the background monitoring results and the simulated CO_2 migration for estimating the probability of leak detection for each monitoring technique given the size of leak, (3) a probabilistic design of CO_2 leak detection for estimating the detection probability of a monitoring technique under different site conditions and monitoring densities, (4) a Bayesian belief network for combining measurements from multiple leak detection technologies at an actual test site, with the site conditions and the probability distributions of leak detection and leakage rate estimated for the site.

All the work in this dissertation was achieved with the support from Carnegie Mellon University (CMU), West Virginia University (WVU), and the National Energy Technology Laboratory (NETL). The monitoring background data at test sites are provided by NETL. The near-surface CO_2 and PFC mitigation modeling was performed by WVU. The statistical analysis and modeling for the development of the BBN model are carried out by the dissertation author with the assistance from the advisor and the committee members at CMU.

The sections below briefly describe the background and the methods associated with the development of the BBN, including the near-surface monitoring methods for leak detection, CO_2 fate and transport modeling for simulating CO_2 migration in the near-surface, Bayesian methods for charactering background (pre-injection) conditions, and the Bayesian belief network for integrating the results from multiple monitoring techniques. Also, the research objectives and the overview of this dissertation are presented in the end of this chapter.

1.1   Near-surface Monitoring Methods for CO_2 Leak Detection

In this dissertation, near-surface monitoring methods are first considered for the use in the BBN due to the data accessibility and collaboration efforts with NETL and WVU. Near-surface monitoring is also an essential component of leak detection at geologic sequestration sites, especially for the risks associated with human beings and ecosystems near the sites. Nevertheless, various technologies for leakage detection are currently being developed and tested by the NETL, including:

Soil gas flux measurements using an accumulation chamber

Soil CO_2 flux monitoring provides a direct estimate of CO_2 exchange between the soil and the atmosphere, and is typically implemented using the accumulation chamber method (*11*). Accumulation chamber monitors have been deployed and tested in a number of pilot projects, such as the Zero Emissions Research and Technology (ZERT) monitoring experiment in Bozeman, Montana (*12-13*). The background flux of CO_2 results from natural soil respiration processes and can be highly variable, depending on local climate and vegetation. It is thus important to account for natural variation of this baseline when attempting to isolate deep source leakage contributions to the monitored soil CO_2 flux. Researchers at NETL currently have measured soil CO_2 fluxes using this method at some test sites like the ZERT site in Montana and the San Juan Basin site in New Mexico. In this dissertation, the background soil CO_2 flux from nine AmeriFlux and CarboEurope sites and the ZERT site are used for building Bayesian hierarchical and nonhierarchical models for soil CO_2 flux and leak detection at geologic sequestration sites.

Perfluorocyclohydrocarbon (PFC) tracer injected with the CO_2 at injection wells

Perfluorocyclohydrocarbon (PFC) is an artificial chemical, which has long lifetime and can be detected at very low concentrations. With no harmful biological effects, PFC is a good choice for being used as a tracer injected along with CO_2 in order to detect leakage at geologic sequestration sites (*9, 14-15*). Although PFC is a strong greenhouse gas, the low dose PFC required for leak detection is insignificant for the environmental effect compared to CO_2. The PFC tracer is detected using soil-gas monitoring with Capillary Adsorption Tube Samplers (CATS) used to collect the tracers. In this research, the PFC tracer is Perfluoromethylcyclohexane (PMCH), tested in the ZERT experiments (*14-15*). Besides the ZERT site, the background PFC concentrations from the San Juan Basin site, the Lower Michigan site in Michigan and the Pines Parking lot of NETL Pittsburgh are used for building a simple Bayesian hierarchical model for CO_2 leak detection.

Shallow soil gas sampling and analysis

CO_2 leakage into vadose zone can cause the changes in the chemical and isotopic compositions of shallow soil gas. Carbon isotopes ($\delta^{13}C$ & $\delta^{14}C$) in soil gas have been mostly tested for detecting CO_2 leakage in recent years (*5-6, 10*). Carbon isotopic ratio shows the compositions and relative ratios of the contributing gas sources. Carbon isotopes are particularly useful in enhanced oil recovery projects since the $\delta^{13}C$ in the gas from fossil-fuel-driven sources is very different form the $\delta^{13}C$ in shallow soil gas, contributed from the atmosphere and biologic activities in the soil, and the $\delta^{14}C$ is

basically absent in fossil CO_2. Therefore, Carbon isotopes are used to distinguish leaking CO_2 from atmospheric and biological background sources. However, soil gas samples for CO_2 concentration and ^{13}C ratios are not included in the BBN for CO_2 leak detection at the idealized ZERT site due to the lack of data for calculating the CO_2 leakage rates from the carbon isotopes observations, which might be solved with the related data or simulations available in the future.

Groundwater chemistry

The chemistry of surface well water is monitored for characteristic changes resulting from the leakage of CO_2 during injection. Some field tests have shown that pH, alkalinity and electrical conductance change significantly and rapidly due to the dissolution of leaking CO_2 into groundwater. Laboratory analyses also indicate that the concentrations of some dissolved inorganic chemicals, like Ca, Mg, Fe and Mn, increase obviously after the injection (*5, 16*). The simulations of the change of groundwater chemistry associated with CO_2 leak flux for deep saline aquifer have been performed (*17-18*), indicating groundwater chemistry monitoring is able to detect median CO_2 leakage. Similarly, the CO_2 release test at the ZERT site 2008 for the changes of shallow groundwater chemistry (*16*) and the ongoing simulations also indicate the good agreement between the observed data and the geochemical modeling (*19*).

1.2   CO$_2$ Fate and Transport Modeling

The simulation of the transport of CO_2 in the near subsurface and lower atmosphere is essential for the success of this study. In the near subsurface zone, where

the pressure is slightly greater than or equal to atmospheric, CO_2 will exist as a colorless, odorless gas or be dissolved in water. It has a density about 50% greater than dry air, therefore, it will tend to sink toward the water table or to collect in surface depressions (*5*).

The simulations focus on the near-surface level where the monitoring networks are installed and tested. This region of interest comprises the saturated zone, the unsaturated zone, and the lower atmosphere. In the saturated zone, the flow can be assumed to follow a two-phase Darcy law since most of the pores are filled with water, but CO_2 is a separate gas migrating upwards within the aquifer. Buoyancy forces due to nonuniform CO_2 concentration and temperature are important. Flow in the saturated zone mainly transports CO_2 gas vertically to the unsaturated zone, as well as dissolved CO_2 horizontally within the aquifer. In the unsaturated or vadose zone, the soil is usually not saturated; and the simultaneous flow of gas and liquid must be considered. The lower atmosphere affects the subsurface conditions varying due to wind, barometric pressure, air temperature and precipitation, etc. and consequently influences CO_2 transport (*20*). A typical simulation might encompass 10 to 50 m of the saturated zone, 10 to 50 m of the unsaturated zone, and about 10 m of the atmosphere. The horizontal extent of the model could range from 10's to 1000's of meters on a side.

Given the complexity of the simulations to be performed and the research advances of multi-phase transport modeling in recent years, the development of a new computer program is not considered. Among the many existing groundwater flow and transport program, such as Eclipse 300 by Schlumberger (*21*), GEM and STARS by Computer Modelling Group (*22*) and TOUGH2 (*23*) by Lawrence Berkeley National

Laboratory, etc., TOUGH2 EOS7C (*24-25*) appears to fulfill the needed capacities for the present application for near surface CO_2 leek seepage simulation. TOUGH2 computes the three dimensional coupled flow of liquid water, water vapor, noncondensible gas, and heat in porous and fractured media. The model includes several options for modeling fractured media. TOUGH2 uses a multi-phase approach, correctly simulating the simultaneous flow of gas and liquid and accounting for transitions between phases. Also, it has been developed and used by Oldenburg and Unger (*26-27*) to perform parametric studies of CO_2 transport in idealized near subsurface and lower atmospheric domains.

1.3   Bayesian Hierarchical Model for Background Site Conditions

Bayesian hierarchical modeling has been applied in a wide range of physical science and engineering applications where statistical models are sought to describe behavior across multiple subpopulations (e.g., sites) thought to exhibit common behaviors, but with a degree of site specificity (*28-33*). Recent advances in Bayesian statistical methodology, including methods for Markov Chain Monte Carlo (MCMC) simulation for parameter estimation, have made models of this complexity easier to solve (*34-39*). The Bayesian hierarchical approach can be viewed as providing a compromise between site-specific and completely-pooled parameter estimates. Sites with small datasets "borrow" information from sites with larger datasets, but their parameter estimates are eventually dominated by their own datasets as these become larger. Joint uncertainty estimates are obtained for all global and site parameters, providing a basis for determining the statistical prediction intervals needed for deciding whether an observed monitoring variable is above that reasonably associated with natural variability at a site.

In this dissertation, the distributions of the background soil CO_2 flux and PFC tracer concentration are estimated through Bayesian hierarchical method.

The estimated posterior global parameter distribution can subsequently be used as the prior distribution for a new site in a later study. Finally, the Bayesian procedure provides a basis for comparing the fit of alternative models for the observed monitoring variable, including those with different numbers of fitted parameters. In this dissertation, soil CO_2 flux was regressed by soil temperature based on the data from nine AmeriFlux sites, and the resulting modeling recommendation is applied to the ZERT site. The PFC concentration was characterized by a simple Bayesian hierarchical normal model across the ZERT site and the other three reference sites.

1.4   Bayesian Belief Network

Bayesian belief network (BBN) has been wildly used in various research fields as a decision support tool. A BBN model combines probabilistic inference from multiple sources of evidence, presented in a graphical format, including node for events, arrows for casual relationship, and tables for probability. The graphical interface and probabilistic expression of BBN have several advantages in describing and modeling an environmental system. A BBN can provide (1) the integration of the system components of different forms and scales, (2) the clarification of a complex environmental system for gaining insights, (3) the basis for a decision support system with the inclusion of utility and decision options, (4) the estimation of the uncertainty associated with the system components, (5) the combination of prior knowledge from experts' belief or historical records and the data from experiments in system modeling (*40-45*).

For the application of CO_2 leak detection, the main nodes for a BBN model are a leak of a given size and a leakage event can cause the measurement results from detection technologies above critical values indicating the occurrence of a leak. The nodes of detection technologies along with their monitoring network designs provide the evidences for evaluating the leakage event. Site conditions that affect leak probability can be listed as other nodes and actually are simulated via the response surface fitted to TOUGH2 simulations. Arrows between events for causal influence are characterized by conditional probabilities. The observations at any combination of nodes propagated through network to compute posterior probabilities. The BBN in this study is designed for the leak detection with a particular concern for leakage rate at a geologic sequestration site, and the systems are divided into the four areas: leakage event (leakage rate), site condition, monitoring network design and detection technology. The methodology and a general framework for a BBN for CO_2 leak detection were developed in this thesis with an application to the ZERT site with two near-surface monitoring.

1.5   Research Objective

The main objective of this dissertation is to build a BBN for CO_2 leak detection with an illustration of the application to a real site. The BBN for CO_2 leak detection is built through an integrated application of a subsurface model for CO_2 migration under different site conditions; field-generated background information on several monitoring techniques; and statistical methods for processing the field background data and the simulation results and for inferring the leak detection threshold for each monitoring technique and the conditional probability values used in the BBN. This dissertation

illustrates the statistical methods applied for the development of the BBN model, and the specific objectives are as follows:

- To characterize the natural background (pre-injection) conditions of the monitoring techniques for leak detection using Bayesian methods.

- To estimate the probability of leak detection for each monitoring technique given the size of leak by combining the characterization of the background monitoring results and the simulations of CO_2 migration.

- To estimate the detection probability of a monitoring technique under different site conditions and monitoring densities through a probabilistic design of CO_2 leak detection

- To build a Bayesian belief network for combining measurements from multiple leak detection technologies at an actual test site, with the site conditions and the probability distributions of leak detection and leakage rate estimated for the site.

1.6   Dissertation Overview

This dissertation consists of five chapters and seven appendices. The main content of the thesis is presented from Chapter 2 to 4, which comprise materials submitted to or in preparation for publication in peer-reviewed journals. Chapter 1 provides a general introduction to the dissertation, including the background of CO_2 leak detection at geologic carbon sequestration sites, the methods used for the development of the BBN, the research objectives and brief overview of the content of this dissertation.

Chapter 2 illustrates the use of Bayesian methods for the background characterization of soil CO_2 flux measurement and the detection threshold of CO_2 leakage events, based on the data from nine AmeriFlux sites. This material, written by Ya-Mei Yang and co-authored by Mitchell J. Small, Brian W. Junker, Grant S. Bromhal, Brian R. Strazisar and Arthur W. Wells is under review in *Environmental Earth Sciences* entitled "Bayesian Hierarchical Models for Soil CO_2 Flux and Leak Detection at Geologic Sequestration Sites".

Chapter 3 presents the core statistical methods developed for estimating the conditional probabilities used in the BBN for CO_2 leak detection at geologic sequestration sites. The methodologies are illustrated for the soil CO_2 flux measurement at the idealized ZERT site. The probability of leak detection for soil CO_2 flux measurement given the size of leak is inferred by combining the characterization of the background monitoring results and the simulations of CO_2 migration. The detection probabilities of soil CO_2 flux measurement under different site conditions and monitoring densities are explored as well. This material, written by Ya-Mei Yang and co-authored by Mitchell J. Small, Egemen O. Ogretim, Donald D. Gray, Grant S. Bromhal, Brian R. Strazisar and Arthur W Wells, is in preparation for publication in *Environmental Science and Technology* under the title "Probabilistic Design of a Near-Surface CO_2 Leak Detection System".

Chapter 4 describes the BBN model developed for CO_2 leak detection and the two major uses of the BBN at geologic sequestration sites. The BBN can be used not only for inferring the probability distribution of leakage rates given the monitoring results, site conditions and monitoring densities, but also for optimizing the design of the monitoring

network of each detection technique. This material, written by Ya-Mei Yang and co-authored by Mitchell J. Small, Egemen O. Ogretim, Donald D. Gray, Grant S. Bromhal, Brian R. Strazisar and Arthur W Wells, will be submitted for publication in a peer-review journal under the title "A Bayesian Belief Network for Combining Sequestration Site Leak Detection Monitoring Results from Near-Surface CO_2 Fluxes and PFC Tracer Concentrations".

Chapter 5 summarizes the major findings and conclusions of this dissertation and provides the suggestions for the ongoing researches and the future work associated monitoring and modeling for leak detection at geologic sequestration.

Appendix A provides the supporting information for Chapter 2; Appendices B and C offer the supplemental materials for Chapter 3; and Appendices D, E and F provides the supporting information for Chapter 4 with a focus on the background characterization and the simulations made for PFC tracer at the idealized ZERT site.

References

(1) U.S. Environmental Protection Agency (2008) Inventory of U.S. Greenhouse Gas Emissions and Sinks: 1990 – 2006. EPA 430-R-08-005. Washington, DC 20460, U.S.A.

(2) Intergovernmental Panel on Climate Change (2005) IPCC Special Report on Carbon Dioxide Capture and Storage. Cambridge University Press, Cambridge, U.K.

(3) U.S. Department of Energy, National Energy Technology Laboratory (2008) Carbon Sequestration Atlas of the United States and Canada, 2nd edit.

(4) Hepple RP, Benson SM (2005) Geologic storage of carbon dioxide as a climate change mitigation strategy: Performance requirements and the implications of surface seepage.

(5) Oldenburg, C.M., J.L. Lewicki, and R.P. Hepple (2003) Near-surface monitoring strategies for geologic carbon dioxide storage verification, Lawrence Berkeley National Laboratory Report LBNL-54089.

(6) Klusman, RW (2003) Evaluation of leakage potential from a carbon dioxide EOR/sequestration project, Energy Conversion and Management, Volume 44, Issue 12, July 2003, Pages 1921-1940

(7) Benson SM, Gasperikova E, Hoversten GM (2004) Monitoring protocols and life-cycle costs for geologic storage of carbon dioxide. In: Proceedings of the 7th International Conferenceon Greenhouse Gas Control Technologies (GHGT-7), Vancouver, Canada, 5–9 September 2004.

(8) Benson SM (2007) Monitoring Geological Storage of Carbon Dioxide, Carbon Capture and Geologic Sequestration: Integrating technology, monitoring, and regulation, E.J. Wilson and D. Gerard (eds.) Blackwell Scientific Publishing, Ames, Iowa, Chapter 4.

(9) Wells, A.W., Diehl, J.R., Bromhal, G., Strazisar, B.R., Wilson, T.H., White, C.M. (2007) The use of tracers to assess leakage from the sequestration of CO_2 in a depleted oil reservoir, New Mexico. USA Appl. Geochem. 22 (5), 996–1016.

(10) Johnson, G, M Raistrick, B Mayer, M Shevalier, S Taylor, M Nightingale, I Hutcheon (2009) The use of stable isotope measurements for monitoring and verification of CO_2 storage, Energy Procedia, Volume 1, Issue 1, Pages 2315-2322

(11) Healy RW, Striegl RG, Russell TF, Hutchinson GL, Livingston GP (1996) Numerical Evaluation of Static-Chamber Measurements of Soil—Atmosphere Gas Exchange: Identification of Physical Processes. Soil Sci Soc Am J 60:740-747.

(12) Lewicki JL, Oldenburg CM, Dobeck L, Spangler L (2007) Surface CO_2 leakage during two shallow subsurface CO_2 releases, Geophys Res Lett 34:L24402.

(13) Strazisar, BR, AW. Wells, JR Diehl, RW Hammack, GA Veloski (2009) Near-surface monitoring for the ZERT shallow CO_2 injection project, International Journal of Greenhouse Gas Control, Volume 3, Issue 6, Pages 736-744

(14) Watson, TB, R Wilke, RN Dietz, J Heiser, P Kalb (2007) The Atmospheric Background of Perfluorocarbon Compounds Used as Tracers, Environ. Sci. Technol., 41 (20), pp 6909–6913

(15) Wells A, Strazisar B, Diehl J, Veloski G (2010) Atmospheric tracer monitoring and surface plume development at the ZERT pilot test in Bozeman, Montana, USA, Environ. Earth Sci. 60 (2): 299-305.

(16) Kharaka, YK, JJ. Thordsen, E Kakouros, G Ambats, WN Herkelrath, SR Beers, JT Birkholzer, JA. Apps, NF Spycher, L Zheng, RC. Trautz, HW Rauch, KS Gullickson (2009) Changes in the chemistry of shallow groundwater related to the 2008 injection of CO_2 at the ZERT field site, Bozeman, Montana, Environ Earth Sci, Special Issue

(17) Zheng, L., Apps, J.A., Zhang, Y., Xu, T., Birkholzer, J.T. (2008): Reactive Transport Simulations to Study Groundwater Quality Changes in Response to CO_2 Leakage from Deep Geological Storage, Proceedings 9th International Conference on Greenhouse Gas Control Technologies, November 2008, Washington, D.C., 2008.

(18) Susan Carroll, Yue Hao, and Roger Aines. Geochemical detection of carbon dioxide in dilute aquifers. Geochemical Transactions 2009, 10:4

(19) Zheng L, Apps J, Spycher N, Birkholzer J, Kharaka YK, Thordsen J, Kakouros E, Trautz R, Rauch H, Gullickson K (2009) Changes in shallow groundwater chemistry at the 2008 ZERT CO_2 injection experiment: II-modeling analysis. Abstract, eight carbon capture and sequestration conference, Pittsburgh, PA, May 4–7

(20) Ogretim E, Donald D. Gray and Grant S. Bromhal (2009) Effects of Crosswind-Topography Interaction on the Near-Surface Migration of a Potential CO_2 Leak, Energy Procedia, Volume 1, Issue 1, Pages 2341-2348

(21) Darvish, G. R., Lindeberg, E., Kleppel, J., Torsaeter, O., "Numerical Simulations For Designing Oil/CO_2 Gravity-Drainage Laboratory Experiments of A Naturally Fractured Reservoir", EOR-OG 320, presented at the 7th International Conference on Greenhouse Gas Control Technologies, Vancouver, Canada, Sep 5 – 9, 2004.

(22) Izgec O., Demiral B., Bertin H.: CO_2 injection into saline carbonate aquifer formations II: comparison of numerical simulations to experiments. Transp. Porous Media 73, 57–74 (2008).

(23) Pruess, K., Oldenburg, C.M., Moridis, G., 1999. TOUGH2 User's Guide, version 2.0. Report LBNL-43134, Lawrence Berkeley National Laboratory, Berkeley, CA, USA.

(24) Pruess K., García, J., Kovscek, T., Oldenburg, C. M., Rutqvist, J., Steefel, C., and Xu, T., 2004. Code intercomparison builds confidence in numerical simulation models for geologic disposal of CO_2. Energy, 29(9-10), 1431-1444.

(25) Oldenburg, C.M., Pruess, K., Benson, S.M., 2001. Process modeling of CO_2 injection into natural gas reservoirs for carbon sequestration and enhanced gas recovery. Energy Fuels 15, 293–298.

(26) Oldenburg, C.M., and A.J.A. Unger. On leakage and seepage from geologic carbon sequestration sites; unsaturated zone attenuation. Vadose Zone Journal (August 2003), 2(3):287-296

(27) Oldenburg, C.M., and A.J.A. Unger (2004) Coupled vadose zone and atmospheric surface-layer transport of CO_2 from geologic carbon sequestration sites, Vadose Zone Journal, 3, 848–857, 2004, LBNL-55510.

(28) Agarwal DK, Silander JA, Gelfand AE, Dewar RE, Mickelson JG (2005) Tropical deforestation in Madagascar: analysis using hierarchical spatially explicit, Bayesian regression models. Ecol Model 185:105–131.

(29) Borsuk ME, Higdon D, Stow CA, et al. (2001) A Bayesian hierarchical model to predict benthic oxygen demand from organic matter loading in estuaries and coastal zones. Ecol Model 143:165–181.

(30) Goyal A, Small MJ, von Stackelberg K, Burmistrov D, Jones N (2005) Estimation of fugitive lead emission rates from secondary lead facilities using hierarchical Bayesian models. Environ Sci Technol 39:4929–4937.

(31) Lockwood, JR, Schervish MJ, Gurian P, Small MJ (2001) Characterization of arsenic occurrence in U. S. drinking water treatment facility source waters. J Am Stat Assoc 96:1184–1193.

(32) Helser TE, Lai HL (2004) A Bayesian hierarchical meta-analysis of fish growth: with an example for North American largemouth bass, Micropterus salmoides. Ecol Model 178:399–416.

(33) Lockwood, JR., Schervish MJ, Gurian P, Small MJ (2004) Analysis of contaminant co-occurrence in community water systems. J Am Stat Assoc 99:45–56.

(34) Berliner LM (2000) Hierarchical Bayesian modeling in the environmental sciences, Allgemeines Statistisches Archiv. J German Stat 84:141–153.

(35) Gelman A, Hill J (2006) Data Analysis Using Regression and Multilevel/Hierarchical Models. Cambridge University Press, New York.

(36) Gelman, A, Carlin, JB, Stern, HS and Rubin, DB (2003) Bayesian Data Analysis, 2nd edn. Chapman & Hall/CRC Press, Boca Raton, FL.

(37) Royle JA, Berliner LM (1999) A Hierarchical approach to multivariate spatial modeling and prediction. J Agric Biol Envir S 4:29–56.

(38) Wikle CK (2003) Hierarchical models in environmental science. Int Stat Rev 71:181–199.

(39) Spiegelhalter DJ, Best NG, Carlin BP, van der Linde A (2002) Bayesian measures of model complexity and fit. J Roy Stat Soc B 64:583–639.

(40) Borsuk ME, Stow CA, Reckhow K (2004) A Bayesian network of eutrophication models for synthesis, prediction and uncertainty analysis. Ecol. Model. 173: 219-239.

(41) Castelletti A, Soncini-Sessa R (2007) Bayesian networks in water resource modelling and management. Environmental Modelling & Software, 22(8): 1073-1074.

(42) Darwiche A (2009) Modeling and Reasoning with Bayesian Networks. Cambridge University Press, New York.

(43) Heckerman D (1999) A Tutorial on Learning with Bayesian Networks. In Learning in Graphical Models, M. Jordan, ed. MIT Press, Cambridge, MA.

(44) Lee DC, Rieman BE (1997) Population viability assessment of salmonids by using probabilistic networks. North Am. J. Fish. Manage. 17: 144–1157.

(45) Ticehurst JL, Newham LHT, Rissik D, Letcher RA, Jakeman AJ (2007) A Bayesian network approach for assessing the sustainability of coastal lakes in New South Wales, Australia. Environ. Model. Softw. 22(8): 1129-1139.

Chapter 2: Bayesian hierarchical models for soil CO_2 flux and leak detection at geologic sequestration sites[1]

Abstract

Proper characterizations of background soil CO_2 respiration rates are critical for interpreting CO_2 leakage monitoring results at geologic sequestration sites. In this paper a method is developed for determining temperature-dependent critical values of soil CO_2 flux for preliminary leak detection inference. The method is illustrated using surface CO_2 flux measurements obtained from the AmeriFlux network fit with alternative models for the soil CO_2 flux vs. soil temperature relationship. The models are fit first to determine pooled parameter estimates across the sites, then using a Bayesian hierarchical method to obtain both global and site-specific parameter estimates. Model comparisons are made using the Deviance Information Criterion (DIC), which considers both goodness of fit and model complexity. The hierarchical models consistently outperform the corresponding pooled models, demonstrating the need for site-specific data and estimates when determining relationships for background soil respiration. A hierarchical model that relates the square root of the CO_2 flux to a quadratic function of soil temperature is found to provide the best fit for the Ameriflux sites among the models tested. This model also yields effective prediction intervals, consistent with the upper envelop of the flux data across the modeled sites and temperature ranges. Calculation of upper prediction intervals using the proposed method can provide a basis for setting critical values in CO_2 leak detection monitoring at sequestration sites.

2.1   Introduction

With geologic sequestration of CO_2 now being considered in a number of nations as a short- to medium-term strategy for reducing carbon emissions, there is a need for CO_2 leak detection monitoring to ensure that the sequestered CO_2 at a site does not return to the atmosphere, yielding the mitigation strategy ineffective (*1-5*).

A number of methods have been proposed for detecting CO_2 leakage at sequestration and storage sites, including: seismic profiling, pressure measurement, and other geophysical methods for detecting changes at the deep reservoir level; groundwater sampling for changes in water chemistry in observation wells; analysis of natural, injected and recovered carbon isotopes; near-surface monitoring of soil-to-air CO_2 fluxes; soil gas measurement for the presence of tracers added to the injected CO_2; and measurement of CO_2, tracers or other indicator gases in the air above (or downwind of) the sequestration site (*6-10*). These alternatives for site monitoring target different locations at or near the site at different stages of the injection and storage process, and it is generally recognized that some combination of methods will ultimately provide for the most cost-effective coverage.

The need to characterize natural background (pre-injection) conditions is common to most methods for leak detection, whether based on ambient air, soil gas, groundwater, CO_2, tracer gas, or isotopic measurements. In each case the natural background must be monitored and/or modeled to provide a baseline against which the operational measurements are compared. Various mechanistic and/or statistical models could be

used to describe background variability. For example, Cortis et al. (11) employ artificial

neural networks (ANN) to model background CO_2 surface concentrations and detect

anomalies possibly caused by CO_2 leakage. In our approach, Bayesian statistical methods

are used to represent both natural variability and the uncertainty present in characterizing

this variability. Statistically, the problem is one of determining the pre-injection

predictive distribution of the measured indicator and its associated prediction intervals

($12-14$). The approach is similar to methods recommended for use by the US EPA for

groundwater leak detection at Resource Conservation and Recovery Act (RCRA) waste

sites (15). The method for determining leak detection prediction intervals is developed

and demonstrated in this paper using surface soil CO2 flux monitoring data.

Soil CO_2 flux monitoring provides a direct estimate of CO_2 exchange between the

soil and the atmosphere, and is typically implemented using the accumulation chamber

method (16). Accumulation chamber monitors have been deployed and tested in a

number of pilot projects, such as the Zero Emissions Research and Technology (ZERT)

monitoring experiment in Bozeman, Montana ($17, 18$). The background flux of CO_2

results from natural soil respiration processes and can be highly variable, depending on

local climate and vegetation. It is thus important to account for natural variation of this

baseline when attempting to isolate deep source leakage contributions to the monitored

soil CO_2 flux.

Predictive models for CO_2 respiration rates generally involve a combination of

mechanistic expressions for biological activity and the fitting of empirical parameters to

observed field data. The explanatory variables most often included in these models

include soil temperature and moisture ($19-24$). Soil temperature is recognized as the

most important and also the most widely used factor for modeling soil respiration rates because of its high degree of correlation with ambient temperature and its essential role in regulating biological mechanisms for energy generation (*24-26*). Generally soil respiration rates increase with soil temperature, but when temperatures become too high, biological activity decreases and thus soil respiration rates are inhibited (*27*). Another important input considered in a number of CO_2 respiration models is soil moisture. As in the case of soil temperature, a non-monotonic relationship is expected with soil moisture, since biological activity is inhibited when soils are dry, but gas transport is blocked when soils become saturated (*23, 28-31*). However, in many cases statistically significant relationships with soil moisture cannot be identified once soil temperature is included in the model (*32, 33*). Recent studies have attempted to include the effects of other factors, like net primary production, or biomass, into soil respiration models (*24, 26*). Nevertheless, these models require more complex functional forms and submodels, more fitted parameters, and a greater amount of field data to support the estimates. While improvements in model prediction performance have been achieved, these applications are usually limited to a single site or biome. Soil respiration can be further partitioned into root respiration and microbial respiration and they may respond differently to soil temperature (*34, 35*), but due to limited data availability, this partition is not considered in this study.

The method for building Bayesian hierarchical models for soil CO_2 flux and leak detection is illustrated using nine sites with soil respiration and temperature data from the Ameriflux database (*36*). The sites are chosen since they have a relatively large number of observations and encompass conditions across a range of climate, vegetation, and soil

conditions. While Hibbard et al. (*36*) performed an extensive study of soil respiration

rates for major Ameriflux sites in the Northern hemisphere, their analysis was limited to a

nonlinear regression model of Lloyd and Taylor (*25*). A number of the Ameriflux sites

were also included in the modeling study of Reichstein et al. (*23*). To demonstrate our

methodology, four alternative models are tested, though all with dependency limited

solely to soil temperature. Subsequently, the best fitting model is expanded to include a

term for soil moisture to see whether the additional complexity is justified using

statistical criteria. For application at potential carbon sequestration sites, soil respiration

models are tested for their ability to estimate both central tendency CO_2 flux rates as a

function of explanatory variables and upper prediction intervals for these relationships,

since it is the latter that determine critical values for leak detection. Bayesian hierarchical

models are fit across the sites to illustrate how multisite information can be used to

provide more-general model selection concurrent with site-specific estimation.

2.2   Data and Methods

2.2.1   Site Data

CO$_2$ respiration and soil temperature data were obtained for nine AmeriFlux and

CarboEurope sites included in the AmeriFlux database (*36*). These nine sites are the

largest in terms of available data, with each having at least 50 concurrent observations of

soil respiration and soil temperature. The nine sites and their data summaries are

presented in Table 2.1. As indicated these sites represent four biomes: the IOM site is

categorized as grasslands (GRS); the HAR and UMB sites represent mixed

deciduous/evergreen forest (MXD); the JUN site belongs to woodland/savannas (WSV); and the remaining five sites are all from evergreen needleleaf forests (ENF). The data were collected over a time period from 1995-2002.

Table 2. 1   Characteristics of Nine AmeriFlux Sites

Site[a]	Site number	Sample Size	Soil Respiration Rate (μmol CO_2 m^{-2} s^{-1}) Mean (Std. Dev.)	Temperature (°C) Mean (Std. Dev.)	Biome[b]
HAR	1	182	3.2 (2.0)	12.0 (5.0)	MXD
HOW	2	149	2.7 (1.7)	9.5 (6.0)	ENF
IOM	3	658	1.6 (1.4)	20.0 (8.6)	GRS
JUN	4	87	0.56 (0.30)	20.0 (6.8)	WSV
MEO	5	302	2.1 (1.1)	13.0 (5.5)	ENF
MEY	6	258	1.5 (0.90)	16.0 (5.8)	ENF
THA	7	278	2.6 (1.7)	6.6 (4.3)	ENF
UMB	8	78	4.6 (2.4)	13.0 (5.8)	MXD
WDN	9	127	2.2 (0.69)	10.0 (3.3)	ENF

[a] HAR = Harvard forest site, Massachusetts; HOW = Howland site, Maine;
IOM = Ione modeled site, California; JUN = Metolius juniper site, Oregon;
MEO = Metolius old site, Oregon; MEY = Metolius young site, Oregon;
THA= Tharandt site, Germany; UMB = University Michigan Biol. Station, Michigan;
WDN = Weidenbrunnen site, Germany
[b] MXD = Mixed deciduous/evergreen forest; ENF = Evergreen needleleaf forests;
GRS = Grasslands; WVS = Woodland/savannas.

The average mean daily soil respiration rate (R_s) across the nine sites was 2.12 μmol m^{-2} s^{-1}. The highest single measurement of soil respiration (9.88 μmol m^{-2} s^{-1}) occurred at the UMB site in July 1999, and the lowest value (0.03 μmol m^{-2} s^{-1}) was measured at the IOM site in October 2001. The UMB site also exhibits the highest average soil respiration rate over the study period, 4.6 μmol m^{-2} s^{-1}, while the lowest average respiration rate is calculated for the JUN site, 0.56 μmol m^{-2} s^{-1}.   Relative

standard deviations (standard deviation divided by the mean) for the soil respiration rates range from 0.52-0.63 for seven of the nine sites, indicating a similar level of variability for each. Somewhat higher variability is exhibited at the IOM site (relative standard deviation = 0.88), while somewhat lower variability is found for the WDN site (relative standard deviation = 0.33). Measured soil temperatures at the sites ranged from 3.0°C to 37.2°C. The highest average soil temperatures are found at the IOM and JUN sites (20.0°C), while the lowest average occurs at the THA site (6.6°C).

2.2.2   Soil Respiration – Temperature Models

A number of preliminary tests of alternative models were conducted for the Ameriflux sites using simple linear or nonlinear regression. Various variable transformations were also considered to insure that the fitted models would yield residuals that were normally distributed or at least approximately normal (*26*). The following four models, representative of a range of previous mechanistic and empirical applications, were chosen for further study: (1) a conventional first-order exponential relationship, often referred to as the van't Hoff simple Q_{10} model; (2) a log- quadratic model (*37*); (3) a modified Davidson model with a formula similar to that of the Michaelis-Menten model (*24*); and (4) a square root-quadratic model (*38*):

$$\text{Simple } Q_{10}: \qquad \ln[CO_2 \ flux] = a + b \, T \qquad\qquad (1)$$

$$\text{Log-quadratic:} \qquad \ln[CO_2 \ flux] = a + bT + cT^2 \qquad\qquad (2)$$

$$\text{Modified Davidson: } [CO_2 \ flux] = \frac{(1+0.2333T) \ 2^{(T-10)/10} \ (10-bT)}{(1+aT) \ 2^{(T-10)/10} + (10-bT)} \qquad (3)$$

$$\text{Square root-quadratic: } [CO_2 \ flux]^{1/2} = a + b \, T + c \, T^2 \qquad\qquad (4)$$

In each case, T is soil temperature (°C) and *CO_2 flux* is the average mean daily soil

respiration rate (μmol m^{-2} s^{-1}). The constants in the modified Davidson model (0.2333, 2

and 10), are adapted from an illustrative model by Davidson et al. (*24*). All four models

can be represented as a general function $g(T/\theta)$ where θ represents a parameter vector (*a*,

b) or (*a*, *b*, *c*). Except for the simple Q_{10} model, all candidate models have the ability to

capture nonmonotonic behavior in the soil respiration-temperature relationship.

2.2.3 *Bayesian Statistical Formulation and Parameter Estimation*

Bayesian hierarchical models have been developed in recent years for a number of

environmental applications (*39-45*). The approach allows model inferences to be shared

across sites (or other subunits, such as species) and yields both global and subunit-

specific parameter estimates. The model structure for the Bayesian hierarchical

regression model is given by:

$$y_{ij} = g(T_{ij}|\theta_j) + \varepsilon_{ij}, \quad \theta_j \sim f_\theta(\theta_j/\gamma) \tag{10}$$

where y_{ij} is the ith observation of soil respiration at site *j* or the appropriate

transformation[2]; $g(T_{ij}|\theta_j)$ is the prediction from one of the four soil respiration models

noted above; and ε_{ij}, is the random error representing the variability that occurs over time

or from point to point at a site due to meteorological, geochemical, and biological

processes not captured by the fitted model. T_{ij} is the ith soil temperature (°C) at site *j*, and

θ_j represents the parameter vector for site *j*, that is, a vector (a_j, b_j) or (a_j, b_j, c_j),

depending on the model. The hierarchical nature of the model is captured by the second

---

[2] Transformations include the logarithm transformation, $\ln[CO_2\ flux]$, for the simple Q_{10} and log-
quadratic models, and the square-root transformation, $[CO_2\ flux]^{1/2}$, for the square-root quadratic model.

part of equation 10, where $f_\theta(\theta_j/\gamma)$ is the global distribution function for θ across sites.

The parameters for this distribution, encompassed in the vector γ, are referred to as the

hyperparameters of the hierarchical model.

      As is common in regression models, the residual error in equation 10 is assumed

to follow a normal distribution with mean zero and common variance, δ_y^2, i.e. $\varepsilon_{ij} \sim N(0,$

$\delta_y^2)$. Consequently, y_{ij} is also normally distributed:

$$y_{ij} \sim N(\, g(T_{ij}|\theta_j),\, \delta_y^2) \tag{11}$$

      Equations 10 and 11 imply that the soil respiration model is hierarchical in terms

of the mean, but non-hierarchical in the variance, that is, a common variance is estimated

across sites.

      The second level of the Bayesian hierarchical model is implemented by assuming

a multivariate normal distribution for $f_\theta(\theta_j/\gamma)$:

$$\theta_j \sim N(\, \mu,\, \delta_\theta^2) \tag{12}$$

where $\gamma = (\mu, \delta_\theta)$ is the hyperparameter vector. The model parameters are assumed a

priori to be normal with respective means and standard deviations. For example, for the

three parameter models with

$$\theta_j = \begin{pmatrix} a_j \\ b_j \\ c_j \end{pmatrix},\ \theta_j \text{ is normal with mean } \mu = \begin{pmatrix} \mu_a \\ \mu_b \\ \mu_c \end{pmatrix},\text{ and standard deviation } \delta_\theta = \begin{pmatrix} \delta_a \\ \delta_b \\ \delta_c \end{pmatrix}.\text{ The}$$

parameters are assumed to be independent a priori, however, covariance in their joint

uncertainties is induced in the posterior estimates through the numerical Markov Chain

Monte Carlo (MCMC) simulation procedure described below.

For the modified Davidson model, two hyperparameter vectors were required in order for the parameter estimation to converge. The vectors differentiate between sites that are fit well by the model and those that are not. This division allows each group to have its own variance, smaller for the former and larger for the latter. The HAR, THA and UMB sites are fit well by the model (with a lower variance), while the remaining sites are assigned to the second, higher-variance group.

The prior distributions of the parameters were chosen to be diffuse and non-informative, since little information is available to suggest particular parameter values over others. Diffuse normal distributions with $\mu = 0$ and $\delta_\theta{}^2 = 10^4$, were selected. The prior distribution for the common standard deviation, δ_y, was assigned a broad uniform distribution, from 0 to 100, to ensure positivity, while still allowing for model convergence.

Parameters are estimated by MCMC simulation, yielding samples of simulation results that are subsequently analyzed to determine parameter central tendencies (means and medians), dispersions (standard deviations and 95% credible intervals), and correlation coefficients. Detailed discussions of MCMC procedures are found in Berliner et al. ([46]), Wikle ([47]), and Gelman et al. ([48, 49]). Gibb's sampling along with the Metropolis-Hastings algorithm are used, implemented by WinBUGS version1.4 ([50]). For models 1, 2 and 4, the initial values for the MCMC chains were first randomly sampled from the diffuse prior distributions. This approach was also initially used for the modified Davidson model; however, successful convergence was not achieved. As such, point estimates of parameters determined by nonlinear regression were used to initiate the MCMC chains, accelerating their convergence. For models 1, 2 and 4, convergence was

achieved by simulating three chains, each with 8,000 iterations. For the modified

Davidson model, 100,000 iterations were required. The last 6,000 iterations for each

model were saved for subsequent statistical analysis.

2.2.4   *Model Evaluation and Comparison*

Models were evaluated and compared using a traditional measure of goodness-of-

fit: the mean square error (MSE) of predicted vs. observed CO_2 flux rates; and a metric

developed specifically for evaluating Bayesian hierarchical models: the Deviance

Information Criterion (DIC) (*48, 51*). In general, the MSE decreases as the model

complexity (number of parameters) increases, particularly when the complex model is a

more generalized version of the less complex model. In contrast, the DIC considers both

the goodness-of-fit and a penalty for model complexity. DIC is defined as

$$DIC = \overline{D} + p_D \tag{13}$$

where $\overline{D}$ is the expected deviance and p_D is the effective number of parameters. The

DIC computes a score based on the likelihood of the observed data given the model, then

applies a penalty based on the number of fitted parameters. The DIC is specifically

designed to overcome the difficulty in determining the effective number of parameters

and degrees of freedom to assign to hierarchical models. For both the MSE and DIC, a

smaller value is preferred.

2.2.5   *Posterior predictive distributions*

The joint parameter distributions simulated for each model with the MCMC

method provide the basis for estimating a predictive distribution and associated

prediction interval for CO_2 flux rates as a function of temperature for each model at each site. The predictive distribution represents the uncertainty in CO_2 flux rate given temperature that results from both the uncertainty in the fitted parameter values of the model and the variability represented by the variance term. The prediction interval identifies a critical percentile along this distribution that may be used to judge the likelihood that a particular flux rate observed at a given soil temperature was sampled from the fitted distribution, reflective of naturally occurring conditions, vs. sampled from a distribution with added CO_2 flux from a possible leak. For example, the 95% prediction interval extends from the 2.5% value of the simulated distribution to the 97.5% value of the distribution, with the latter providing a possible critical value for leak detection. In this paper, a value of 97.5%, corresponding to the upper bound of 95% prediction intervals, is chosen for illustrative purposes.

The steps in estimating the predictive distribution for each model at each site are as follows:

1. The last 6000 sets of parameter values of the simulated MCMC chain constitute samples from the joint parameter distribution.

2. For each parameter set a mean CO_2 flux rate is computed for the chosen soil temperature.

3. The error variance for each parameter set is used to simulate a normally distributed error term for addition to the mean from b), then this sum is transformed if needed (depending on the model) to obtain a sample of the CO_2 flux rate corresponding to the predictive distribution.

4. The resulting sample of predicted CO_2 flux rates (n = 6000) is analyzed to estimate targeted percentiles, e.g., the 2.5, 50, and 97.5% values, for the given temperature, model, and site.

2.3   Results

2.3.1   *Parameter estimation*

The full sets of parameters estimated for the four Bayesian hierarchical models are shown in Table 2.2, including the Bayesian posterior median of each parameter and their 95% credible intervals. Median and 95% credible intervals are likewise reported for the model standard deviations, δ_y. Estimates for Bayesian pooled models, in which data from all sites are combined to fit a single (pooled) model across sites, are also presented in Table 2.2 for comparison. The fitted models yield statistically significant parameter estimates in all but a few cases. Further interpretation of the specific parameter estimates for each model is found in Appendix A and graphical presentations of the fitted relationships are shown below for selected sites. As expected, the estimated $\delta_{y(hierarchical)}$ of the Bayesian hierarchical model is smaller than the $\delta_{y(pooled)}$ of the Bayesian pooled model, indicating that the hierarchical structure allows more accurate prediction, though at the cost of greater model complexity and a higher effective number of model parameters.

Table 2. 2   Summary of Markov Chain Monte Carlo Parameter Estimates for Bayesian Hierarchical Model Fit for each CO_2 Flux - Temperature Model for each Site

A. Simple Q_{10} (log-linear) Model

Parameter:	a			b		
Site	2.50%	median	97.50%	2.50%	median	97.50%
HAR	-1.30	-1.07	-0.84	0.14	0.16	0.17
HOW	-0.88	-0.70	-0.52	0.13	0.14	0.16
IOM	1.76	1.88	1.99	-0.10	-0.10	-0.09
JUN	-2.04	-1.65	-1.26	0.03	0.05	0.06
MEO	-0.68	-0.52	-0.35	0.08	0.09	0.10
MEY	-0.63	-0.42	-0.21	0.03	0.04	0.05
THA	-0.39	-0.26	-0.14	0.13	0.15	0.17
UMB	-0.39	-0.09	0.24	0.09	0.11	0.13
WDN	-0.75	-0.42	-0.09	0.08	0.11	0.14
Bayesian Pooled	0.77	0.85	0.93	-0.04	-0.03	-0.03
$\sigma_{y(hierarchical)}$	0.578	0.596	0.614			
$\sigma_{y(pooled)}$	0.945	0.972	1.004			

B. Log-quadratic Model

Parameter:	a			b			c		
Site	2.50%	median	97.50%	2.50%	median	97.50%	2.50%	median	97.50%
HAR	-1.64	-1.59	-1.31	0.17	0.22	0.28	-0.01	-3.0E-03	-9.2E-04
HOW	-1.09	-1.05	-0.87	0.17	0.23	0.28	-0.01	-4.9E-03	-1.9E-03
IOM	1.00	1.05	1.27	-0.06	-0.03	0.00	-2.5E-03	-1.8E-03	-1.0E-03
JUN	-2.62	-2.49	-1.88	-0.04	0.07	0.15	-2.8E-03	-7.1E-04	2.4E-03
MEO	-1.07	-1.02	-0.78	0.09	0.14	0.19	-4.1E-03	-2.1E-03	-1.1E-04
MEY	-1.06	-1.00	-0.69	0.03	0.08	0.13	-2.9E-03	-1.4E-03	3.0E-04
THA	-0.54	-0.52	-0.37	0.16	0.21	0.27	-0.01	-4.7E-03	-1.5E-03
UMB	-0.71	-0.63	-0.29	0.11	0.16	0.24	-0.01	-2.3E-03	2.4E-04
WDN	-1.05	-0.99	-0.64	0.11	0.17	0.26	-0.01	-3.3E-03	-9.6E-05
Bayesian Pooled	-0.71	-0.70	-0.61	0.19	0.21	0.22	-0.01	-0.01	-0.01
$\sigma_{y(hierarchical)}$	0.572	0.589	0.608						
$\sigma_{y(pooled)}$	0.758	0.781	0.805						

C. Modified Davison Model

Parameter:	a			b		
Site	2.50%	median	97.50%	2.50%	median	97.50%
HAR[a]	18.2	62.1	139.2	-319.8	-144.9	-41.7
HOW[b]	0.01	0.04	0.21	-0.04	0.38	0.43
IOM[b]	0.32	0.34	0.37	0.31	0.32	0.32
JUN[b]	2.99	6.87	27.04	-2.09	-0.25	0.16
MEO[b]	1.46	3.17	9.38	-7.43	-2.14	-0.72
MEY[b]	1.54	2.78	7.51	-2.30	-0.53	-0.07
THA[a]	-17.41	-6.44	0.40	-338.5	-168.9	-33.17
UMB[a]	11.0	30.9	64.0	-330.4	-163.4	-58.0
WDN[b]	0.27	1.24	6.47	-9.45	-1.27	0.26
Bayesian Pooled	0.22	0.23	0.24	0.32	0.32	0.33
$\sigma_{y(hierarchical)}$	0.849	0.874	0.901			
$\sigma_{y(pooled)}$	1.288	1.327	1.371			

D. Square Root Quadratic Model

Parameter:	a			b			c		
Site	2.50%	median	97.50%	2.50%	median	97.50%	2.50%	median	97.50%
HAR	0.22	0.37	0.54	0.07	0.11	0.13	-1.2E-03	-1.0E-04	1.4E-03
HOW	0.55	0.65	0.75	0.09	0.11	0.12	-1.9E-03	-8.9E-04	1.8E-04
IOM	1.42	1.56	1.68	0.00	0.01	0.03	-1.9E-03	-1.5E-03	-1.2E-03
JUN	0.04	0.37	0.71	-0.01	0.02	0.06	-1.2E-03	-2.4E-04	7.4E-04
MEO	0.48	0.63	0.78	0.04	0.07	0.09	-1.3E-03	-3.1E-04	6.6E-04
MEY	0.51	0.68	0.89	0.02	0.04	0.07	-1.4E-03	-6.8E-04	2.4E-04
THA	0.75	0.83	0.90	0.09	0.11	0.13	-2.0E-03	-7.2E-04	7.0E-04
UMB	0.61	0.79	0.97	0.07	0.10	0.13	-1.3E-03	-1.3E-04	1.3E-03
WDN	0.50	0.69	0.88	0.05	0.09	0.12	-2.7E-03	-8.2E-04	7.2E-04
Bayesian Pooled	0.62	0.68	0.74	0.12	0.13	0.13	-4.5E-03	-4.3E-03	-4.0E-03
$\sigma_{y(hierarchical)}$	0.294	0.303	0.312						
$\sigma_{y(pooled)}$	0.432	0.445	0.458						

2.3.2   *Model comparison for Bayesian pooled and hierarchical models*

The selected predictions of the four Bayesian hierarchical models and their

Bayesian pooled versions are presented in Figure 1 below. The predictions represent the

median values of the simulated predictive distributions of soil respiration as a function of

temperature. The four sites shown represent the four different biomes in the dataset, the

HAR site (MDF biome), HOW site (ENF), IOM site (GRS) and JUN site (WVS). As

shown in Figure 1, the hierarchical models fit the site data better than the pooled models

do. At the HAR site (Figure 1 (a)), the four hierarchical models' predictions are very

close and exhibit similar upward-sloping convex shapes as a function of temperature for

the soil respiration rate. For the HOW site (Figure 1 (b)), differentiation between the

fitted model predictions is apparent above 15°C. The Q_{10} model keeps rising up steeply,

the log-quadratic model and the square root-quadratic model go up mildly and are close

to each other, and the modified Davidson model starts decreasing with temperature at

around 18°C. In contrast, the IOM site (Figure 1 (c)) exhibits a clear decrease in soil

respiration rate at high temperature, which is common for the GRS biome. All four

models capture this behavior, except for the pooled modified Davidson estimate. All of

the hierarchical models for the IOM site predict monotonically decreasing relationships

over the observed temperature range $(6 - 35^{o}C)$, except for the modified Davidson model

which initially increases with temperature, then decreases. The JUN site has very low,

relatively constant soil respiration rates across the range of observed temperatures, and

this behavior is captured reasonably well by each of the hierarchical models.
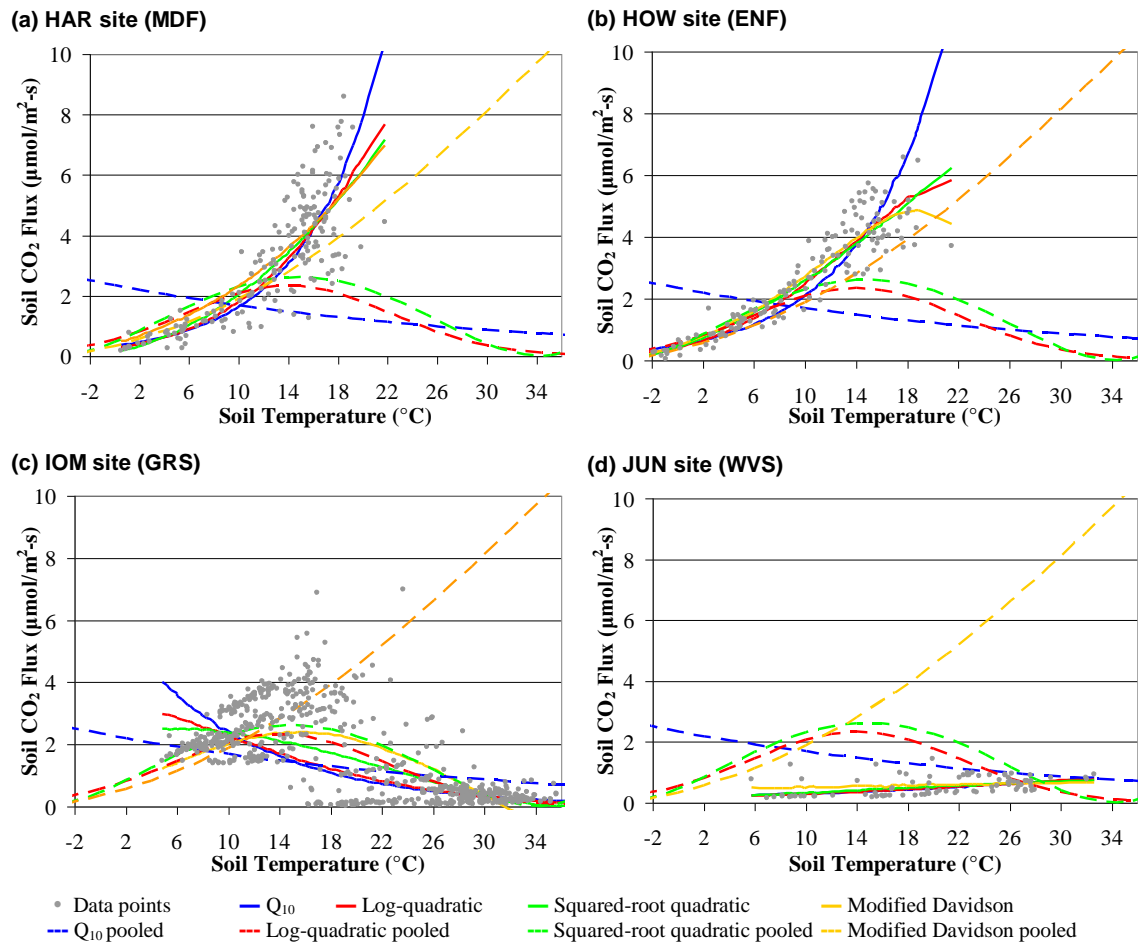
Figure 2. 1   Comparison of Bayesian Pooled and Bayesian Hierarchical Model Prediction for Median CO_2 flux for Four Models of Soil Respiration. The solid lines represent the prediction from Bayesian hierarchical models (different for each site), and the grid lines represent the prediction from Bayesian pooled models (same across all sites). Blue color is for simple Q_{10} model; red color is for log-quadratic model; green color is for square root-quadratic model; yellow color is for modified Davidson model: (a) HAR site for mixed deciduous/evergreen forest biome; (b) HOW site for evergreen needleleaf forest biome; (c) IOM site for grassland biome; and (d) JUN site for woodland/savannas biome.

The predictions of the Bayesian pooled models reveal a strong averaging effect across sites. For instance, the pooled Q_{10} model is greatly influenced by the largest site (IOM), which exhibits a significant drop in soil respiration rates at high soil temperature, and the pooled data thus lead to an atypical (downward sloping) curve for the fitted Q_{10} model. The other two-parameter (modified Davidson) function also yields a monotonic

33

pooled function, though in this case upward sloping. In contrast, the three-parameter

models (log-quadratic and square-root quadratic) provide sufficient flexibility to yield a

non-monotonic pooled relationship, better able to capture the range of behavior exhibited

across sites.

The goodness of fit of the alternative models and modeling approaches is

summarized in Table 2.3. For all four models there is a substantial decrease in the mean

square error in moving from the single pooled model applied to all sites to the

hierarchical model that provides for site-specific parameter estimates. However, this

requires an increase in the effective number of parameters from approximately 3-4

(depending on the model), to between 12 and 25. The DIC, which penalizes models for

the number of fitted parameters, is nevertheless consistently lower (better) for the

hierarchical models. As such, the added complexity of hierarchical models is indeed

worth it. By all measures the best fitting model is the hierarchical square-root quadratic,

with a DIC value of 978. The square-root quadratic also provides the best fitting (lowest

DIC) pooled model, and has the lowest MSE for both the pooled and hierarchical fits.

Table 2. 3   Mean Square Error (MSE) and Deviance Information Criterion (DIC) of Four Bayesian Hierarchical and Pooled Models of Soil Respiration (see Equation 13 for parameter definitions)

Model	MSE (Pooled)	MSE (Hierarchical)	DIC (Pooled)			DIC (Hierarchical)		
			p_D	$\overline{D}$	DIC	p_D	$\overline{D}$	DIC
Simple Q_{10}	3.11	1.00	3	5891	5894	18.9	3817	3836
Log-quadratic	1.99	0.849	3.9	4962	4966	25.4	3769	3794
Modified Davidson	10.03	0.759	3	7213	7216	11.7	5441	5453
Square root-quadratic	1.78	0.749	3.9	2583	2587	23.2	955	978

2.3.3 *Posterior Predictive Distribution and Prediction Intervals*

Figure 2 illustrates the resulting predictive distributions from this procedure for the IOM and the HAR site, at a temperature of $15^{\circ}C$, based on parameter sets from the four Bayesian hierarchical models. Each cumulative distribution function is computed from 6000 samples generated as described above. In the case of the IOM site, the models tend to converge at higher percentile values of the distribution, so that the 97.5% value is approximately 4 μmol CO_2 m^{-2} s^{-1} in each case. The overall shapes of the four predictive distribution curves are somewhat similar for the IOM site, with some differentiation between the Q_{10} and log-quadratic models vs. the modified Davidson and square-root quadratic models. At the HAR site, the models show significant disagreement at higher percentage values of the distribution, and the two groups of curves are obviously distinguished from each other. The 97.5% values of the modified Davidson and square-root quadratic models are approximately 5-6 μmol CO_2 m^{-2} s^{-1}; however, the 97.5% values of the Q_{10} and log-quadratic models are higher, approximately 9 μmol CO_2 m^{-2} s^{-1}.
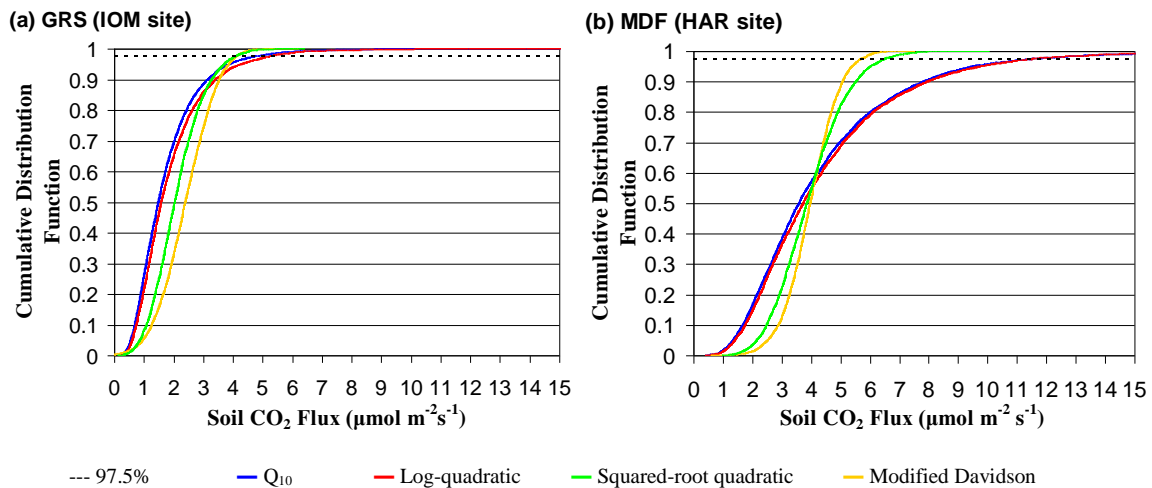
Figure 2. 2   Cumulative distribution function of posterior predictive distribution of the CO_2 flux at T = $15^{\circ}C$ for the four Bayesian hierarchical models at the IOM and HAR sites.

35

The 95% prediction intervals computed using the Bayesian hierarchical models for the four sites shown in Figure 1 are presented in Figure 3, along with the original data. The models yield similar results, especially for the lower (2.5%) prediction interval value, however, it is the upper value that is our primarily concern, since this (or a similar upper percentile) will be used as a critical value for leak inference. A consistent pattern is present at three of the sites: HAR, HOW, and IOM. In each case the four models yield similar 97.5% values over approximately half of the observed temperature range – for the HAR and HOW sites this occurs at lower soil temperatures, while for the IOM site this occurs at higher soil temperatures (in all three cases corresponding to lower flux rates). However, for the remaining portion of the curve the Q_{10} and log-quadratic models predict 97.5% flux rates much higher than the other two models and much higher than any of the observations made at those temperatures. In contrast, the modified Davidson and square-root quadratic models provide 97.5% estimates that reasonably track the upper envelope of the observed data, as would be targeted for leak detection applications. Given this result and the strong performance of the square-root quadratic model in the goodness of fit comparisons presented above, this model would appear to provide a preferred basis for modeling the soil temperature – CO_2 flux relationship and associated prediction intervals at these sites.
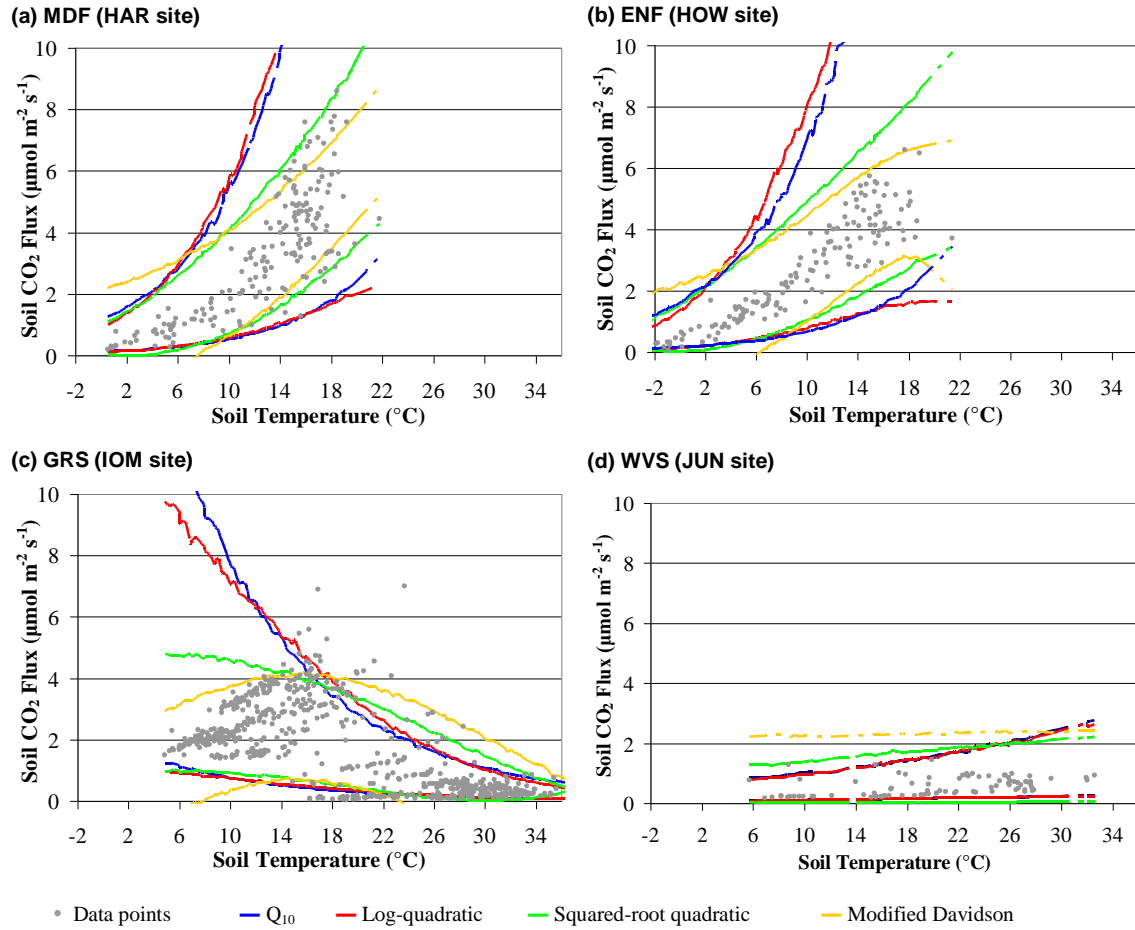
Figure 2. 3   95% Prediction Intervals of Four Models of Soil Respiration. Blue color denotes Q_{10} model; red color denotes log-quadratic model; green color represents square root-quadratic model; the yellow represents modified Davidson model: (a) HAR site for mixed deciduous/evergreen forest biome; (b) HOW site for evergreen needleleaf forest biome; (c) IOM site for grassland biome; and (d) JUN site for woodland/savannas biome.

To illustrate the effect of including soil moisture as an additional explanatory variable in the hierarchical model, the square-root quadratic model was refit using both soil temperature and soil moisture data for the nine Ameriflux sites (due to data limitations, the total sample size is reduced from 2119 to 1840). This was implemented by modifying Equation 4 to include an additional linear term for soil moisture on the right-hand-side of the equation. While the soil moisture term is statistically significant in single-site regression models for five of the nine sites, for three of these sites the fitted

37

coefficient is positive while for the other two it is negative. Furthermore, for the

Bayesian hierarchical model, addition of the soil moisture term yields a fitted model with

a much higher DIC value (4575 for the model with the soil moisture term vs. 978 for the

model with only the soil temperature terms). As such, use of the additional parameters

(the soil moisture term coefficients for each site and the hyperparameters across sites) is

not statistically justified for the hierarchical model. While the use of additional

explanatory variables, such as soil moisture, can be readily accommodated in the general

methodology proposed here, this use should be justified using appropriate statistical

measures (such as the DIC) that consider the tradeoff between goodness-of-fit and model

complexity.

2.4   Discussion and Conclusion

In this study Bayesian pooled and hierarchical models have been successfully

developed and applied to predict soil CO_2 respiration rates as a function of temperature at

nine AmeriFlux sites. The hierarchical approach allows determination of a global

parameter distribution for the set of sites, the sharing of information across sites, and site-

specific parameter estimates for each. The Bayesian MCMC method allows

determination of the joint uncertainty of model parameters across sites, facilitating the

calculation of predictive distributions for each site and the comparison of alternative

models. The comparison of goodness of fit between the pooled and hierarchical models

shows that the hierarchical structure enables much better prediction by providing site-

specific parameter estimates. The greater model complexity required by the hierarchical

models is more than compensated for by the improved fit, as reflected in their lower DIC

values. The ability to characterize the uncertainty at each site allows estimation of prediction intervals, which can provide a first basis for determining critical values of measured CO_2 fluxes (conditioned on temperature) representing higher-than-natural values. Measurements above these flux rates could thus be indicative of a possible leak at a sequestration site.

Among the four selected soil respiration models, the square root-quadratic model has the best performance in fitting the site data and providing reasonable prediction intervals. The square root-quadratic model has the lowest DIC and MSE for both hierarchical and pooled versions. Furthermore, the model's upper prediction intervals reasonably match the upper envelope of observed values across different sites and different temperature ranges. This is a desirable feature for a model that may be applied for general use in leak detection applications. This model should thus be among those considered for fitting respiration-temperature relationships and determining critical values for leak detection at planned CO_2 sequestration sites.

The Bayesian hierarchical approach illustrated here for determining the critical values of soil CO_2 flux for leak detection can also be applied to other CO_2 leak detection monitoring techniques, such as carbon isotopes or injected tracers. In each case, the natural background data from multiple sites are characterized by the Bayesian hierarchical method in order to obtain the predictive distribution of the natural background data at each site. The predictive distribution is used to estimate the prediction intervals, and the upper value of the prediction intervals is the critical value of leak identification for the monitoring technique. The critical value is needed to determine

when a measurement is statistically significantly different from that expected normal range for a given site and site conditions.

Prediction intervals result from the combined effects of measurement error; variability in local climate, site geology, and soil conditions; and the uncertainty inherent in fitting models with finite datasets. When measurements are available across multiple sites, Bayesian hierarchical models provide a basis for pooling this information, thereby reducing the overall uncertainty, while still maintaining site-specific model estimates.

References

(1) Hepple RP, Benson SM (2005) Geologic storage of carbon dioxide as a climate change mitigation strategy: Performance requirements and the implications of surface seepage. Environ Geol 47:576–585

(2) Wilson EJ, Friedmann SJ, Pollack MF (2007) Research for deployment: incorporating risk, regulation, and liability for carbon capture and sequestration. Environ Sci Technol 41:5945–5952

(3) Bachu, S (2008) CO2 storage in geological media: Role, means, status and barriers to deployment, Prog Energ Combust Sci 34:254–273

(4) de Coninck H, Stephens JC, Metz B (2009) Global learning on carbon capture and storage: A call for strong international cooperation on CCS demonstration. Energ Policy, 37:2161–2165

(5) van Alphen K, Hekkert MP, Turkenburg WC (2009) Comparing the development and deployment of carbon capture and storage technologies in Norway, the Netherlands, Australia, Canada and the United States – An innovation system perspective. Energy Procedia 1:4591–4599

(6) Klusman, RW (2003) Evaluation of leakage potential from a carbon dioxide EOR/sequestration project. Energ Convers Manage 44:1921–1940

(7) Oldenburg CM, Lewicki JL, Hepple RP (2003) Near-surface monitoring strategies for geologic carbon dioxide storage verification. Lawrence Berkeley National Laboratory, LBNL-54089

(8) Benson SM, Gasperikova E, Hoversten GM (2004) Monitoring protocols and life-cycle costs for geologic storage of carbon dioxide. In: Proceedings of the 7th International Conferenceon Greenhouse Gas Control Technologies (GHGT-7), Vancouver, Canada, 5–9 September 2004.

(9) Benson SM (2007) Monitoring Geological Storage of Carbon Dioxide, Carbon Capture and Geologic Sequestration. In: E.J. Wilson and D. Gerard (eds.) Integrating technology, monitoring, and regulation, Blackwell Scientific Publishing, Ames, Iowa, pp 73-100

(10) Leuning R, Etheridge D, Luhar A, Dunse B (2008) Atmospheric monitoring and verification technologies for CO2 geosequestration. Int J Greenh Gas Con 2(3):401–414

(11) Cortis A, Oldenburg CM, Benson SM (2008) The role of optimality in characterizing CO2 seepage from geologic carbon sequestration sites. Int J Greenh Gas Con 2:640–652

(12) Colosimo BM, Del Castillo E (eds.) (2007) Bayesian Process Monitoring, Control and Optimization. Chapman & Hall/CRC Press, London/Boca Raton, FL

(13) Downes BJ, Barmuta LA, Fairweather PG, Faith DP, Keough MJ, Lake PS, Mapstone BD, Quinn GP (2002) Monitoring Ecological Impacts: Concepts and Practice in Flowing Waters. Cambridge University Press, Cambridge UK

(14) Tsiamyrtzis P, Hawkins DM (2005) A Bayesian scheme to detect changes in the mean of a short run process. Technometrics 47:446–456

(15) US Environmental Protection Agency (2009) Statistical Analysis of Groundwater Monitoring Data at RCRA Facilities—Unified Guidance, EPA 530-R-09-007, March at:

http://www.epa.gov/epawaste/hazard/correctiveaction/resources/guidance/sitechar/gwstats/index.htm

(16) Healy RW, Striegl RG, Russell TF, Hutchinson GL, Livingston GP (1996) Numerical Evaluation of Static-Chamber Measurements of Soil—Atmosphere Gas Exchange: Identification of Physical Processes. Soil Sci Soc Am J 60:740-747

(17) Lewicki JL, Oldenburg CM, Dobeck L, Spangler L (2007) Surface CO_2 leakage during two shallow subsurface CO_2 releases, Geophys Res Lett 34:L24402

(18) Strazisar BR, Wells AW, Diehl JR, Hammack RW, Veloski GA (2009) Near-surface Monitoring for the ZERT shallow CO_2 injection Project. Int J Greenhouse Gas Cont 3:736–744

(19) Buchmann N (2000) Biotic and abiotic factors controlling soil respiration rates in Picea abies stands. Soil Biol Biochem 32:1625–1635

(20) Carlyle JC, Than UB (1988) Abiotic control of soil respiration beneath an eighteen-year-old pinus radiate stand in south-eastern Australia. J Ecol 76:654–662

(21) Davidson EA, Belk E, Boone RD (1998) Soil water content and temperature as independent or confounded factors controlling soil respiration in a temperate mixed hardwood forest. Glob Change Biol 4:217–227

(22) Raich JW, Schlesinger WH (1992) The global carbon dioxide flux in soil respiration and its relationship to vegetation and climate. Tellus B 44:81–99

(23) Reichstein M, Rey A, Freibauer A et al. (2003) Modelling temporal and large-scale spatial variability of soil respiration from soil water availability, temperature and vegetation productivity indices. Global Biogeochem Cy 17(4):15.1-15.15

(24) Davidson EA, Janssens IA, Luo Y (2006) On the variability of respiration in terrestrial ecosystems: moving beyond Q10. Glob Change Biol 12:154–164

(25) Lloyd J, Taylor JA (1994) On the temperature dependence of soil respiration. Funct Ecol 8:315–323

(26) Richardson AD, Braswell BH, Hollinger DY, Prabir Burman P, Davidson EA, Evans RS, Flanagan LB, Munger JW, Savage K, Urbanski SP, Wofsy SC (2006) Comparing simple respiration models for eddy flux and dynamic chamber data. Agr Forest Meteorol 141:219–234

(27) Smith KA, Ball T, Conen F, Dobbie KE, Massheder J, Rey A (2003) Exchange of greenhouse gases between soil and atmosphere: interactions of soil physical factors and biological processes. Eur J Soil Sci 54:779–791

(28) Jassal RS, Black TA, Drewitt GB, Novak MD, Gaumont-Guay D and Nesic Z (2004) A model of the production and transport of CO_2 in soil: predicting soil CO_2 concentrations and CO_2 efflux from a forest floor. Agr Forest Meteorol 124 :219–236

(29) Jassal RS, Black TA, Novak MD, Gaumont-Guay D, Nesic Z (2008) Effect of soil water stress on soil respiration and its temperature sensitivity in an 18-year-old temperate Douglas-fir stand. Glob Change Biol 14:1305–1318

(30) Moncrieff JB and Fang C (1999) A model for soil CO_2 production and transport 2: application to a Florida Pinus elliotte plantation. Agr Forest Meteorol 95:237–256

(31) Pumpanena J, Ilvesniemib H, Kulmala L, Siivola E, Laakso H, Kolari P, Helenelund C, Laakso M, Uusimaa M, Hari P (2008) Respiration in boreal forest soil as determined from carbon dioxide concentration profile. Soil Sci Soc Am J 72:1187–1196

(32) Davidson EA, Verchot1 LV, Cattânio JH, Ackerman IL, Carvalho JEM (2000) Effects of soil water content on soil respiration in forests and cattle pastures of eastern Amazonia. Biogeochemistry 48: 53–69

(33) Reth S, Reichstein M, Falge E (2005) The effect of soil water content, soil temperature, soil pH-value and the root mass on soil CO2 efflux – A modified model. Plant Soil 268:21–33

(34) Hanson PJ, Edwards NT, Garten CT, Andrew JA (2000) Separating root and soil microbial contributions to soil respiration: A review of methods and observations. Biogeochemistry 48: 115–146

(35) Wang W, Feng J and Oikawa T (2009) Contribution of root and microbial respiration to soil CO2 efflux and their environmental controls in a humid temperate grassland of Japan. Pedosphere 19(1): 31–39

(36) Hibbard KA, Law BE, Reichstein M (2005) An analysis of soil respiration across northern hemisphere temperate ecosystems. Biogeochemistry 73:29–70

(37) O'Connel AM (1990) Microbial decomposition (respiration) of litter in eucalypt forests of South-Western Australia: An empirical model based on laboratory incubations. Soil Biol Biochem 22:153–160

(38) Fang C, Moncrieff JB (2001) The dependence of soil CO2 efflux on temperature. Soil Biol Biochem 33:155–165

(39) Agarwal DK, Silander JA, Gelfand AE, Dewar RE, Mickelson JG (2005) Tropical deforestation in Madagascar: analysis using hierarchical spatially explicit, Bayesian regression models. Ecol Model 185:105–131

(40) Borsuk ME, Higdon D, Stow CA, et al. (2001) A Bayesian hierarchical model to predict benthic oxygen demand from organic matter loading in estuaries and coastal zones. Ecol Model 143:165–181

(41) Cable JM, Ogle K, Tyler AP, Pavao-Zuckerman MA, Huxman TE (2009) Woody plant encroachment impacts on soil carbon and microbial processes: results from a hierarchical Bayesian analysis of soil incubation data. Plant and Soil 320: 153-157

(42) Goyal A, Small MJ, von Stackelberg K, Burmistrov D, Jones N (2005) Estimation of fugitive lead emission rates from secondary lead facilities using hierarchical Bayesian models. Environ Sci Technol 39:4929–4937

(43) Lockwood, JR, Schervish MJ, Gurian P, Small MJ (2001) Characterization of arsenic occurrence in U. S. drinking water treatment facility source waters. J Am Stat Assoc 96:1184–1193

(44) Lockwood, JR., Schervish MJ, Gurian P, Small MJ (2004) Analysis of contaminant co-occurrence in community water systems. J Am Stat Assoc 99:45–56

(45) Patrick, LD, Ogle K, Tissue DT (2009) A hierarchical Bayesian approach for estimation of photosynthetic parameters of C3 plants. Plant, Cell & Environment 32: 1695-1709

(46) Berliner LM (2000) Hierarchical Bayesian modeling in the environmental sciences, Allgemeines Statistisches Archiv. J German Stat 84:141–153

(47) Wikle CK (2003) Hierarchical models in environmental science. Int Stat Rev 71:181–199

(48) Gelman, A, Carlin, JB, Stern, HS and Rubin, DB (2003) Bayesian Data Analysis, 2nd edn. Chapman & Hall/CRC Press, Boca Raton, FL

(49) Gelman A, Hill J (2006) Data Analysis Using Regression and Multilevel/Hierarchical Models. Cambridge University Press, New York

(50) Lunn, DJ, Thomas A, Best N, Spiegelhalter D (2000) WinBUGS -- a Bayesian modelling framework: concepts, structure, and extensibility. Stat Comput 10:325–33

(51) Spiegelhalter DJ, Best NG, Carlin BP, van der Linde A (2002) Bayesian measures of model complexity and fit. J Roy Stat Soc B 64:583–639

Chapter 3: Probabilistic Design of a Near-Surface CO_2 Leak Detection System[3]

Abstract

A methodology is developed for predicting the performance of near-surface CO_2 leak detection systems at geologic sequestration sites. The methodology integrates site characterization and modeling to predict the statistical properties of natural, pre-injection CO_2 fluxes; the transport of potential CO_2 leakage from the subsurface reservoir; and the detection of CO_2 transport, surface fluxes, or other signals measured by the monitoring network. The probability that a leakage event will be detected is computed as the probability that the leakage signal is sufficient to increase to total flux beyond a statistically-determined threshold for a presumptive leak. The methodology is illustrated assuming a monitoring network utilizing CO_2 surface flux chamber measurements on a uniform grid. A highly idealized site is assumed, with simple subsurface layering, horizontally homogeneous permeability, and a uniform probability of leakage across the site. The TOUGH2 model is used to predict the spatial profile of surface CO_2 fluxes resulting from different leakage rates and different soil permeability. A response surface is fit to the TOUGH2 results to allow interpolation across continuous values of permeability and leakage rate. Nonlinear, non-monotonic relationships of network performance with soil permeability and network density are evident, and in general dense networks (with ~10-20 meters between monitors) are required to ensure a moderate to

---

high probability of leak detection. Therefore, surface soil CO_2 flux measurement is unlikely to be feasible as a stand-alone technology for leak detection. Rather, it will most likely be applied in high risk locations, such as areas around wells and features, during the injection and post-injection period. Extensions to consider detection networks using multiple monitoring technologies at real sites with complex, nonhomogeneous site conditions, are discussed.

3.1   Introduction

Fossil fuel combustion is the principal source of anthropogenic CO_2 emissions globally and in the U.S. In 2007, electric power plants and industrial sources together resulted in the majority of US CO_2 emissions (42% from power plants, 15% from industrial sources) ([1, 2]). Coal-fired power plants constitute the largest single emitter of CO_2 and despite efforts to transition to alternative sources of energy, they are likely to remain so in the near future.

As a near-term solution the U.S. and many other nations are pursuing the implementation of carbon capture and sequestration (CCS) to reduce CO_2 emissions from electric power plants and industrial sources. CCS involves the post-combustion capture of CO_2 and its subsequent injection into geologic formations. However, to ensure that CCS is effective, leak detection monitoring is required to verify that a significant portion of the captured CO_2 does not return to the atmosphere. To ensure that greenhouse emissions credits are fairly applied, performance criteria proposed for the U.S. dictate monitoring technologies capable of detecting small leaks of no more than 1% of the amount of injected carbon dioxide ([3]).

Several monitoring technologies have been developed to detect CO_2 leakage at sequestration sites, including: observation of reservoir seismic and pressure profiles; ground water chemistry monitoring; near-surface measurements of soil CO_2 fluxes, carbon isotopes and tracer compounds injected with the sequestered CO_2; and nearby atmospheric monitoring of CO_2 and tracer gases (*4-8*). However, as a CCS site may span several square kilometers, many hundreds of monitors may be needed to cover such a large area, potentially at a significant cost. Additionally, more than one type of monitoring technology may be needed at a site to ensure early detection and allow quantitative estimation of leakage rates. Operators could incur high costs or risk non-detection if such monitoring networks are designed poorly. Methodologies are thus needed that can utilize site-specific information to design efficient networks with high probabilities of leak detection, but also with low false positive rates. Furthermore, an effective design methodology should be able to consider the application of multiple monitoring technologies at a site.

This paper provides a probabilistic methodology for assessing the performance of a monitoring network, using characterizations of leak occurrence, CO_2 transport and flux in the subsurface, and statistical attribution of changes in monitored values that could be induced by these fluxes. While the methodology is introduced in this paper for a single type of measurement, the general approach is broadly applicable and subsequent applications will demonstrate the combination of leak inferences and designs for systems that deploy multiple measurement technologies. The specific objective of the proposed methodology is to estimate the probability that a monitoring network will detect CO_2 leakage rates of a given size. The methodology is illustrated for a CO_2 surface flux

monitoring network in which measurements of CO_2 flux (or "seepage") rates are taken at fixed locations at a site using a chamber accumulation method or similar technique (*7, 9-11*). Background (pre-injection) monitoring at the site is used to determine critical threshold values for leak detection and ongoing (post-injection) monitoring is used for presumptive leak inference. A presumptive leak is inferred when the measured flux rate at a monitor exceeds a critical threshold value, determined to occur with low probability under the background (no-leak) condition. The statistical approach for leak inference is thus similar in concept to that used for groundwater leak detection at waste sites (*12-15*).

To evaluate the relationship between leakage events and possible incremental fluxes, a subsurface simulation model, TOUGH2 (*16*), is applied under a range of scenarios for the leakage rate, leakage location (relative to monitors), and subsurface conditions of interest (in particular, permeability). The TOUGH2 model is able to simulate multiphase, multicomponent fluid flow through porous media, allows for flexible representation of physical processes and site hydrogeology (*17*), and has been applied to simulate near surface CO_2 seepage in a number of recent studies (*18-20*). Other recent studies have considered the risk of transport from a sequestration reservoir to the surface through fissures, wells, and other subsurface features (*21*). Here we consider the transport and detection of such a leakage event only after it has reached the near-surface vadose zone. However, the general methodology is applicable to leak detection at any stage in the post-injection process using any technology where a leakage signal must be distinguished from background variability (*22*).

3.2   Methodology

The approach is first presented in a general manner, followed by idealizations to facilitate demonstration of the overall methodology. These idealizations include the assumption of a spatially homogeneous (though temporally varying) distribution of background CO_2 flux rates; a uniform leakage occurrence probability across the site; isotropic, homogeneous subsurface properties resulting in a radially symmetric spatial profile of CO_2 flux around a leakage point; and leakage flux detection occurring (or missed) only at the monitor closest to the point of leakage. These assumptions allow for a number of computational simplifications, including the substitution of the TOUGH2 model flux profile results with a nonparametric response surface for flux vs. distance. These simplifications allow a full illustration of the conceptual methodology, setting the foundation for subsequent applications requiring additional data to characterize site heterogeneity and greater computational resources to model the subsurface transport of potential CO_2 leakage plumes.

While a highly idealized site model is assumed, the parameters of the model are chosen to roughly correspond to conditions found at the Zero Emission Research and Technology Center's (ZERT) testing field site at Bozeman, Montana. The ZERT site is a collaborative research effort designed to advance scientific understanding of site hydrogeology, injection, potential leakage, monitoring, and modeling dimensions of geologic CO_2 sequestration sites (http://www.montana.edu/zert/). ZERT conditions and data are used to characterize the background CO_2 flux rates and to prescribe the range of leakage rates and soil permeability considered in demonstrating the methodology.

3.2.1 General framework for leak detection

Consider a leakage event releasing CO_2 to the subsurface above a sequestration reservoir at source location s, at steady leakage rate L_s [M/T]. This leakage is assumed to result in a steady seepage flux rate at surface monitoring location m, of S_m [M/L^2-T]. The first step is to determine the functional relationship (FR) between S_m and L_s:

$$S_m = FR(L_s, s, m) \tag{1}$$

This can be generally accomplished through use of a subsurface fate and transport model, such as TOUGH2, applied to a fully specified sequestration site. Leaks of size L_s are simulated with the model at location s and the seepage rate S_m is computed at location m. The model may be as complex as needed to accurately capture the source-receptor relationship, e.g., including multiple layers of varying thickness and permeability. However, when a complex heterogeneous system is assumed, all combinations of possible source points s and monitoring locations m must be simulated, creating a very high computational demand.

In this first demonstration of the methodology, we assume a homogeneous, isotropic subsurface, resulting in a radially symmetric functional relationship (RSFR):

$$S_m = RSFR(L_s, \phi, r_{s,m}) \tag{2}$$

where ϕ is a vector of subsurface properties input to the fate and transport model (in this case, permeability) and $r_{s,m}$ is the radial distance from source point s to monitoring location m.

The steady seepage from the leakage event is assumed to be superimposed on the naturally occurring CO_2 respiration rate at the monitoring location, Y_m [M/L^2-T], to yield a total flux X_m [M/L^2-T]:

$$X_m \;=\; Y_m \;+\; S_m \qquad\qquad\qquad (3)$$

The monitoring device measures X_m and an inference is drawn regarding the potential presence of a leak at the site. If X_m equals or exceeds a critical threshold value β_m, then a presumptive leak is inferred. Otherwise, no leak is implied. The threshold β_m is chosen so that there is a very small probability that it will be exceeded under the (no-leak) condition of natural variability (the exceedance probability chosen for the threshold corresponds to the false positive rate for an individual measurement). In practice, β_m could vary with time (e.g., seasonally), location at the site, and site conditions, such as soil temperature and moisture. In Yang et al. (*23*) we develop Bayesian statistical models to relate natural CO_2 surface flux to soil temperature, and upper prediction intervals from these models are employed here to illustrate the methodology. A single threshold is assumed to apply at all locations at the idealized site.

With this formulation, the probability of detecting a leak of size L_s at monitoring location m is the probability that the total flux that results, X_m, is above the detection threshold β_m. This probability, $P[D_m | S_m = FR(L_s,s,m)]$ is given by:

$$P[D_m | S_m = FR(L_s, s, m)] \quad = \quad P[X_m \geq \beta_m]$$

$$= \quad P[Y_m + S_m \geq \beta_m]$$

$$= \quad P[Y_m \geq (\beta_m - S_m)]$$

$$= \quad 1 - P[Y_m < (\beta_m - S_m)]$$

$$= \quad 1 - F_{Ym}(\beta_m - S_m) \qquad\qquad (4)$$

where $F_{Ym}( )$ is the cumulative distribution function (cdf) of the naturally occurring CO_2 flux rate. The problem is thus reduced to one of computing the functional relationship between S_m and L_s, specifying the probability distribution of naturally occurring measured CO_2 flux at the monitoring locations, and choosing an appropriate threshold β_m. In our analysis, β_m is determined as a function of soil temperature using a relationship fit to pre-injection baseline data, then subsequently applied with soil temperature measurements taken concurrently with the CO_2 flux samples collected during detection monitoring. The detailed assumptions and simplifications needed to provide a first demonstration of the methodology are provided in the sections that follow.

3.2.2 *Distribution of background CO_2 flux rate and determination of critical value for leak detection*

A variety of statistical methods can be used to characterize background variability for carbon sequestration sites. For example, Cortis et al. (*24*) apply artificial neural networks (ANN) to model background CO_2 surface concentrations. To demonstrate our methodology, a Bayesian statistical method is used to fit a soil temperature-CO_2 flux relationship and calculate upper prediction intervals for measured values (*23*). The fitted posterior distribution of model parameters and the resulting predictive distribution for individual measurements reflect the high variability and uncertainty of natural background soil CO_2 fluxes typically encountered at sites. The upper prediction interval for the natural flux provides a rational basis for selecting the leak detection threshold and facilitates the subsequent analysis of the probability that the monitoring threshold will be exceeded, with and without incremental flux from the occurrence of a leak.

Natural background soil CO_2 flux rates (Y_m, $\mu mol/m^2$-s) are characterized using empirical regression models to predict the probability distribution function of Y_m at a site as a function of the soil temperature, T (^{o}C). In Yang et al. (*23*) several Bayesian hierarchical regression models were built and tested using soil CO_2 flux measurements obtained from the nine largest sites in the Ameriflux database (*25*). Among the four empirical models considered, a square root-quadratic relationship with soil temperature was found to provide the best goodness of fit and the most stable estimates for the upper prediction intervals (needed to determine β_m). In this study new temperature-flux data were obtained from the ZERT site. Using a model selection procedure that considers the tradeoff between model complexity and prediction errors (see Appendix B), a simpler

square root-linear relationship was found to provide the best fit for these data. The square-root linear relationship is assumed to apply at all locations *m* at the site, with the background CO_2 flux rate given by:

$$[Y_m]^{1/2} = a + bT + \varepsilon \tag{5}$$

where *a*, *b*, and c are fitted constants and ε is an error term, normally distributed with mean zero and variance σ_ε^2. As described in Yang et al. (*23*), Equation 5 is estimated using Markov Chain Monte Carlo (MCMC) simulation. Each sample in the simulation provides an estimate for a, b, and σ_ε. These vectors are sampled uniformly and the predictive distribution of $[Y_m]^{1/2} | T$ is simulated by drawing multiple normal samples with a mean of $a + bT$ and a standard deviation of σ_ε. The empirical cumulative distribution function of the simulated predictive distribution is then evaluated to determine the upper prediction interval value, β_m, used for leak detection. For example, if the upper limit of the 99% prediction interval is desired (this upper limit corresponds to the 99.5 percentile value of the empirical distribution) and 10,000 values are simulated from the predictive distribution and ranked from smallest to biggest, then β_m is assigned the value of the 9,950[th] value in this sample.

The chamber CO_2 flux measurements at the ZERT site were collected from September 2006 – June 2007, yielding a total of 105 CO_2 flux – soil temperature measurements. Parameter estimation for Equation 5 was conducted using the MCMC procedure in WinBUGS14 (http://www.mrc-bsu.cam.ac.uk/bugs/winbugs/contents.shtml)

with three chains, each with 10,000 iterations (burn-in of 2500), and the last 7,500

iterations saved for analysis. The posterior parameter estimates are summarized in Table

3.1, including the parameter medians, standard deviations, 95% probability intervals, and

correlation coefficients. Figure 3.1 presents the resulting 99% prediction interval for CO_2

flux as a function of soil temperature.   As shown, the upper prediction interval (99.5%

estimate) does appear to provide a reasonable envelope for the natural, pre-injection

conditions, with only one of the 105 observations above the threshold. This upper

prediction interval is used for the leak detection threshold, β_m, in the analysis that

follows.

Table 3. 1   MCMC posterior estimates for parameters in square root linear model (Eq. 5) for ZERT site (n = 105). Based on MCMC sample size of 7,500

A. Posterior parameter estimates

	a	b	σ_ε
Median	0.21	0.0855	0.545
Std. Dev.	0.220	0.00967	0.0388
95% Interval	(-0.219, 0.635)	(0.0668, 0.105)	(0.478, 0.629)

B.

X. Posterior parameter correlations

Parameters	ρ
a, b	-0.969
a, σ_ε	0.00678
b, σ_ε	-0.00507
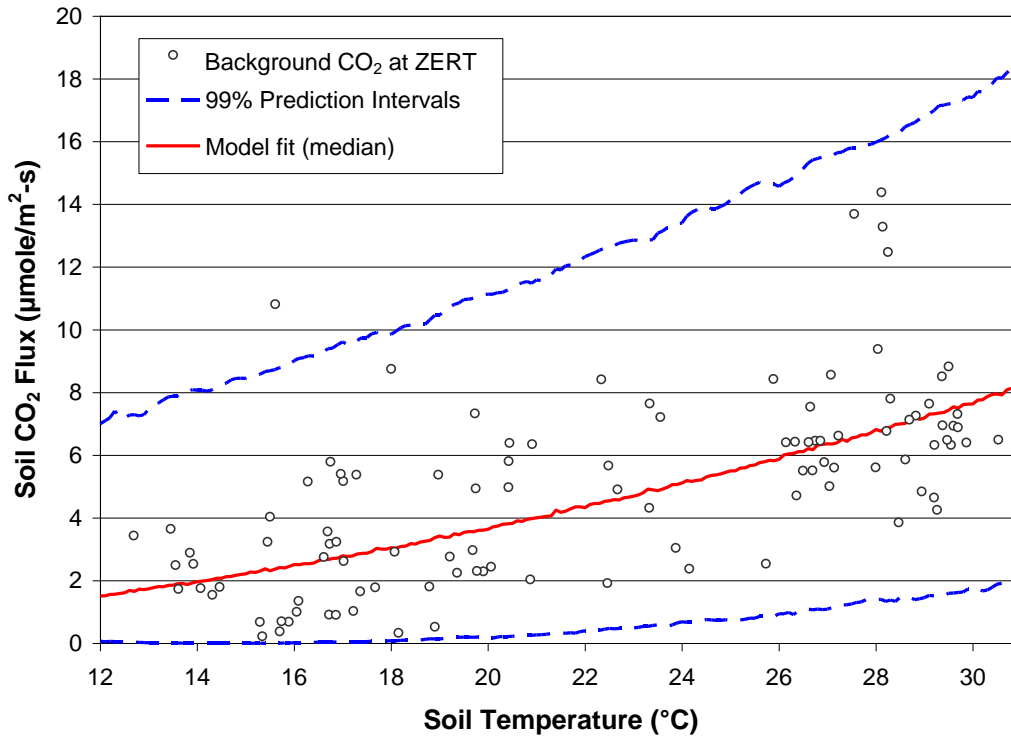
Figure 3. 1 CO_2 flux vs. soil temperature relationship fit for ZERT site.   The 99% prediction intervals are shown for square root linear model (0.5% and 99.5% values) along with observed ZERT site data.

3.2.3   *Simulation of seepage rate profile from a leakage event*

In order to produce a simulated data base for the spatial distribution of CO_2 seepage flux around a point source, the TOUGH2 code with the EOS7CA module was used. This module is capable of including water, air, and CO_2, making it suitable for simulating two-phase flow in the vadose zone. For the sake of selecting a reference setting, conditions similar to those at the ZERT test site are assumed (*10*), though simplifications are made consistent with the goal of demonstrating the methodology for an idealized site.

Similar to the ZERT field tests, our base case includes a CO_2 leakage source 2.45 m below the soil surface with a leakage rate of 1.93×10^{-4} kg/s (16.67 kg/day). Unlike

the ZERT field tests which included multiple leakage points along a pipe, our simulations

represent only a single point source, since the aim of this study is to quantify the

likelihood of detection as a function of distance from a source. The topsoil in the domain

is assumed to be a 1.2 m thick silty soil with high capillary retention properties. The

lower 8.8 m of the domain is a cobble-type layer with very low capillary retention. To

mimic the presence of the atmosphere above the domain, a hypothetical soil layer is

added with a porosity of 0.99, high relative permeability and no capillary retention. The

total flux rate from the soil to the atmosphere is computed as the sum of the computed

fluxes due to diffusion and convection into this atmospheric layer. Please see Figure 3.2

below for the physical scenario with an example CO_2 plume given 1.93 x 10^{-7} kg/s

leakage rete, 1mD permeability and 1.35 vadose zone thickness.
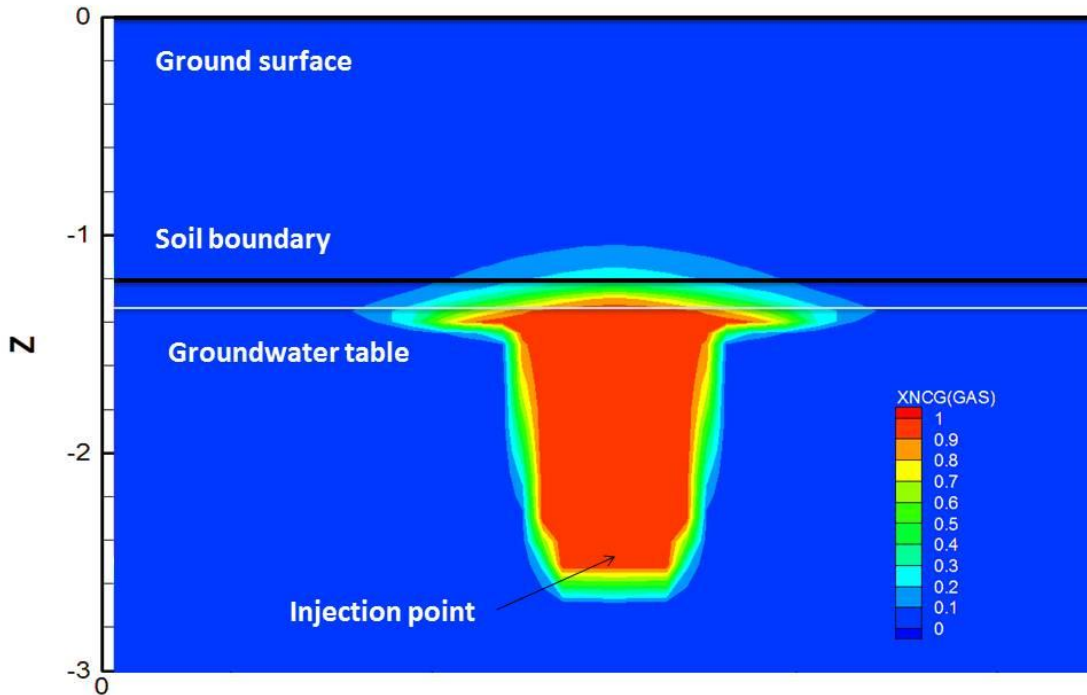
Figure 3. 2 Example CO$_2$ seepage simulation by TOUGH2 for leakage rate L1 = 1.93 x 10^{-7} kg/s, permeability P1=0.001 Darcy and vadose zone thickness = 1.35m.

The leakage event is simulated for 50 days, and the resulting seepage distribution as a function of radius is computed. In order to populate the data base for the response surface model, three parametric studies were performed. First, the topsoil permeability was modeled with seven different values varying from 1 mD to 1000 D, by factors of 10. Second, the leakage rate was varied over the range from 1.93 x 10^{-7} to 1.93 x 10^{-1} kg/s, again by factors of 10. The four extreme cases with combinations of the highest and lowest permeabilities and leakage rates were also evaluated. Overall, a total of 17 cases

were simulated using a main effects centered statistical design to fit the response surface relationships.

3.2.4 *Nonparametric response surface modeling of TOUGH2 simulations*

While each of the 17 initial TOUGH2 simulations were conducted for particular values of the leakage rate and permeability we seek to estimate the key model output, CO_2 seepage rate as a function of distance from the leak, as a continuous function of leakage rate and permeability. In the subsequent analysis, this allows us to compute the leak detection probability for arbitrary (i.e., continuous) combinations of permeability and leakage rate (within the range used to generate the TOUGH2 simulations). This is accomplished using a nonparametric cubic spline function (*26*) to determine the seepage rate S_r as a function of distance r for each of the 17 TOUGH2 model simulations with specified permeability and leakage rate, then applying 2D kriging at a given r to interpolate estimates of S_r for other (unmodeled) values of the leakage rate and permeability. An intermediate vadose zone thickness of 1.35 m is assumed in this analysis.

Figure 3.3 shows the CO_2 seepage rate as a function of distance (r, in meters) from the point of leakage, for the intermediate case permeability = 1 Darcy, for each of the leakage rates tested, ranging from 1.93 x 10^{-7} kg/s (L1) to 1.93 x 10^{-1} kg/s (L7). Figure 3.3 is a similar plot, showing the effect of varying permeability, while keeping the leakage rate at the intermediate value, L4 = 1.93 x 10^{-4} kg/s. In both figures, the original TOUGH2 results are shown as points and the fitted spline curves are shown as solid lines.

Figure 3.3 indicates a monotonically increasing response in the seepage rate as the leakage rate increases, as would be expected. Figure 3.4 indicates somewhat more complex behavior as the permeability changes with a fixed leakage rate. At low permeability, the seepage rate vs. distance profiles are relatively flat, yielding lower seepage rates near the source of the leakage, but higher seepage rates (relative to the high permeability cases) at larger distances. The high permeability cases yield very high seepage rates near the source, but the zone of influence is limited to a smaller distance of ~8 meters or less. For Figure 3.3 it is found that the increase of leakage rate increases the diffusion flux of the seepage, but for Figure 3.4 the diffusion fluxes keep similar values in all cases as the permeability increases. The advection part of the seepage only increases monotonically as the leakage rate increases. For the permeability study, the advection part of the seepage also increases with permeability until around 100D (P6 case), and the advection part in the P7 case drops back to the magnitude similar to that in the P4 case.

Figures 3.3 and 3.4 demonstrate that the spline function for seepage rate as a function of distance is able to provide an excellent representation of the original TOUGH2 results. To validate the ability of the 2-D kriging prediction for other values of permeability and leakage rate, a cross-validation is performed (see Appendix C). The cross-validations indicate a very good correspondence between the TOUGH2 simulation results and the values estimated by the combined spline-kriging interpolation method. For a given leakage rate and permeability this algorithm is used in subsequent analysis to estimate the seepage rate, S_m, at a distance $r_{m,s}$ from the point of leakage.
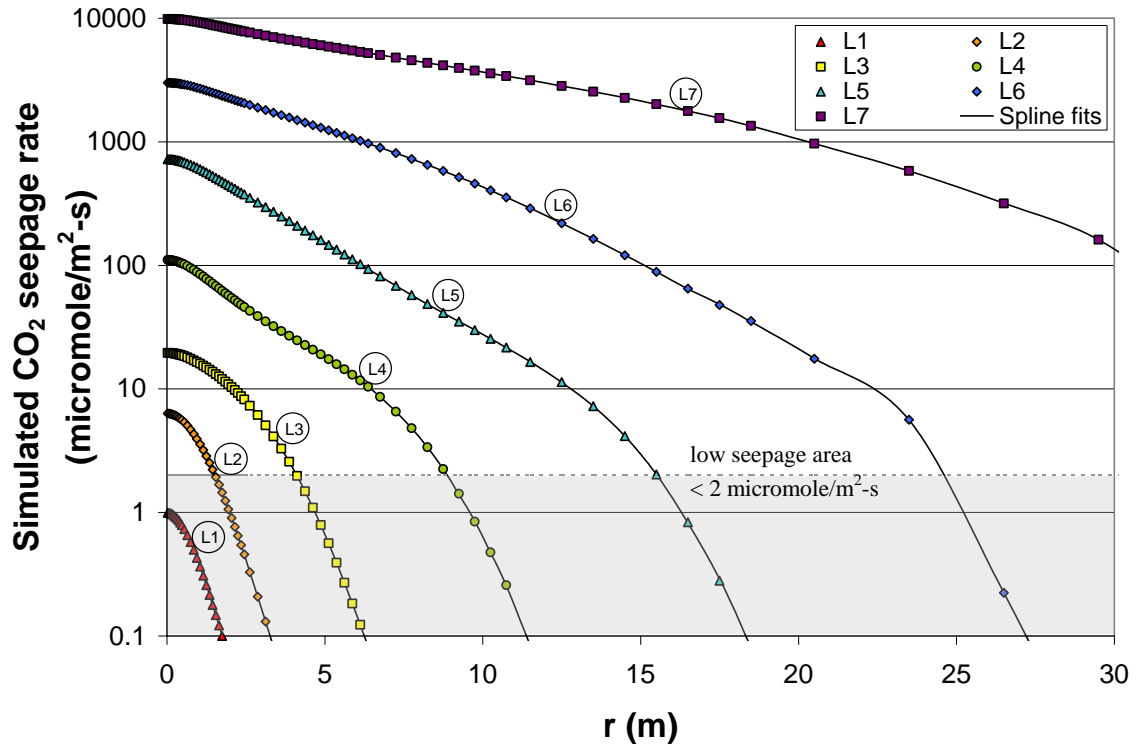
Figure 3. 3   Simulated CO$_2$ seepage rates for different leakage rates, ranging from L1 = 1.93 x 10^{-7} kg/s to L7 = 1.93 x 10^{-1} kg/s, by factors of 10.   For all cases, permeability = 1 Darcy, vadose zone thickness = 1.35m.   Points are TOUGH2 simulation results, solid lines are fitted cubic spline prediction.   Low seepage rate area shown in grey is unlikely to be distinguished from background.
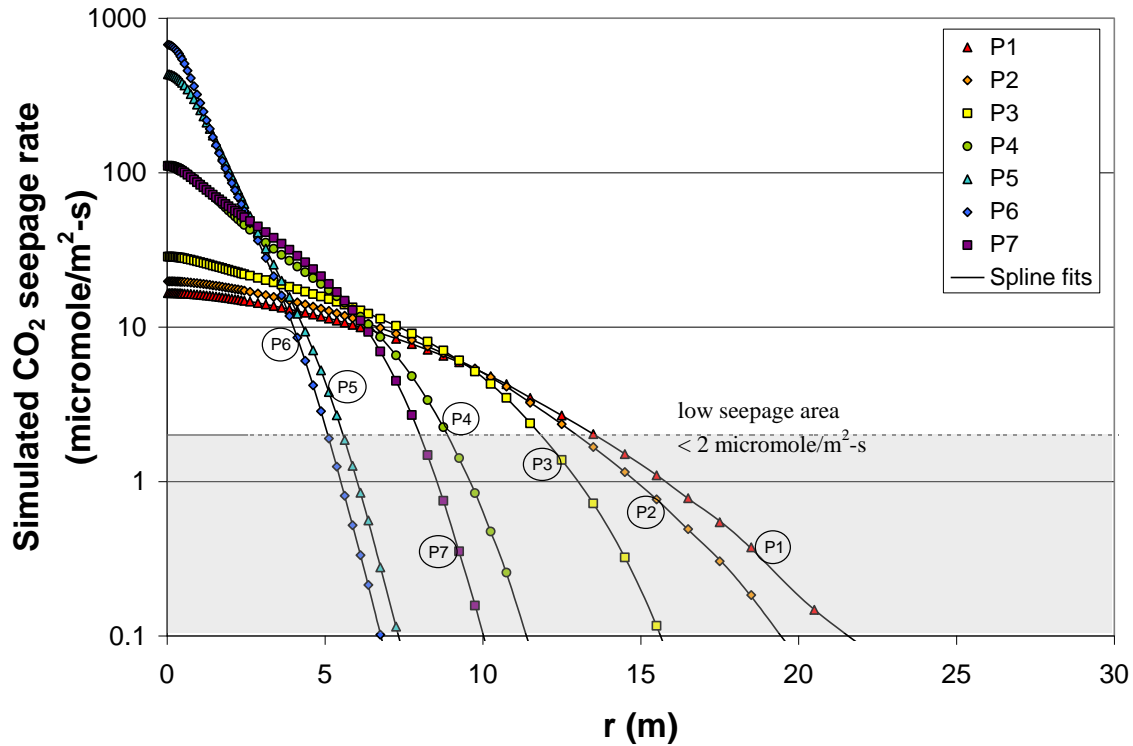
Figure 3. 4   Simulated CO_2 seepage rates for different soil permeability, ranging from P1 = 0.001 Darcy to P7=1000 Darcy, by factors of 10. For all cases, leakage rate = 1.93 x 10^{-4} kg/s, vadose zone thickness = 1.35m. Points are TOUGH2 simulation results, solid lines are fitted cubic spline prediction. Low seepage rate area shown in grey is unlikely to be distinguished from background.

3.2.5   *Idealized site and monitoring network layout*

Calculations are made for a hypothetical homogeneous site, 1 km x 1 km. Monitoring points are placed at center points of a square grid (see Figure 3.5), with the distance between adjacent monitors ranging from d = 100 m (this is the case shown in Figure 3.5, a sparse grid with a total of n=100 monitors distributed across the site) to d = 10 m (a dense grid with n = 10,000). Leaks are assumed to occur with uniform probability across the site. The probability distribution function of the distance from a random leakage point to the nearest monitor can be calculated analytically or generated with a simple Monte Carlo routine. The latter simulates many potential leakage points

uniformly within a square domain and computes the distance from each point to its

domain center (where the monitor is located). For nonuniform leak occurrence

probabilities (e.g., where there are wells, fissures, or other features that cause leaks to be

more likely to occur at particular locations within the site), the Monte Carlo method is

readily adapted by generating proportionally more random points at these locations. The

Monte Carlo method is used here with a sample size of 10^6, yielding the distribution

functions for the distance to the nearest monitor shown in Figure 3.6. These distributions

are sampled randomly to determine the distance $r_{m,s}$ for use in the spline functions used to

calculate S_m in Eq. 4.
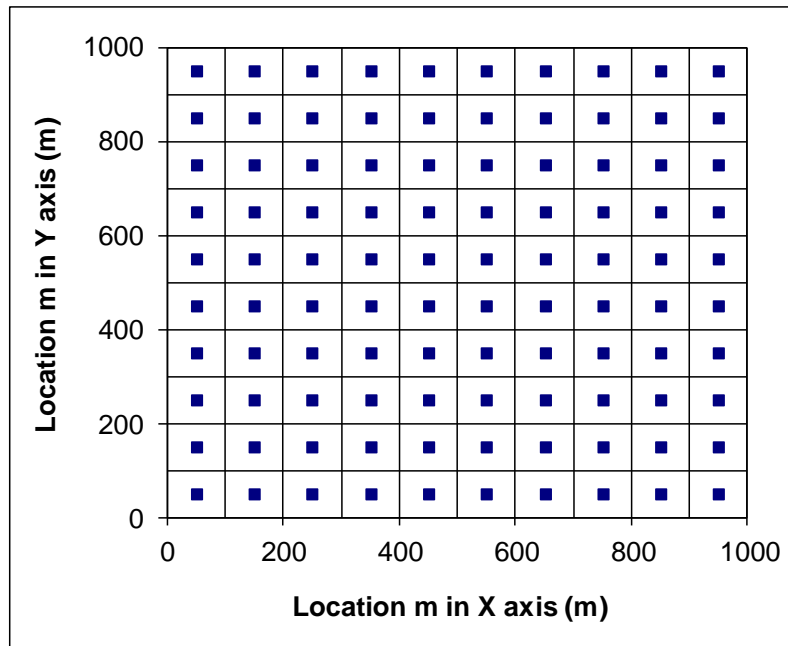
Figure 3. 5   Idealized site with homogeneously distributed monitoring points (distance between monitors, d=100 m). Each monitoring point is located at the center of the square defining its domain for calculating the distance to the nearest monitor.
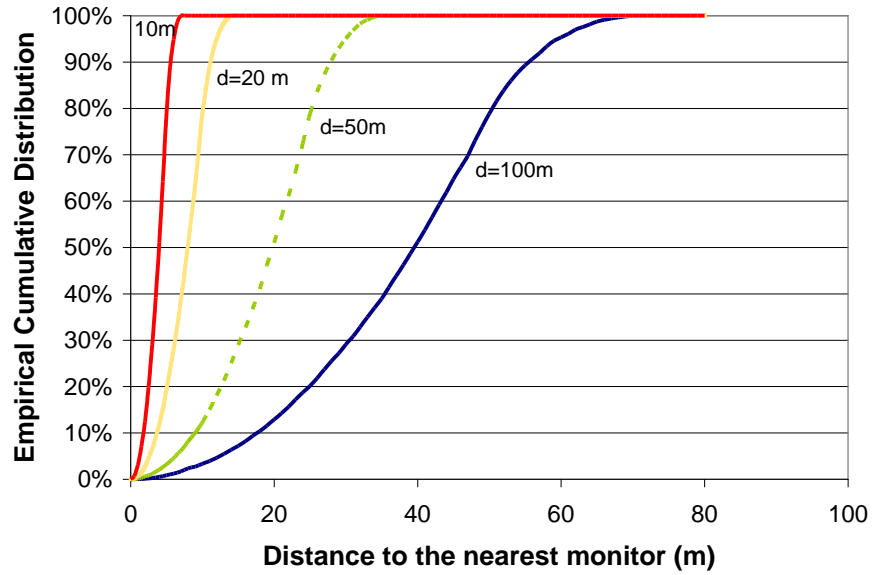
Figure 3. 6 **Empirical cumulative distribution of the distance to the nearest monitor for a random leak location in a square grid monitoring network (results shown for networks with distance between monitors ranging from d = 10m to d = 100m).**

3.2.6 Computing the probability of seepage detection and the probability of leakage detection

The probability of detection for a given size leak, L_s, occurring randomly (in this case uniformly) across the site is computed with the following steps.

    i. For the given monitoring density, randomly select a distance to the nearest monitor, r_{nm}, from the appropriate empirical distribution shown in Figure 3.6.

    ii. For the given leakage rate (L_s) and subsurface properties (ϕ = permeability in this case), determine the seepage rate at distance r_{nm} by evaluating the radially symmetric functional relationship in Equation 2: $S_m = RSFR\left(L_s, \phi, r_{s,m}\right)$,

with $r_{s,m} \leftarrow r_{nm}$. This evaluation is made using the cubic spline – kriging

estimates determined as a function of L_s and permeability.

iii. Given S_m, the leak detection threshold β_m, and the soil temperature T, evaluate

Equation 4 to determine the probability of detection $P[D_m| S_m]$, that is, the

probability that the background seepage rate plus the leak-induced seepage rate

$(X_m = Y_m + S_m)$ exceeds the leak detection threshold β_m. This calculation is

made using the same predictive distribution of $Y_m|T$ simulated in Section 2 to

estimate the threshold β_m, except in this case we determine what fraction of this

sample is greater than β_m - S_m.

iv. Repeat steps i. through iii. for different values of r_{nm}, sampled from the

simulated distribution of distance to the nearest monitor for the given

monitoring density.   Then average the values of $P[D_m| L_s]$ computed for each to

determine the overall probability of detection for a randomly located leak of

size L_s at the site.

3.3   Results

The methodology is demonstrated for the range of leakage rates, site conditions,

and monitoring densities described above. A soil temperature of $T = 15$ °C is assumed,

resulting in a detection threshold of $\beta_m \approx 8.5$ μmole/m^2-s for the CO_2 seepage rate

(computed from Equation 5, see also Figure 3.1). Equation 4 is then evaluated to

determine the probability of detection at a monitor as a function of the seepage rate.

The result, $P[D_m| S_m]$, is shown in Figure 3.7. Comparing Figure 3.7 to Figure 3.1, it is not surprising that the probability of detection begins to increase measurably at seepage rates S_m between 1 and 2 μmole/m^2-s, approaching nearly 1.0 (nearly assured detection) as S_m increases from 8 to 9 μmole m^{-2}s^{-1}.
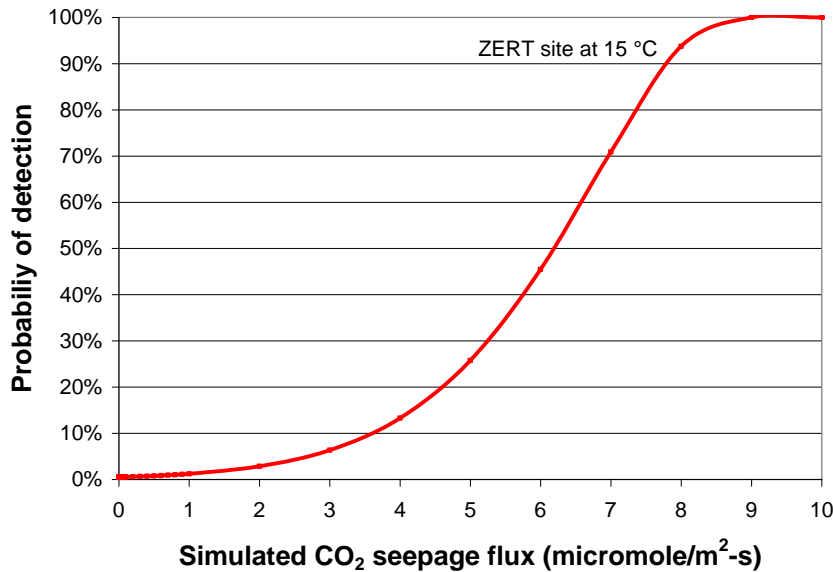
Figure 3. 7   Probability of detection at ZERT site for different leak-related seepage rates, for soil temperature $T = 15°C$.

Equation 4 is evaluated multiple times (for a given leakage rate and permeability) using seepage fluxes corresponding to randomly sampled values of the distance to the nearest monitor (calculated from the TOUGH2 response surface). The computed probabilities of detection are then averaged across the sampled distances to compute the overall probability of detection for a randomly located leak event. Figures 3.8a, b and c illustrate the results for the idealized ZERT site given permeabilities of 0.01, 1 and 100 Darcy, respectively, with soil temperature T = 15°C, vadose zone thickness = 1.35 m and monitoring densities ranging from d=100 to 10m.

The principal inferences that can be drawn from Figure 3.8 include:

- As expected, the probability of detection increases with increasing leakage rate.

- Transitions from low to high detection probability as a function of leakage rate tend to occur more rapidly in high-density networks.

- Transitioning from low (d = 100m) to high density (d = 10m) networks results in very large increases in the probability of detection for all values of permeability considered. This reflects the relatively small radius of influence associated with a point source released near the surface.

- Permeability affects detection probability in a more complex, non-monotonic manner, depending upon the monitoring network density:

  o For the dense network (d = 10 m), moving from the low permeability case in Figure 3.8a (corresponding to P2 in Figure 3.4) to the intermediate permeability case in Figure 3.8b (corresponding to P4 in Figure 3.4), results in an increase in detection probability, since seepage rates for the latter increase to high, easily detectable values over most of the range from $r = 0$ - 7 meters (these inferences are limited to cases with intermediate to high leakage rates that are potentially detectable). Further increases in near-source seepage rates do occur at high permeability (P6 in Figure 3.4), however these are limited to the range from 0-3 meters (where seepage rates are already high enough to yield a high probability of detection for the intermediate permeability case) and are associated with a sharp drop-off in the seepage rate beyond three meters. As a result,

moving from the intermediate permeability case in Figure 3.8b to the high

permeability case in Figure 3.8c for the dense network (d = 10 m) results

in an overall decrease in the probability of detection.

o   In contrast, for a sparse network (d = 100m) increases in permeability lead

to decreases in detection probability throughout, since the upward

channeling and reduction in the horizontal extent of the plume they induce

preclude the occurrence of increased seepage rates at the greater distances

where monitoring locations are now more likely to be located.

Of particular interest for network design is the monitoring density necessary to

achieve a high probability of leak detection for a leakage rate large enough to cause

safety, economic, and/or regulatory concerns. Assume a site where 1 million

tonnes of CO_2 per year (1 Mt CO_2/yr) has been injected for the first 10 years (*27*) , with a

design lifetime of 100 years. If 1% of the total injected CO_2 is lost over the 100 year

period (essentially equivalent to the 0.01% annual seepage rate proposed as a cap by

Hepple et al., 2004 (*28*)), this scenario corresponds to a maximum leakage rate of 0.0336

kg/s (or $10^{-1.47}$ kg/s). Assume further that a probability of leak detection of 90% is

sought. For the intermediate permeability case in Figure 3.8b, this is achieved with a

monitoring density between d=50 and d=20m (assuming the 0.0336 kg/s leakage rate

occurs at a single point). However, leakage could also occur in a distributed manner

across multiple point locations, such as wells and features. For example, with a well

density of 1 per km^2 (within the range of 0.01- 20 wells per km^2 reported in recent studies

(*23, 29, 30*)), and a distributed CO_2 footprint of 100 km^2 (*28*), the leakage event would be

distributed among 100 wells, requiring a 100-fold reduction in the leakage rate targeted

for detection, i.e., 3.36×10^{-4} kg/s (or $10^{-3.47}$ kg/s). Again for the intermediate permeability

case in Figure 3.8b, with a goal of detecting leakage with a probability of 90%, a higher

monitoring density with d=10m is now required.
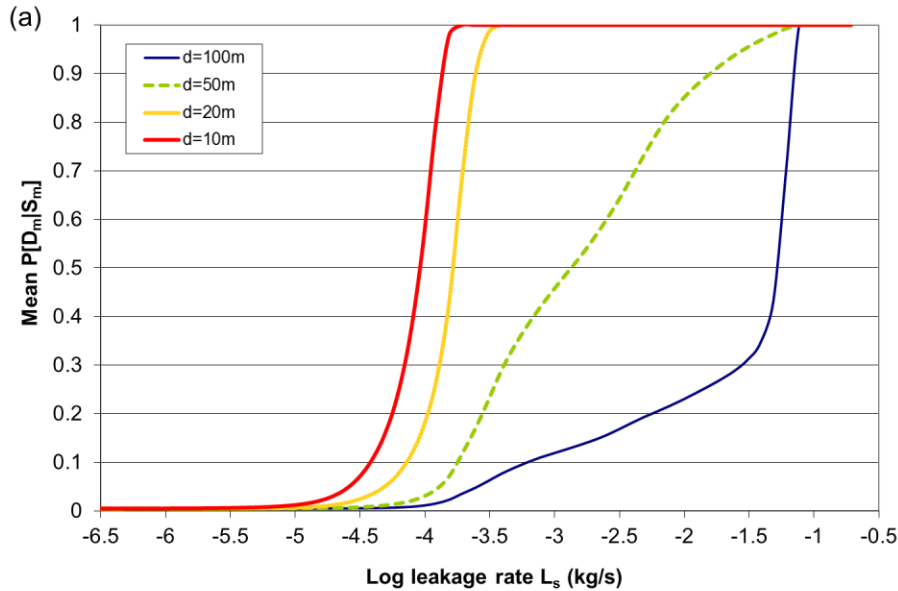
Figure 3. 8(a)   Probability of detection as a function of CO$_2$ leakage rate for different density monitoring networks, ranging from sparse (d = 100m between monitors) to dense (d = 10m between monitors) given low permeability = 0.01 Darcy, and vadose zone thickness = 1.35m. Leakage rate shown as base 10 logarithm.

(b)
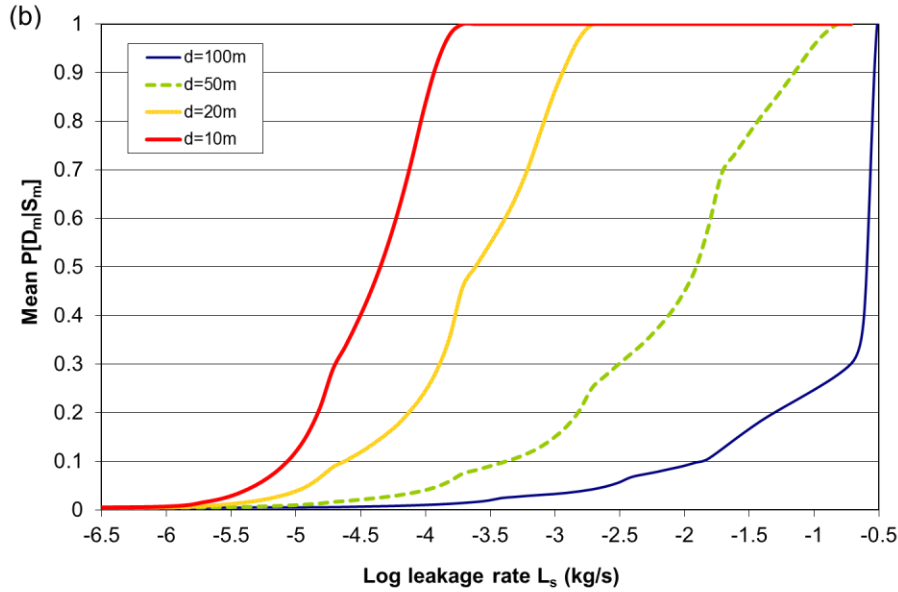
Figure 3. 9 (b)   Probability of detection as a function of CO$_2$ leakage rate for different density monitoring networks, ranging from sparse (d = 100m between monitors) to dense (d = 10m between monitors) given intermediate permeability = 1 Darcy, and vadose zone thickness = 1.35m. Leakage rate shown as base 10 logarithm.

(c)
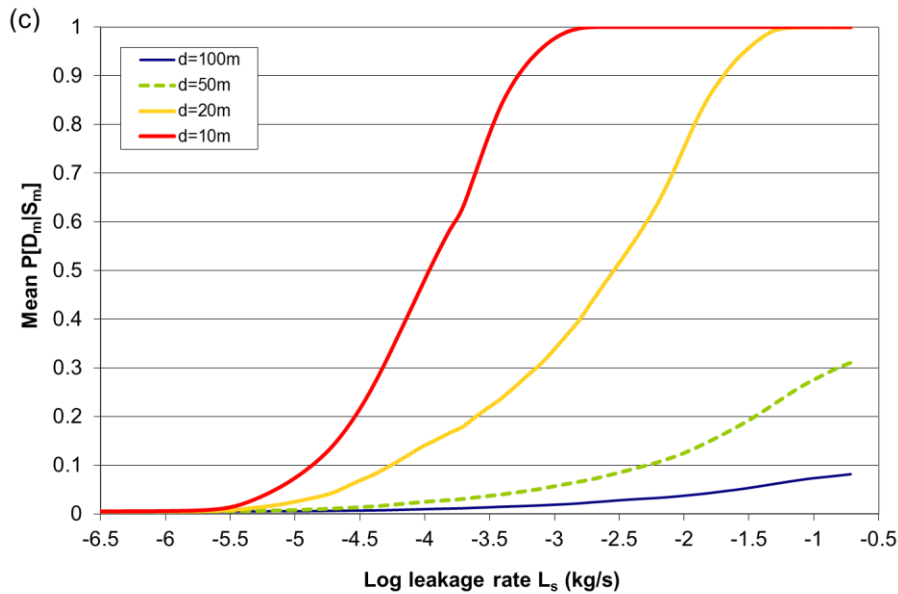
Figure 3. 10 (c)   Probability of detection as a function of CO$_2$ leakage rate for different density monitoring networks, ranging from sparse (d = 100m between monitors) to dense (d = 10m between monitors) given high permeability = 100 Darcy, and vadose zone thickness = 1.35m. Leakage rate shown as base 10 logarithm.

3.4   Discussion

The results presented above provide useful initial insights on monitoring network performance and the factors that affect it. Even for the idealized site considered, nonlinear/non-monotonic relationships are apparent between site conditions, monitoring design (density), and the resulting detection probability. These effects are likely to be even more pronounced when the method is applied to actual site conditions with potential releases from deep formations; complex non-homogeneous site geology; facilitated transport through fissures, wells, and zones of high permeability; and spatial variation in pre-injection soil respiration rates. The purpose of this paper is to formulate and illustrate (here using multiple simplifying assumptions) the overall framework for integrating site characterization, site modeling, and monitoring device and network specification, to compute the likely performance of a network. Application to actual sites will require more detailed site characterization data and modeling tools for estimating the relationships between leakage events and monitoring results, and adaptation of the methodology will be required to address these complexities. For example, methods will be needed to account for partial (imperfect) knowledge of more-likely leak locations and the need for denser monitoring coverage at or near these portions of the site.

For the simple cases considered here, relatively dense monitoring networks with distances between monitors ranging from 10 to 20 meters were required to assure a high probability of detection at leakage rates likely to be of concern. At even a small 1 km square site, this corresponds to be between 2500 and 10,000 surface flux monitoring points. This is clearly impractical from both an administrative and an economic

perspective. Furthermore, with such a large number of monitors, the risk of a false positive is substantial.

As such, surface soil CO_2 flux measurement is unlikely to be feasible as a stand-alone technology for leak detection. Rather, it will most likely be applied in high risk locations, such as areas around wells and features, during the injection and post-injection period. As now recognized, a mix of complementary technologies targeting signals from potential leaks at different locations and in different ways, will be needed to allow for practical and affordable designs that achieve high levels of assurance (*10, 24, 31*). The methods proposed here for computing detection probabilities are generally applicable, and our ongoing research considers the joint deployment of technologies targeting both deep and near-surface leakage signals.

Acknowledgements

References

(1) U.S. Environmental Protection Agency. *Inventory of U.S. Greenhouse Gas Emissions and Sinks: 1990-2007*. EPA 430-R-09-004; EPA: Washington, DC, 2009.

(2) U.S. Energy Information Administration, Independent Statistics and Analysis. *International Energy Outlook 2009*. DOE/EIA-0484(2009); EIA: Washington, DC, 2009.

(3) U.S. Department of Energy, National Energy Technology Laboratory. *Carbon Sequestration Technology Roadmap*. DOE: Washington, DC, 2007.

(4) Oldenburg, C. M.; Lewicki, J. L.; Hepple, R. P. *Near-surface monitoring strategies for carbon dioxide storage verification*. Lawrence Berkeley National Laboratory Report LBNL-54089, 2003.

(5) Benson, S. M. Monitoring Geological Storage of Carbon Dioxide, In *Carbon capture and sequestration: Integrating technology, monitoring, and regulation*; Wilson, E.J., Gerard, D., Eds.; Blackwell Scientific Publishing, Ames, Iowa, 2007; pp 73-100.

(6) Leuning R.; Etheridge, D.; Luhar, A.; Dunse, B. Atmospheric monitoring and verification technologies for CO_2 geosequestration. *Int J Greenh Gas Con*. **2008**, 2(3), 401–414.

(7) Strazisar, B. R.; Wells A.W.; Diehl, J. R.; Hammack, R.W.; Veloski, G. A. Near-surface monitoring for the ZERT shallow CO_2 injection. *Int J Greenh Gas Con*. **2009**, 3(6), 736-744.

(8) Johnson, G.; Raistrick, M.; Mayer, B.; Shevalier, M.; Taylor, S.; Nightingale, M.; Hutcheon, I. The use of stable isotope measurements for monitoring and verification of CO_2 storage. *Energy Procedia*. 2009, 1(1), 2315-2322.

(9) Chiodini, G.; Cioni, G. R.; Guidi, M.; Raco, B.; Marini L. Soil CO_2 flux measurements in volcanic and geothermal areas. *Appl Geochem*. **1998**, 13, 543–552.

(10) Lewicki, J. L.; Oldenburg C. M.; Dobeck L.; Spangler, L. Surface CO_2 leakage during two shallow subsurface CO_2 releases. *Geophys Res Lett*. **2007**, 34, L24402.

(11) Oldenburg C. M.; Lewicki, J. L.; Dobeck L.; Spangler, L. Modeling gas transport in the shallow subsurface during the ZERT CO_2 release test. *Transp Porous Med*. **2010**, 82(1), p. 77-92.

(12) Gibbons, R. D. Statistical prediction intervals for the evaluation of ground water quality. *Ground Water*. **1987**, 25(4), 455–465.

(13) Small, M.J. Groundwater detection monitoring using combined information from multiple constituents. *Water Resour Res*. 1997, 33(5), 957-969.

(14) Gibbons, R. D.; Coleman, D. E. *Statistical Methods for Detection and Quantification of Environmental Contamination*; John Wiley & Sons: New York, 2001.

(15) U.S. Environmental Protection Agency, Office of Resource Conservation and Recovery. *Statistical Analysis of Groundwater Monitoring Data at RCRA Facilities - Unified Guidance*. EPA 530-R-09-007; EPA: Washington, DC, 2009.

(16) Pruess, K.; Oldenburg, C.; Moridis, G. *TOUGH2 User's Guide, Version 2.0*, Lawrence Berkeley National Laboratory Technical Report No. LBL-43134, 1999.

(17) Finsterle, S.; Doughty, C.; Kowalsky, M. B.; Moridis, G. J.; Pan, L.; Xu, T.; Zhang, Y.; Pruess, K. Advanced vadose zone simulations using TOUGH. *Vadose Zone Journal*. **2008**, 7, 601–609.

(18) Oldenburg, C.M.; Unger, A.J.A. Coupled vadose zone and atmospheric surface-layer transport of CO_2 from geologic carbon sequestration sites. *Vadose Zone Journal*. **2004**, Vol. 3, 848-857.

(19) Lewicki, J. L.; Hilley, G. E.; Fischer, M. L.; Pan, L.; Oldenburg, C. M.; Dobeck, L.; Spangler, L. Eddy covariance observations of surface leakage during shallow subsurface CO_2 releases. *J. Geophys. Res.* **2009**, 114, D12302.

(20) Ogretim, E.; Gray, D. D.; Bromhal, G. S. Effects of crosswind-topography interaction on the near-surface migration of a potential CO_2 leak. *Energy Procedia*. **2009**, 1(1), 2341-2348.

(21) Celia, M. A.; Nordbotten, J. M.; Bachu, S.; Dobossy, M.; Court, B. Risk of leakage versus depth of injection in geological storage. In *Proceedings of the GHGT−9 Conference*, Washington, DC, November 2008.

(22) Cortis, A.; Oldenburg, C. M; Benson, S. M. The role of optimality in characterizing CO_2 seepage from geologic carbon sequestration sites. *Int J Greenh Gas Con*. **2008**, 2, 640–652.

(23) Yang, Y.; Small, M. J.; Junker, B. W.; Bromhal, G. S.; Strazisar B. R.; Wells A.W Bayesian hierarchical models for soil CO_2 flux and leak detection at geologic sequestration sites. *Environ. Earth Sci*. (in review).

(24) Seto, C. J.; McRae, G. J. Reducing risk in basin scale CO_2 sequestration: A framework for integrated monitoring design. *Environ. Sci. Technol*. in press.

(25) Hibbard, K. A.; Law, B. E.; Reichstein, M. An analysis of soil respiration across northern hemisphere temperate ecosystems. *Biogeochemistry*. **2005**, 73, 29–70.

(26) Durrleman, S.; Simon, R. Flexible regression models with cubic splines. *Stat. Med*. **1989**, 8, 551-561.

(27) Benson, S.M.; Hepple, R. P. Detection and options for remediation of leakage from underground CO_2 storage projects. In *Proceedings of the 7th international conference on greenhouse gas technologies*. Rubin, E. S.; Keith, D.W.; Gilboy, C. F., Eds.; Elsevier: London, 2005; pp1329-1338.

(28) Hepple, R. P.; Benson, S. M. Implications of surface seepage on the effectiveness of geologic storage of carbon dioxide as a climate change mitigation strategy: Performance requirements and the implications of surface seepage. *Environmental Geology*. **2004**, 47(4), 576-585.

(29) Nordbotten, J. M.; Celia, M. A.; Bachu, S.; Dahle, H. K. Semianalytical solution for CO_2 leakage through an abandoned well. *Environ. Sci. Technol*. **2005**, *39* (2), 602–611.

(30) Zhou, W.; Stenhouse, M. J.; Arthur, R.; Whittaker, S.; Law, D.; Chalaturnyk, R.; Jazrawi, W. The IEA Weyburn CO_2 monitoring and storage project – modelling of the long-term migration of CO_2 from Weyburn. In *Proceedings of the 7th international conference on greenhouse gas technologies*. Rubin, E. S.; Keith, D.W.; Gilboy, C. F., Eds.; Elsevier: London, 2005; pp 721-29.

(31) Benson, S. M.; Gasperikova, E.; Hoversten, G. M. Monitoring protocols and life-cycle costs for geologic storage of carbon dioxide. In *Proceedings of the 7th*

international conference on greenhouse gas technologies. Rubin, E. S.; Keith, D.W.; Gilboy, C. F., Eds.; Elsevier: London, 2005.

Chapter 4: A Bayesian Belief Network for Combining Sequestration Site Leak Detection Monitoring Results from Near-Surface CO$_2$ Fluxes and PFC Tracer Concentrations[4]

Abstract

To incorporate the use of multiple geologic sequestration monitoring techniques, a Bayesian Belief Network (BBN) for leak detection inference is applied to integrate the information provided by different techniques deployed at a site. In this study, two monitoring methods, near-surface soil CO$_2$ flux and perfluorocarbon (PFC) tracer concentration, are included in the BBN. First, possible near-surface flux rates for CO$_2$ and PFC tracer as a function of distance from a leakage point are simulated by TOUGH2, given different leakage rates and permeabilities. Then, the natural near-surface CO$_2$ flux and background PFC tracer concentration measured at the Zero Emission Research and Technology (ZERT) site are used to determine critical values for leak inference and to calculate the probabilities of leak detection given a monitoring network. A BBN of leak detection is established by combing the TOUGH2 simulations and the background characterization of near-surface CO$_2$ flux and PFC tracer at the sequestration site. The results show a positive correlation between the detection abilities of PFC tracer and soil CO$_2$ flux, but the PFC tracer is more sensitive for detecting a leak in most cases. The BBN of leak detection including both soil CO$_2$ flux and PFC tracer concentration gives an integrated probability estimation of leak detection for different permeability and leakage rates for a given monitoring network. The results show that with sufficient

---

[4] Coauthored by Mitchell J. Small, Egemen O. Ogretim, Donald D. Gray, Grant S. Bromhal, Brian R. Strazisar and Arthur W Wells and in preparation for publication.

monitoring density, PFC tracer monitoring can generally detect the leakages greater than 10^{-6} kg/s, while soil CO_2 flux measurement can effectively detect the leakage greater than 10^{-4} kg/s, based on the ZERT site condition. Considering the pros and cons of the two monitoring techniques, soil CO_2 flux measurement is recommended for regions where the large size leaks might occur, such as the area around wells and features. PFC tracer monitoring is more flexible with regard to the location of monitors due to its sensitivity to small sized leaks. A BBN developed using the proposed methodology can be used to help site engineers and decision makers to evaluate leakage signals and the risk of undetected leakage, given a suite of monitoring techniques and site conditions.

4.1 Introduction

Geologic carbon sequestration is a promising and feasible solution to the reduction of the CO_2 emission from large anthropogenic sources to the atmosphere. In order to achieve long-term storage of CO_2 successfully, minimum 99% retention of the injected CO_2 is needed in geological sequestration (*1*), or equivalently 0.01% annual seepage rate (*2*). To ensure the effectiveness of geologic carbon sequestration and to early detect the unexpected leakage, assurance monitoring is extremely important and necessary in a geologic sequestration project.

A number of monitoring techniques have been developed at some test sites (*3-10*) and have been tested and applied to several large geologic sequestration projects (*11, 12*). These monitoring techniques include (1) subsurface monitoring, like seismic methods, well fluids sampling, pressure and tiltmeter measurement; and (2) near-surface and surface monitoring such as soil gas sampling, soil CO_2 flux and atmospheric CO_2 flux

measurement, satellite remote sensing, carbon isotopes and tracers added to the sequestered CO_2. With different strengths and weaknesses for every monitoring technique, an evaluation tool is needed to integrate the information provided by different techniques deployed at a site. More importantly, an evaluation that is able to provide the assessment of possible size of a leak based on the multiple monitoring results further helps the managers and decision makers to know whether the unexpected leakage event is still smaller than the 0.01% annual seepage rate required for effective long-term storage.

Bayesian belief network (BBN) is a very useful and powerful tool for integrating the information from different components of various formats and scales in an environmental system (*13, 14*). A Bayesian belief network, a graphical model representing the probabilistic relationships between variables of interest (*15*), has several advantages in describing and modeling an environmental system. First, the system components of different forms and scales can be integrated via their probabilistic expressions in a BBN model, so a complicated system can be easily represented without the difficulties encountered in system dynamics (*16*). Second, a BBN represents the causal or evidential relationships between system components (or variables) based on experts' prior knowledge in a graphical interface, which summarizes a complex environmental system into a simpler concept (*13, 17*). Therefore, it is more intuitive and easier to gain insight from a BBN model. Third, it is readily to expend a BBN model to a decision support system with the inclusion of utility and decision options (*14*). Moreover, it provides the uncertainty estimation for each system component due to its probabilistic formulation and shows how the uncertainty of each component affects the predictions or the decisions possibly made (*13, 15*). Thus, it helps decision makers see

79

the effect of each component systematically. Finally, a BBN model is an excellent

approach combing prior knowledge from experts' belief or historical records and the data

from experiments in system modeling. However, the prior and conditional probability

estimations for each variable usually require a lot of work since these values are obtained

from data, expert elicitations or simulations of other models (*14, 18*), and sometimes

these values are hard to estimated.

Many applications of BBN can be found in the field of environmental and natural

resource management since 1990s. Most of the studies are found in the water resource

management area. For example, an overview of BBN with some case studies from water

resource management and fisheries was made by Varis and Kuikka (*19*); Borsuk et al.

(*11*) developed a very comprehensive BBN for eutrophication problem; Castelletti and

Soncini-Sessa (*14*) thoroughly studied the application of BBN to water research

management and addressed the related issues; and Tiecehurst et al. (*16*) used BBN model

for assessing the sustainability of costal lakes in Australia. Other applications of BBN

include fisheries (*20, 21*), fish and wildlife (*22*), water distribution (*23*), groundwater

contamination (*24*) and risk assessment (*25, 26*).

The objective of this research is to develop a Bayesian Belief Network (BBN) for

CO_2 leak detection in order to integrate the information provided by different near-

surface monitoring techniques deployed at a site and to infer the probability that a CO_2

leakage event occurs, expressed in a probability distribution of CO_2 leakage rate.

Meanwhile, this BBN model is used to evaluate the performance of an integrated

monitoring network with different monitor densities. To illustrate the methodology

developed for a geologic sequestration site, the information from the Zero Emission

Research and Technology (ZERT) site is used for the BBN model. The parameters used for simulating leakage events are tuned using ZERT site data, given various leakage rates and permeabilities. The background data of two monitoring methods, near-surface soil CO_2 flux and perfluorocarbon (PFC) tracer concentration measured at the ZERT site are characterized for leak detection. The probabilistic relationships between leakage rate, soil CO_2 flux, PFC tracer concentration and permeability are obtained by a subsurface simulation model, TOUGH2 (*27*) under a range of scenarios for the leakage rate, leakage location (relative to monitors), and subsurface conditions (permeability). While this study focuses on the near-surface monitoring techniques, other monitoring methods can be added to the BBN model as well. Similarly, this BBN model includes only permeability as the site condition variable due to the simulation cost of time, however, other site conditions can be included if needed for the future applications.

4.2   Methods

First, the methodology and a general framework for the development of a Bayesian Belief Network (BBN) for CO_2 leak detection are described, and then the illustration of the application to the ZERT site with two near-surface monitoring techniques is followed.

4.2.1   *Bayesian Belief Network for CO₂ Leak Detection at a Geologic Sequestration Site*

A Bayesian Belief Network (or Bayesian Network or Bayesian probability network) is a graphical model representing the probabilistic relationships between variables of interests (*15*). According to Heckerman's notation (*15*), a BBN includes (i) a

set variables X={X1, …, Xi, …, Xn}, i.e. system components, (ii) a set of local probability distributions P related to each variable, and (iii) a directed acyclic graphical structure representing the probabilistic relationships between the variables of interest in the system . In the directed acyclic graph, the variables are represented as nodes, and the conditional dependence between these variables is expressed as a series of arcs. The lack of arcs between variables indicates conditional independence, a key feature of a BBN that allows the estimation of joint distribution of X to be logically simplified into steps and thus reduce the complexity of computations and modeling. Therefore, the conditional probability of Xi given other variables is reduced to those variables on which Xi is dependent, known as "parents" (or "parent nodes") Pai. The conditional probability P (Xi|Pai) refers to the local probability distributions of Xi mentioned above.

The development of a BBN model starts with the selection of the variables in the system, then the network structure is identified by assigning causal relationships among the variables, and finally the probability $P(X_i|Pa_i)$ is assessed based on the inference made from any related data, model simulations or expert elicitation (*15, 20*). All the steps of the BBN model development require an understanding and knowledge of the problem and the system of interest. In our study, the variables were chosen by the authors, and the general structure of the model structure was reviewed by experts in the Monitoring, Measurement and Verification (MMV) group at the National Energy Technology Laboratory (NETL) and other experts in the field of geologic carbon sequestration at the Sixth Annual Conference on Carbon Capture & Sequestration (*28*).

The BBN in this study is designed for the leak detection with a particular focus on the leakage rate at a geologic sequestration site. This problem involves two major

aspects: the occurrence of a leakage event and the detection of the leak by various monitoring techniques and network designs. The occurrence of a leakage event includes the possible factors that make the leakage event happen   and the parameters that affect how the leak spreads and where the leak moves once it begins, including the physical and geological conditions of the site such as temperature, porosity, permeability, vadose zone thickness, rock types, etc. The second aspect of the CO_2 leak detection problem involves the monitoring plan at the site, including the monitoring techniques chosen for the pre-injection, operation and post-injection stages as well as the number of monitors needed and the monitoring location for each monitoring technique. The monitors can be evenly distributed throughout a site or located around possible leak spots like wells and faults. Figure 4.1 below shows the general BBN framework CO_2 leak detection problem. In this figure, the systems are divided into four areas with respect to the two major aspects mentioned above. The areas with solid lines are included in the ZERT case, but the area surrounded by the dotted line is not included due to the lack of data; however, it is part of the original BBN model developed in the first place.
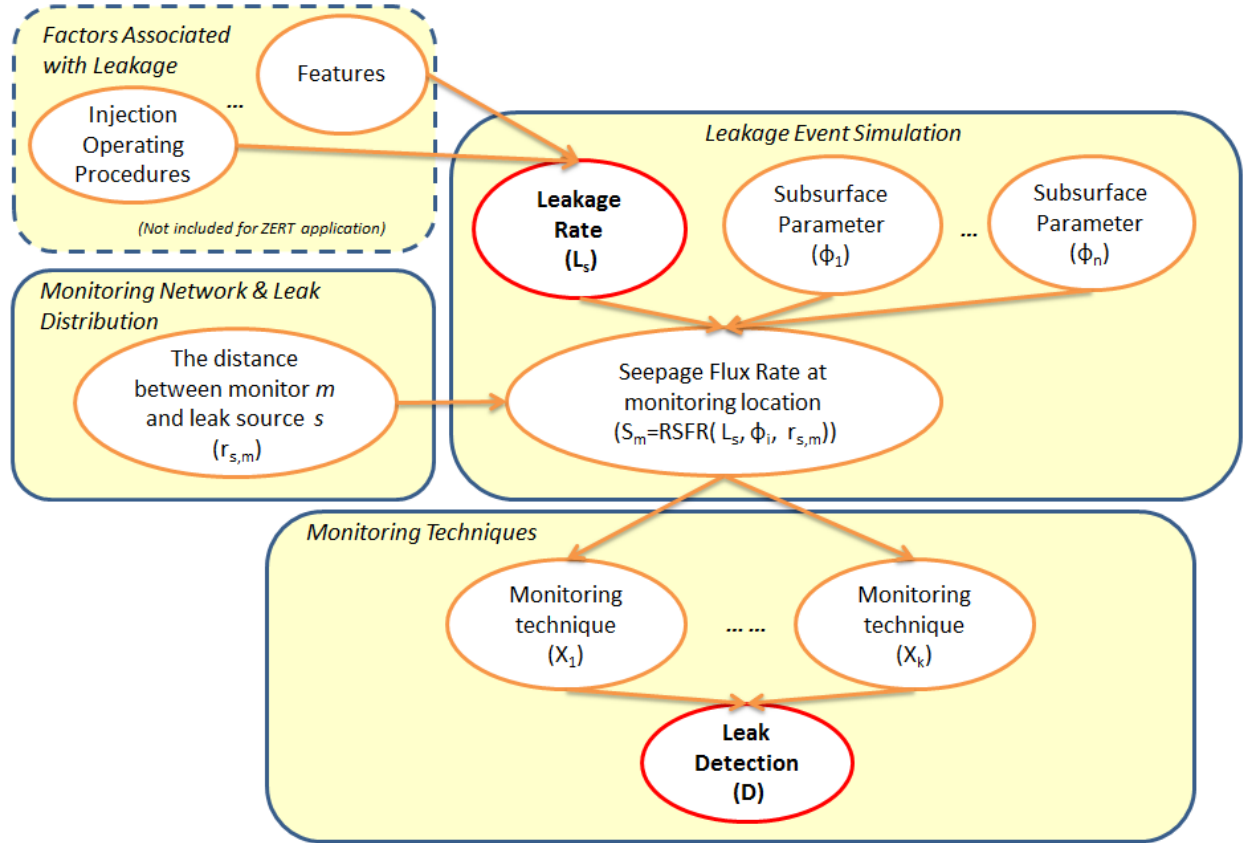
Figure 4. 1   General Framework of Bayesian Belief Network for CO_2 Leak Detection at Geologic Sequestration Site

In Figure 4.1, a leakage event can be simulated by models like TOUGH2 using the designed leakage rates and the parameters as the inputs for the simulations. Then, the simulations create the geological patterns showing how the leakage flux spreads out, that is, the relationship between the simulated CO_2 leak flux and a particular location at a sequestration site. The methodology for predicting the performance of near-surface CO_2 leak detection systems geologic sequestration sites earlier developed by Yang et al. (**29**) was adapted for the current research. A radially symmetric functional relationship (RSFR) of CO_2 seepage flux S_m given leakage rate L_s sub-surface parameters ϕ and the leak source location s at the monitor location m is expressed as $S_m=RSFR(L_s, \phi, r_{s,m})$,

where $r_{s,m}$ is the distance between the source of the leak and the monitor. A number of leakage rates L_s are given in the simulations in order to estimate the probability distribution of possible size leaks based on the multiple monitoring inputs. The sub-surface parameters ϕ are site specific, mostly depending on the geological information available at the site. The distance distribution of $r_{s,m}$ for each monitoring technique can be calculated given a monitoring network design and possible leak sources. For any given measurement made using each monitoring technique, the corresponding CO_2 seepage flux S_m was estimated in order to calculate the probability of detecting a leak. This estimation of S_m for each monitoring technique could be made based on either the field data, experimental data, or related simulations. This is one of the main reasons that near-surface CO_2 fluxes and PFC tracer concentrations were chosen for this research.

4.2.2   *Application to the ZERT site*

A BBN for combining the leak detection monitoring results from near-surface CO_2 fluxes measurement and PFC tracer monitoring was built based on the information provided at the ZERT site. This site was selected to demonstrate the BBN model due to the abundance of data available there. The shallow CO_2 release experiments were carried out at the ZERT site in the fall of 2006 and the summers of 2007 and 2008. The modeling of CO_2 transportation accompanied these experiments by TOUGH2/EOS7CA (*30, 31*) provided the calibration and verification information for our simulations. Several near-surface monitoring methods were tested and verified during the experiments (*9, 32-34*). Two near-surface monitoring methods, the CO_2 flux (or soil CO_2 flux) and PFC tracer monitoring, were selected for the BBN model.

Leakage Event Simulation

Simulations of leakage events involving both CO_2 seepage flux and the PFC tracer fluxes were implemented using TOUGH2/EOS7CA. Simulation scenarios and assumptions followed the methodology described in Yang et al. (*29*), which considered combinations of different values of leakage rates and top-soil permeabilities (the one subsurface parameter), for a total of 17 cases. The base leakage rate was 1.93×10^{-4} kg/s, twice the value used in the MMV test at the ZERT site, and varied from a factor of $1/10^3$, $1/10^2$… to 10^3. Similarly, the permeability ranged over factors of 10 from 1 mD to 1000 D, using 1 D as the base value. Four cases combining the highest and lowest permeability and leakage rate were included as well. The PFC tracer was Perfluoromethylcyclohexane (PMCH), tested in the ZERT experiments, and the tracer leakage rate was assumed to be proportional to the CO_2 leakage rate. The ratio of CO_2 and PMCH leakage rates by weight was 3107.28, between the values found in the ZERT tests (*9*) and the Frio test (*4, 5*). Consequently, a PMCH leakage rate of 1.24×10^{-7} kg/s was thus obtained for the base case. The simulations of the 17 cases provided the basis for estimating both CO_2 seepage flux S_m given different leakage rates L_s and permeability (ϕ_1), as well as the corresponding PMCH seepage flux, Sp_m, in the near-surface area. The simulation results of CO_2 seepage flux were taken from the study by Yang et al., 2010 (*29*), and the simulations of PMCH seepage were implemented in our study using the settings above. The results of simulated PMCH seepage flux for different leakage rates and permeabilities are shown in Appendix D.

Monitoring Network and Leak Distribution

The simulations of leakage events for both the CO_2 and PFC fluxes were used to test the design of four monitoring densities, d=100 m, d=50m, d=20m and d=10m, where d indicates the distance between adjacent monitors. A random leak field for a hypothetical homogeneous site of 1 km x 1 km was assumed. Then, the distance $r_{m,s}$ from a random leakage point s to the nearest monitor m was calculated. The distribution of the distance $r_{m,s}$ was estimated by random sampling within the random leak field, as described in Yang et al. (*29*), where the distance distributions of $r_{m,s}$ for the four monitoring densities can also be found. These distance distributions of $r_{m,s}$ were used as the inputs in the radially symmetric functional relationship S_m for near-surface CO_2 flux and the Sp_m for near-surface PMCH flux. The resulting seepage flux distributions of S_m and Sp_m were then used to calculate the probability of detection in the following section.

Monitoring Technique and Detection

The natural near-surface CO_2 flux (or soil CO_2 flux rate) and the background PMCH tracer concentration measured at the ZERT site were used to determine critical values for leak inference and to calculate the probabilities of leak detection given a monitoring network. In Yang et al. (*35*), the natural soil CO_2 flux rates ($\mu mol/m^2$-s) at the ZERT site were characterized by a Bayesian square-root linear model that predicted the background flux as a function of soil temperature. Therefore, this square-root linear model was also assumed to apply for all locations m at the ZERT site, and the 15 °C simulation temperature in TOUGH2 was used for this model. The natural background PMCH concentrations (fL/L) were characterized by a Bayesian hierarchical model that

predicted the background tracer concentration based on the measurements obtained from the four sites in 2007: the ZERT site in Montana (9), the Lower Michigan Basin site near Gaylord, Michigan (36), the San Juan Basin site in New Mexico, and the Pines parking lot at NETL, Pittsburgh, Pennsylvania. The Bayesian hierarchical model was used to characterize the PMCH concentration because of the small number of observations at the ZERT site. Thus, a Bayesian hierarchical model combining information from other similar sources was the best alternative in this situation. The summary of the simulations for the Bayesian hierarchical modeling of background PMCH concentrations can be found in Appendix E.

The probability distributions of the background soil CO_2 flux, Y_1, and the background PMCH tracer concentration, Y_2, were obtained once the characterization of background data had been made. The resulting predictive distribution from the Bayesian hierarchical or nonhierarchical model was then used to determine the upper prediction interval value of each monitoring technique for leak detection (35). In this study, the upper bound of the 99% prediction interval was chosen as the threshold for detecting a leak for both CO_2 flux measurement and PMCH concentration.

The probability of leak detection for each monitoring technique is defined as the probability that the total CO_2 flux or tracer concentration, i.e. the observed value, exceeds the threshold estimated based on the background information. The total CO_2 flux (X_1) is the sum of the natural background CO_2 flux (Y_1) and the simulated leak seepage flux (S_m). Similarly, the total tracer concentration (X_2) is the sum of the natural background concentration (Y_2) and the additional tracer concentration from the simulated leak seepage flux (Sp_m). At the ZERT site, PMCH flux was converted to PMCH concentration

by assuming a circular influence area of 1.5 m in diameter and a 10-day exposure period for each PMCH monitor. Since the simulated seepage flux is a function of leakage rate (L_s), site parameters (ϕ) and the distance between adjacent monitors ($r_{m,s}$), the probability of detection for a given size leak, L_s, could be obtained through the simulated seepage flux (S_m) or tracer concentration (Sp_m) (**29**).

The Detection node represents the detection done by any of the monitoring techniques. The joint distributions for leak detection were estimated assuming conditional independence between monitoring techniques given a particular size of leak. The joint distributions of X_1 and X_2 above their detection thresholds, i.e., the joint probability distribution of the detection node, were calculated by combining the distributions of Y_1 and Y_2 with the relationship between S_m and Sp_m. Since the tracer leakage rate was assumed to be a portion of the CO_2 leakage rate, the simulated S_m and Sp_m had a clear relationship which could easily be modeled (See Appendix F). Here a nonparametric cubic spline function was applied for determining Sp_m as a function of S_m, including the estimation of the distribution of the prediction error. The joint probability distribution of the detection node was generated with a Monte Carlo integral over of Y_1 and Y_2 along with the error distribution and the inherent variability from S_m due to the distance distribution $r_{s,m}$, given a particular leakage rate and permeability.

Figure 4.2 below shows the BBN applied to the idealized ZERT site. In this study, the leakage rates were discretized and range from tiny leakage rates below 10^{-6} kg/s to the explosion size of 1 kg/s based on the range of the TOUGH2 simulations. A power distribution with a slope factor of 1 was assumed for the prior distribution of the leakage rate (**37-38**), i.e. the probability density function $p(L_s)=(4.54 \times 10^{-7})L_s^{(-1)}$. The distribution

of distance $r_{m,s}$ depends on the designed monitoring density: d=100m, d=50m, d=20m and d=10m (**29**). In order to focus on the leakage rate distribution, the subsurface parameter, soil permeability, is limited to three deterministic options: high (100 D), median (1 D) and low (0.01 D). The simulated CO_2 leak seepage node is also hidden in the Results section below in order to directly represent the probabilistic relationships between the monitoring results and the corresponding distribution of leakage rates. The BBN was constructed using the software package Netica 4.16 (**39**).
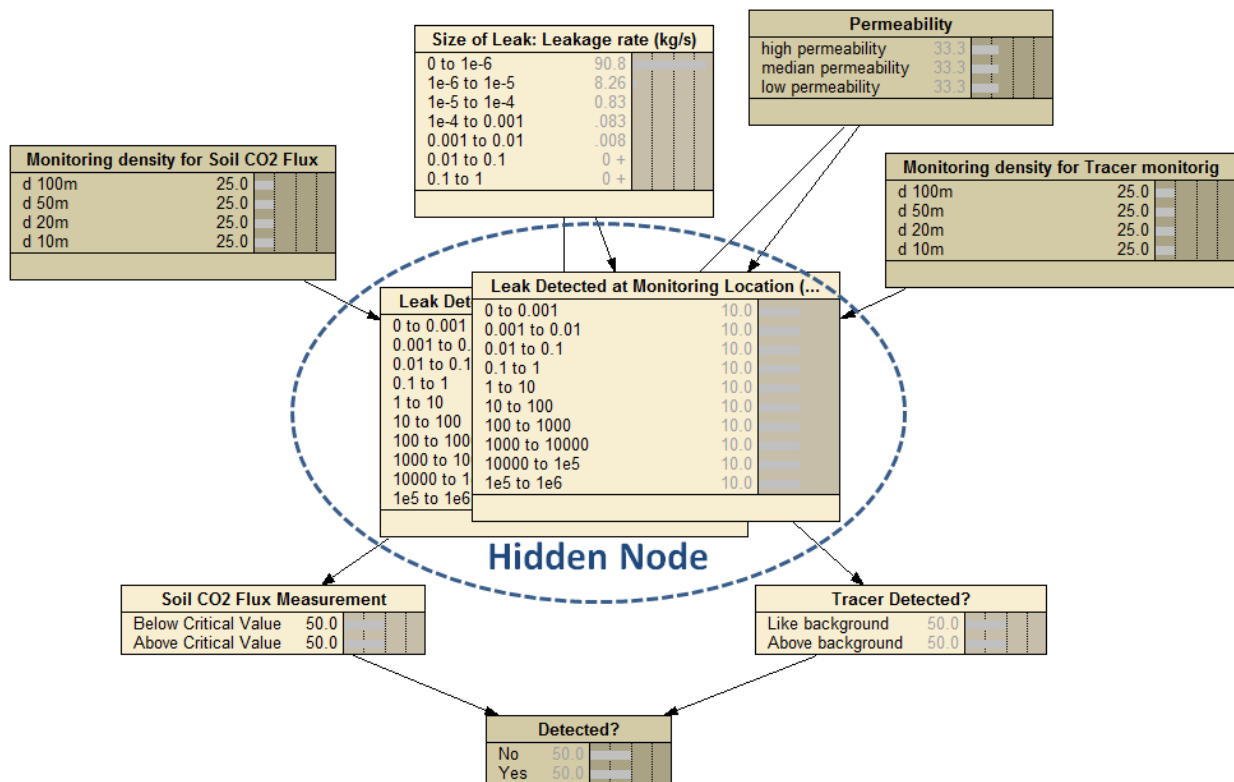
Figure 4. 2   Bayesian Belief Network for CO_2 Leak Detection for the Idealized ZERT Site

4.3   Results

4.3.1   The probabilities of CO_2 leak detection and CO_2 leakage rate

The relationships between the probability of CO_2 leak detection and the CO_2 leakage rate for the PFC tracer, the soil CO_2 flux measurement, and the joint measurement of both the soil CO_2 flux and the PFC tracer are shown in Figures 4.3-4.5 below, for the low, median and high permeability rates, respectively, given different monitoring densities. These probabilistic relationships form the content of   the conditional probability tables in the BBN model for the idealized ZERT site (see Appendix G). The probability of CO_2 leak detection for soil CO_2 flux measurement given different permeabilities and leakage rates were discussed in the research reported in Yang et al. 2010. Here these cases are presented again for comparison with the PFC tracer monitoring and the joint measurement of both soil the CO_2 flux and PFC tracer.

In Figures 4.3- 4.5, the PFC tracer reading is shown to be much more sensitive for detecting a leak than soil CO_2 flux measurement in all twelve cases with combinations of the four monitoring densities and three permeabilities. Therefore, the probabilities for the joint leak detection are almost the same as for the PFC tracer alone. Like soil CO_2 flux measurement, the probability of leak detection by the PFC tracer increases with rising leakage rate. Also, the probability of leak detection increases as the monitoring density increases from low (d=100m) to high (d=10m). Moreover, the overall probabilities of leak detection for both monitoring methods decrease with increases in permeability, unlike the soil CO_2 flux measurement in median permeability with monitoring density d=10 m and 25m, where the shape of the CO_2 seepage plume becomes important in leak

91

detection (*29*). However, the abilities of detecting minimal-sized leaks are very different in tracer and soil CO_2 flux measurement.
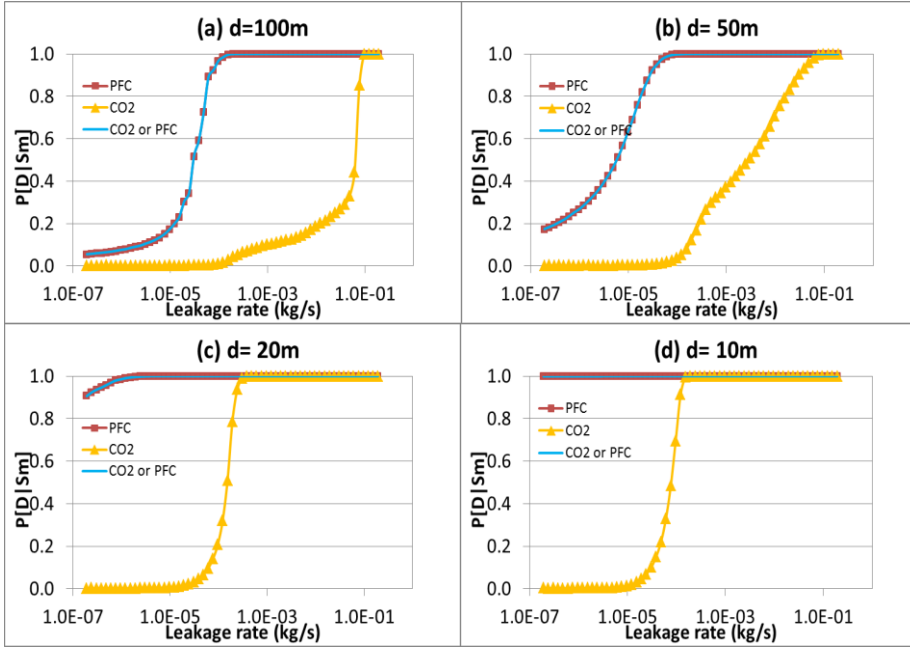
Figure 4. 3   **Probability of detection as a function of CO_2 leakage rate for different monitoring densities, (a) 100m (b) 50m (c) 20m and (d) 10m between monitors, and for different monitoring techniques, PFC tracer and/or CO_2 flux measurement, given low permeability = 0.01 Darcy.**
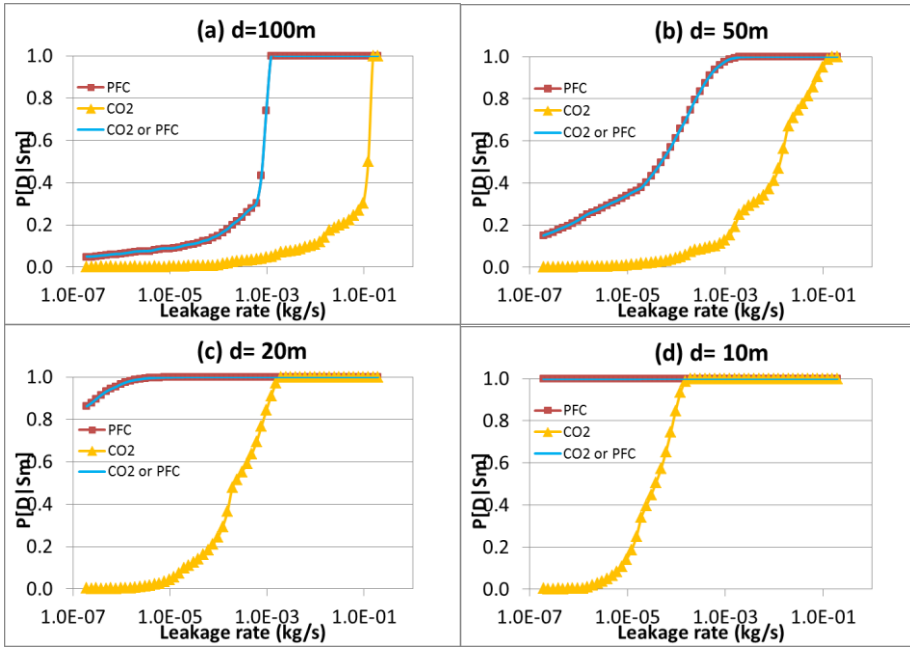
Figure 4. 4   **Probability of detection as a function of CO_2 leakage rate for different monitoring densities (a) 100m (b) 50m (c) 20m and (d) 10m between monitors, and for different monitoring techniques PFC tracer and/or CO_2 flux measurement, given median permeability = 1 Darcy.**
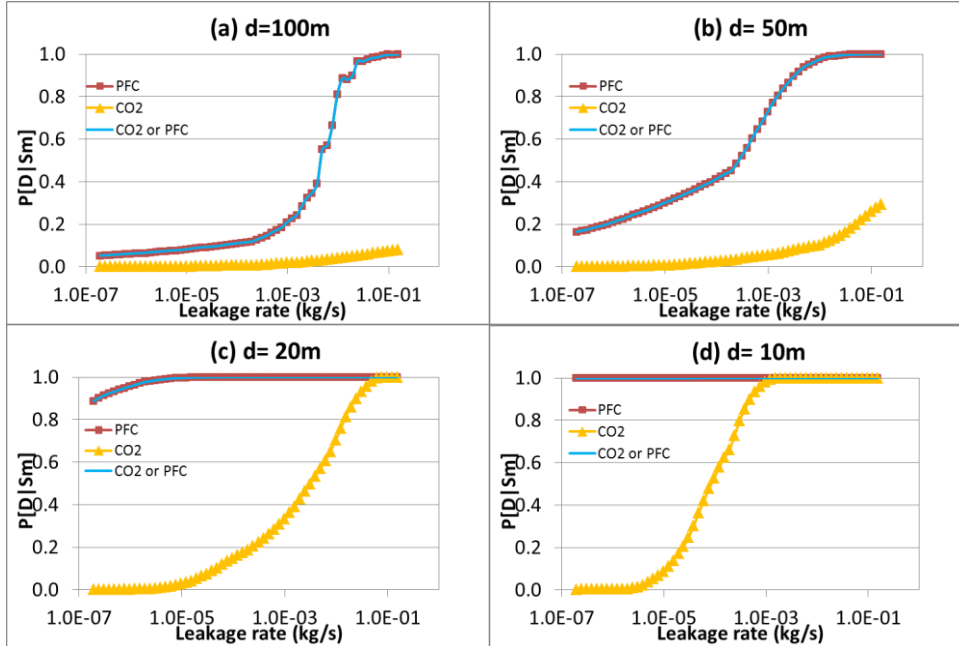
Figure 4. 5   Probability of detection as a function of CO_2 leakage rate for different monitoring densities (a) 100m (b) 50m (c) 20m and (d) 10m between monitors, and for different monitoring techniques PFC tracer and/or CO_2 flux measurement, given high permeability = 100 Darcy.

For PFC monitoring, permeability only has an effect on the probability of detection with the less dense (d=50m and d=100m) networks. In Figure 4.3 showing the cases with low permeability, the probabilities of leak detection by PFC tracer remain close to 1 at the higher monitoring densities (d=20 m and d=10 m). The PFC tracer can nearly fully detect the CO_2 leak seepage signals generated by any leakage rate above 10^{-6} kg/s when the distance between adjacent monitors is less than 20 m. Under the same monitoring network (d=20 m), soil CO_2 flux only starts detecting the seepage signal at leakage rate around 10^{-4} kg/s. Additionally, the detection ability of the PFC tracer starts decreasing as the leakage rate decreases to 10^{-4} kg/s, given the monitoring network d=50 m. Nevertheless, the probability of leak detection with the PFC tracer in the d=100 m case is still comparable to that with soil CO_2 flux in the d=10 m case. Similarly, in Figures 4.4 and 4.5, for the median and high permeability cases, respectively, the nearly full detection made by the PFC tracer is still achieved for denser monitoring networks

(d=10 m and 20 m)), while for sparse monitoring networks, d=50 m and d=100 m, the full detection probability is reached at leakage rates of 10^{-3} and 10^{-2} kg/s respectively. Compared to soil CO_2 flux measurement for sparse networks in cases of high permeability, the leakage rate above 10^{-2} kg/s, which is hardly detected by soil CO_2 flux measurement, can still be detected by PFC tracer monitoring. However, though the PFC tracer provides a better coverage for detecting a leak, there are a few drawbacks with PFC tracer monitoring, which are explained in the discussion section.

4.3.2 *Probability inference of the Bayesian Belief Network Model for the Idealized ZERT site*

The probability of any node in the model can be inferred with the BBN model, given any evidence, monitoring network designs, or site conditions. The calculation is made based on the conditional probabilities shown in the previous section. Two types of probability inferences made by the BBN model are illustrated here: (1) the inference regarding the possible size of a leak, i.e. the leakage distribution given the monitoring results (evidence), monitoring network design or site parameters, and (2) the use of the BBN model to calculate the probability of leak detection for an acceptable minimum leakage rate in order to optimize a monitoring network design or to select monitoring techniques to be deployed at a site.

First, the BBN model in Figure 4.6 shows the posterior distributions of the leakage rates for the high (d=10m) and low (d=100m) monitoring density networks, given that both soil CO_2 flux and PFC tracer measurements detect the leak. The expected size of the leakage and the variance found in the high density case are smaller than those

in the low density case. As can be seen in Figure 4.6a for the high monitoring density, the

expected leakage size is 1.41×10^{-4} kg/s with a variance of 5.1×10^{-3}, while in Figure 4.6b,

the expected leakage size for the low density case is shown to be 2.26×10^{-3} kg/s with a

variance of 0.035. The increase in monitoring density increases the ability of detecting

smaller leaks and thus decreases the expected leakage size and the variance once the leak

is found.   Although the leakage rate distribution in Figure 4.6b seems to focus on the

category of the smallest leaks (0 to 10^{-6} kg/s), the substantially increased portions of the

large leakage rates, from 0.001 to 1, increase the expected values about one order of

magnitude.
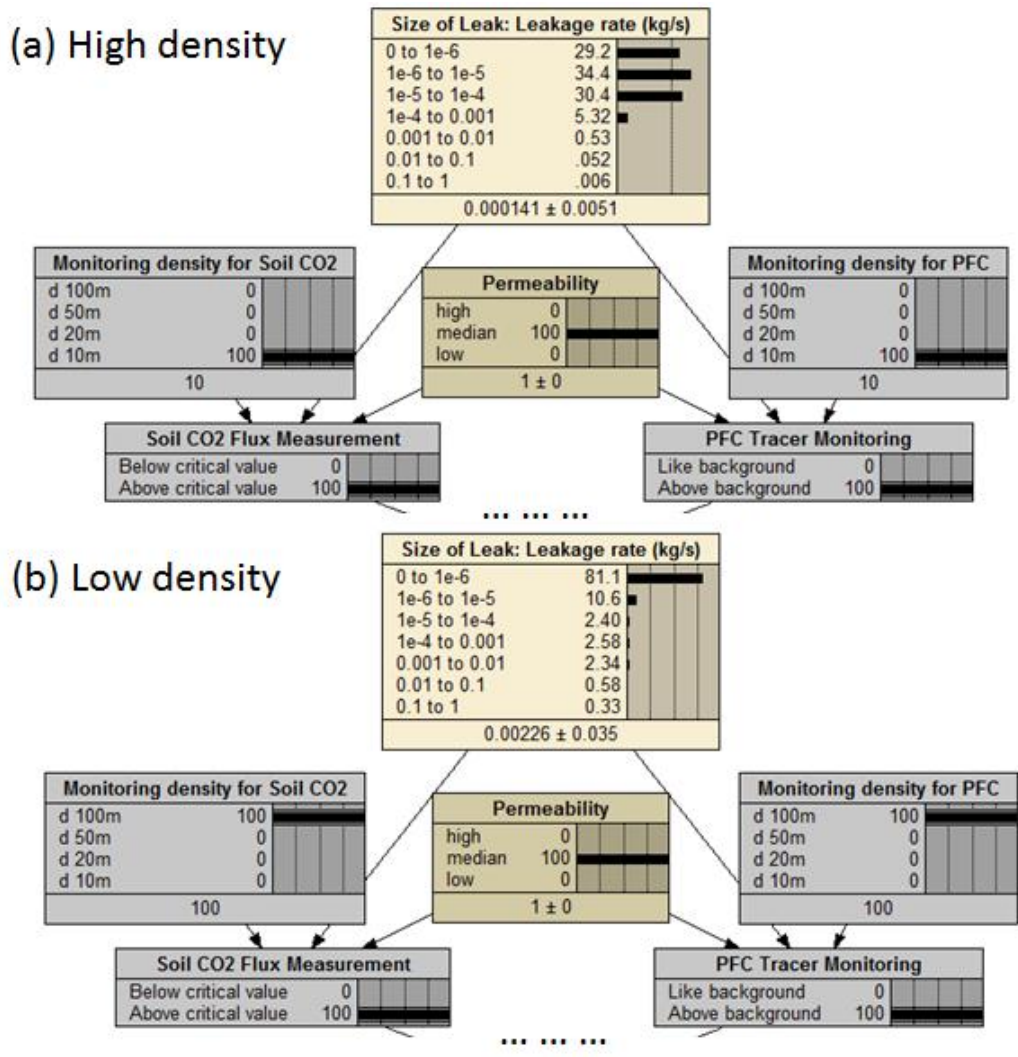
Figure 4. 6   The leakage rate distributions for the network of (a) high monitoring density (10m) and (b) low monitoring density (100m), given the detection made using both soil CO$_2$ flux and PFC tracer measurements.

Second, the posterior distributions of the leakage rate can also be inferred from the multiple monitoring results, analogous to a medical diagnosis. In Figure 4.7 the posterior distributions of leakage rate for the detection made by the two techniques or the PFC tracer alone are shown given median permeability and monitoring density d=20m. In Figure 4.7a, the expected leakage rate for the joint measurements is 2.29x10^{-4} kg/s

96

with a variance of $7.1x10^{-3}$. For a leak detected with the use of both monitoring

techniques, a larger sized leak is expected because the soil CO_2 flux measurement

discovers larger sized leaks. Figure 4.7b shows the leakage distribution when both

monitoring techniques are applied but only PFC tracer monitoring detects the leak. With

the no-detection input from soil CO_2 flux measurement, the expected leakage rate is

much smaller, with a mean of $1.52x10^{-6}$ kg/s and a variance of $1.2x10^{-5}$ since PFC tracer

monitoring is able to detect smaller sized leaks. Figure 4.7c shows the leak detection

done using only the PFC tracer monitoring result without the use of soil flux

measurement. The leakage distribution has a slightly higher mean of $3.45x10^{-6}$ kg/s and a

larger variance of $6.6x10^{-4}$, similar to the result shown in Figure 4.7b.
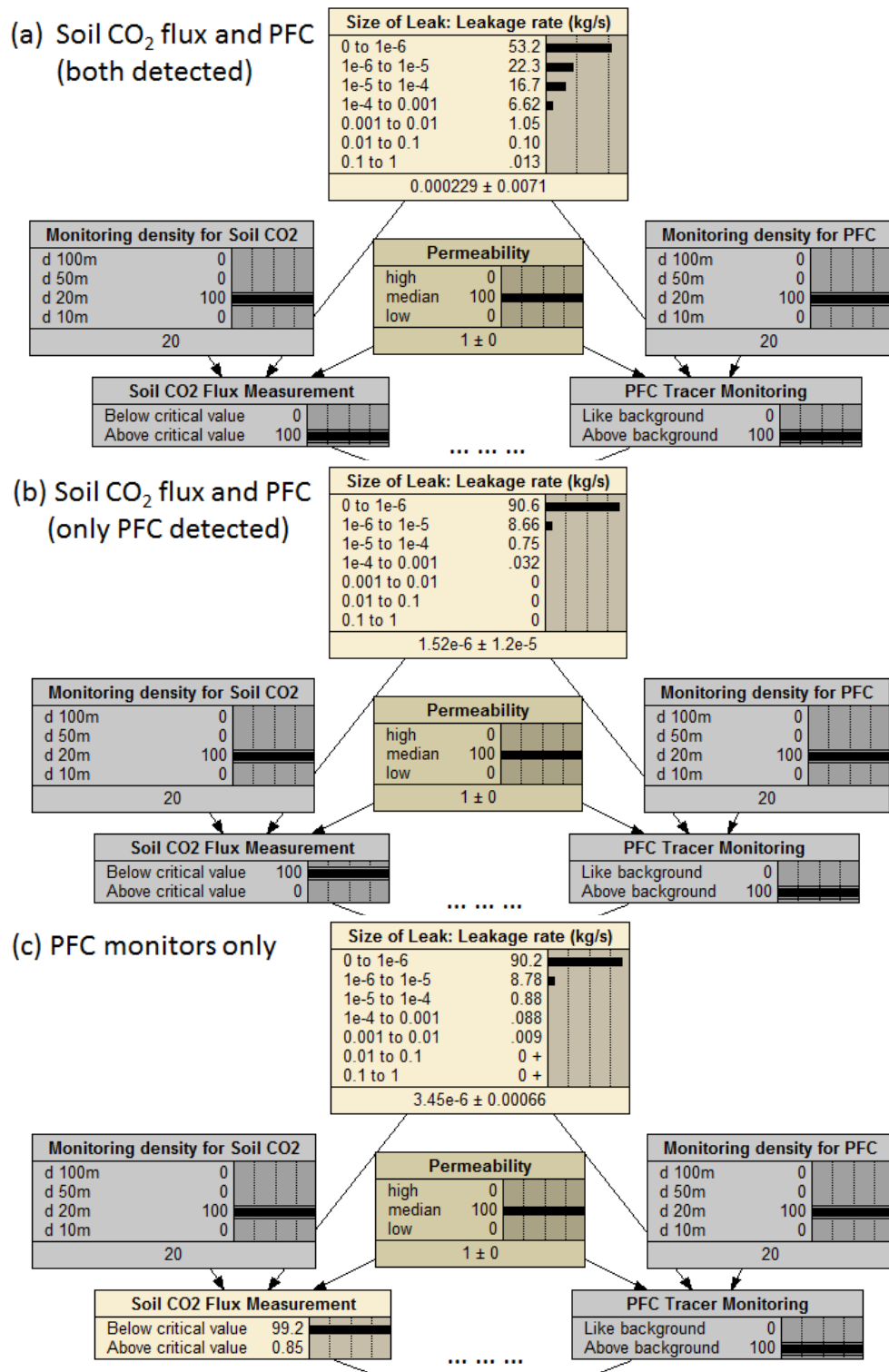
Figure 4. 7 The leakage rate distributions for detection made using PFC tracer and soil CO$_2$ flux measurement with **(a)** both techniques indicating positive findings, **(b)** PFC tracer indicating positive finding and soil CO$_2$ flux indicating none, and **(c)** only PFC tracer monitoring implemented and indicating positive, given median permeability and monitoring density d=20m.

Another important use of the BBN model is to calcualte the probability of leak detection for an acceptable minimum leakage rate in order to optimize a monitoring network design or to select the monitoring techniques deployed at a site. Considering the different coverage ability of the two monitoring techniques, the monitoring density can be assigned to each node specifically for its individual design. Figure 8 illustrates the probability of leak detection at a desired level of leakage rate (10^{-4} to 10^{-3} kg/s) for two different monitoring designs, d=20m for soil CO_2 flux and d=50m for PFC tracer, given median permeability. This leakge rate catetory (10^{-4} to 10^{-3} kg/s) correponds to the leakage rates used in our base case simulation and the ZERT tests. Figure 4.8 shows that the overall probability of detection is 0.967, and the individual probability of detection is 0.636 for for soil CO_2 flux given the monitoring network design d=20m and 0.919 for PFC tracer when the design of d=50m. Similarly, the same computation can be made for all possible combinations of monitoring densities and monitoring techniques so that a subsequent optimization of monitoring network design that includes other considerations such as cost or labor can take place. Therefore, the overall and individual probabilities of detecting the leakage rate from 10^{-4} to 10^{-3} kg/s are calculated for all combinations of the four monitoring densities and the two monitoring techniques, given high, median, and low permeability, as shown in Table 4.1 below.
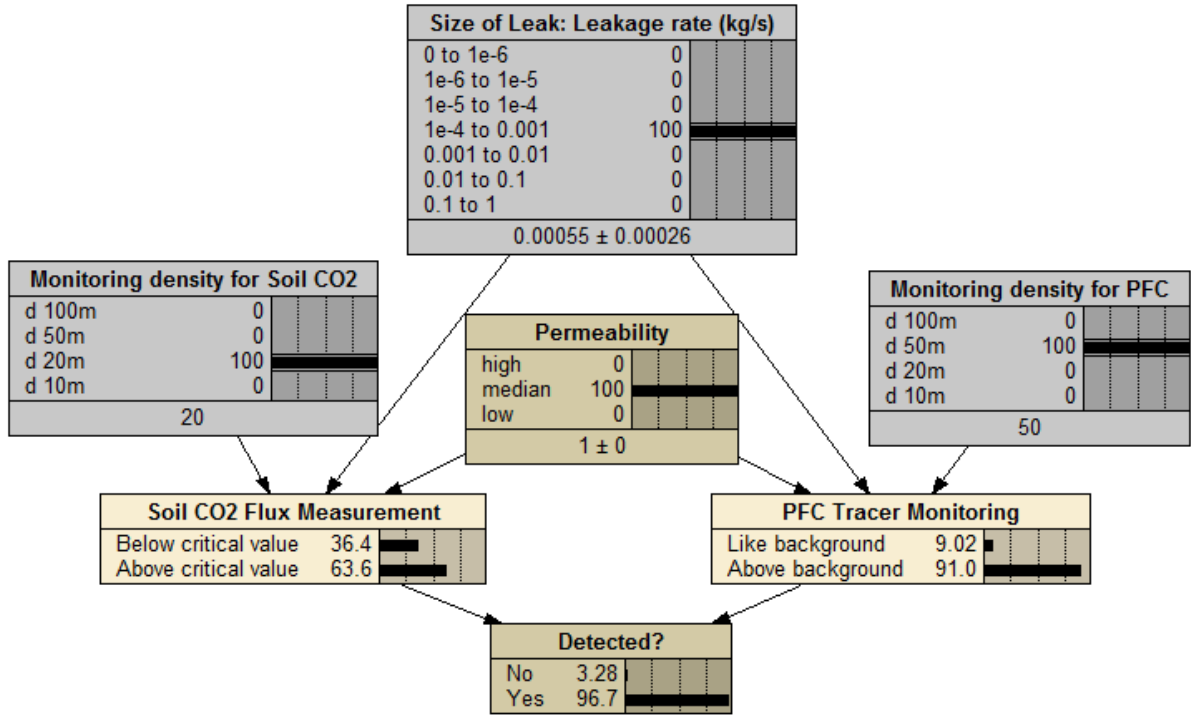
Figure 4. 8   The probability of leak detection for a desired level of leakage rate (10^{-4} to 10^{-3} kg/s) using the network design of monitoring density of 20m for soil CO_2 flux and 50m for PFC tracer, given median permeability.

Table 4. 1   Probability of Leak Detection for 10^{-4} to 10^{-3} kg/s Leakage Rate for Soil CO_2 Flux and PFC Tracer

High permeability		PFC tracer			
Soil CO_2 flux	na	100 m	50 m	20 m	10 m
na	0	15.90%	60.40%	100%	100%
100 m	1.29%	17.00%	60.90%	100%	100%
50 m	4.67%	19.80%	62.20%	100%	100%
20 m	26.30%	38.00%	70.80%	100%	100%
10 m	89.90%	91.50%	96.00%	100%	100%
Median permeability		PFC tracer			
Soil CO_2 flux	na	100 m	50 m	20 m	10 m
na	0	27.80%	91.00%	100%	100%
100 m	3.44%	30.30%	91.30%	100%	100%
50 m	9.70%	34.80%	91.90%	100%	100%
20 m	63.60%	73.70%	96.70%	100%	100%
10 m	99.90%	99.90%	100%	100%	100%
Low permeability		PFC tracer			
Soil CO_2 flux	na	100 m	50 m	20 m	10 m
na	0	100%	100%	100%	100%
100 m	7.89%	100%	100%	100%	100%
50 m	30.00%	100%	100%	100%	100%
20 m	100%	100%	100%	100%	100%
10 m	100%	100%	100%	100%	100%

With Table 4.1, the lowest density of the monitoring network required for each monitoring technique can easily be found given a required detection probability under different permeability conditions. If a minimum 95% detection probability is required, a monitoring network of d=20m for PFC tracer alone or the combination of d=50m network for PFC tracer and d=10m network for soil CO_2 flux is sufficient in the case of high permeability. Likewise, the target probability of 95% detection can be met one of three ways: by using the d=50m network for PFC tracer and d=20m monitoring network for soil CO_2 flux, merely a d=10m monitoring network for soil CO_2 flux, or a d=20m

network for PFC tracer in the median permeability case. For low permeability, either a monitoring network of d=100m for PFC tracer or a monitoring network of d=20m for soil CO_2 flux can achieve the same target detection probability. The trade-offs between the two methods can be seen in this analysis, which provides a basis for the following decision making process to obtain an optimized monitoring network design for an acceptable minimum leakage rate. Besides detection ability, the determination of the optimized network design usually involves other factors such as the cost of monitoring, labor and technology availability.

4.4   Discussion

The two monitoring techniques, soil CO_2 flux measurement and PFC tracer monitoring, show different results for detecting the size of leak in the BBN model for the idealized ZERT site. With sufficient monitoring density, PFC tracer monitoring can generally detect the leakages greater than 10^{-6} kg/s, while soil CO_2 flux measurement can effectively detect the leakage greater than 10^{-4} kg/s, based on the ZERT site condition. PFC tracer monitoring is more sensitive in detecting leaks. In Figure 4 for median permeability, the monitoring density required for 90% detection is d=10 m for soil CO_2 flux measurement and d=20 m ~ 50 m for PFC tracer monitoring. These numbers tell us that PFC monitoring has better performance in detecting a leak compared to soil CO_2 flux measurement for the same monitoring density and site conditions.

However, PFC tracer monitoring is not as fast and direct as soil CO_2 flux measurement. It usually takes from a couple of weeks to a couple of months to complete PFC tracer sampling (*9, 40*). In contrast, the daily average of soil CO_2 flux measured by

102

accumulated chamber is obtained and used for leak detection; thus, the feedback using soil CO_2 flux measurement is faster. Also, because of the possible contamination of PFC tracer during the injection stage, which changes the original background concentration, the injection procedure of PFC tracer must be done especially carefully (*36, 41, 42*), while soil CO_2 flux is less delicate and provides direct measurement on the spot. Nevertheless, the coverage of soil CO_2 flux measurement is small compared to that provided with PFC tracer monitoring, so many more monitors are needed to achieve the same probability of detection, making this technique cost- and labor-intensive.

Considering the pros and cons of the two monitoring techniques, soil CO_2 flux measurement is recommended for regions where the large size leaks might occur, such as the area around wells and features. PFC tracer monitoring is more flexible with regard to the location of monitors due to its sensitivity to small sized leaks. Actually, these concerns with regard to coverage area, sampling time and cost can be integrated to the BBN to build a decision support system for CO_2 leak detection for application in the future. Take the cost for example: if the use of a PFC tracer is relatively more expensive than soil CO_2 flux measurement, a combination of the two monitoring techniques may be preferred. If it's not more expensive, soil CO_2 flux is suggested for use in high risk regions because of its quick feedback. Since the use of different monitoring strategies is suggested, in our ongoing research, we will consider the monitoring network designed specifically for each monitoring technique for each particular situation, considering high-risk leakage pathways like fractures, faults and abandoned wells. The optimization of these network designs in order to achieve a minimum acceptable leakage rate is indeed

site-specific; therefore, more information from a sequestration site is needed to obtain a refined monitoring network design.

This study presents a general and applicable framework of the Bayesian Belief Network (BBN) for CO_2 leak detection deployed at a site, illustrating the use of the two monitoring techniques for the idealized ZERT site. However, more monitoring technologies can be added to the BBN for a more fully integrated assessment of CO_2 leak detection in the application stage. Moreover, each monitoring node can be further categorized into several states in order to better characterize leakage distribution. Other site parameters of interest, such as vadose zone thickness or porosity, can be added into the BBN as well. Additionally, the prior distribution of leakage rate can be further explored, rather than simply assuming a power-low distribution based on the natural analogue like volcanic CO_2 fluxes. Some operational or natural factors associated with leakage rate, or site characterization generally, are worth studying. Finally, as mentioned above, the BBN can be expanded into a decision support system with the addition of other elements reflecting important operational, economic, and social concerns.

References

(1) U.S. Department of Energy, National Energy Technology Laboratory (2007) Carbon Sequestration Technology Roadmap. DOE: Washington, DC.

(2) Hepple RP and Benson SM (2005) Implications of Surface Seepage on the Effectiveness of Geologic Storage of Carbon Dioxide as a Climate Change Mitigation Strategy: Performance Requirements and the Implications of Surface Seepage. Environmental Geology 47(4): 576-585.

(3) Oldenburg CM, Lewicki JL, Hepple RP (2003) Near-surface monitoring strategies for carbon dioxide storage verification. Tech Report LBNL-54089, Lawrence Berkeley National Laboratory.

(4) McCallum SD, Phelps TJ, Riestenberg DE, Friefeld BM, Trautz RC (2005) Interpretation of perfluorocarbon tracer data collected during the Frio carbon dioxide sequestration test: presented at the American Geophysical Union Fall Meeting, San Francisco, California, December 5–9, 2005, paper GC13A-1214. GCCC Digital Publication Series #05-03f, pp. 1-2.

(5) Hovorka SD, Benson SM, Doughty C, Freifeld BM, Sakurai A, Daley TM, et al. (2006) Measuring permanence of CO2 storage in saline formations: the Frio experiment. Environ Geosci, 13(2):105–21.

(6) Wells A, Hammack R, Veloski G, Diehl J, Strazisar B (2006) Monitoring, mitigation, and verification at sequestration sides: Sequre technologies and the challenge for geophysical detection. The Leading Edge, 10: 1264-1270.

(7) Benson SM (2007) Monitoring Geological Storage of Carbon Dioxide, Carbon Capture and Geologic Sequestration: Integrating technology, monitoring, and regulation, E.J. Wilson and D. Gerard (eds.) Blackwell Scientific Publishing, Ames, Iowa, Chapter 4.

(8) Leuning R, Etheridge D, Luhar A, Dunse B (2008) Atmospheric monitoring and verification technologies for CO_2 geosequestration. Int J Greenh Gas Con 2(3):401–414

(9) Strazisar BR, Wells AW, Diehl JR, Hammack RW, Veloski GA (2009) Near-surface monitoring for the ZERT shallow CO2 injection project. International Journal of Greenhouse Gas Control, 3(6): 736-744.

(10) Johnson, G, M Raistrick, B Mayer, M Shevalier, S Taylor, M Nightingale, I Hutcheon (2009) The use of stable isotope measurements for monitoring and verification of CO2 storage, Energy Procedia, Volume 1, Issue 1, Pages 2315-2322

(11) Preston C, Monea M, Jazrawi W, Brown K, Whittaker S, White D, Law D, Chalaturnyk R, Rostron B (2005) IEA GHG Weyburn CO_2 monitoring and storage project. Fuel Processing Technology, 86(14-15): 1547-1568.

(12) Wildenborg T, Bentham M, Chadwick R, David P, Dillen M, Gronenberg H, Kirk K and Le Gallo Y (2009) Large-scale CO_2 injection demos for the development of monitoring and verification technology and guidelines (CO2ReMoVe). Energy Procedia 1: 2367–2374.

(13) Borsuk ME, Stow CA, Reckhow K (2004) A Bayesian network of eutrophication models for synthesis, prediction and uncertainty analysis. Ecol. Model. 173: 219-239.

(14) Castelletti A, Soncini-Sessa R (2007) Bayesian networks in water resource modelling and management. Environmental Modelling & Software, 22(8): 1073-1074.

(15) Heckerman D (1999) A Tutorial on Learning with Bayesian Networks. In Learning in Graphical Models, M. Jordan, ed. MIT Press, Cambridge, MA.

(16) Ticehurst JL, Newham LHT, Rissik D, Letcher RA, Jakeman AJ (2007) A Bayesian network approach for assessing the sustainability of coastal lakes in New South Wales, Australia. Environ. Model. Softw. 22(8): 1129-1139.

(17) Darwiche A (2009) Modeling and Reasoning with Bayesian Networks. Cambridge University Press, New York.

(18) Lee E, Park Y, Shin JG (2009) Large engineering project risk network. Expert Syst Appl. Volume 36 Issue 3, April, 2009

(19) Varis O, Kuikka S (1999) Learning Bayesian decision analysis by doing: lessons from environmental and natural resources management. Ecological Modelling. 119 (2-3): 177-195.

(20) Borsuk ME, Reichert P, Peter A, Schager E, Burkhart-Holm P (2006) Assessing the decline of brown trout (Salmo trutta) in Swiss rivers using a Bayesian probability network. Ecol. Model. 192: 224–244.

(21) Lee DC, Rieman BE (1997) Population viability assessment of salmonids by using probabilistic networks. North Am. J. Fish. Manage. 17: 144–1157.

(22) Marcot, B. G., Holthausen, R. S., Raphael, M. G., Rowland, M. M. and Wisdom, M. J. (2001). Using Bayesian belief networks to evaluate fish and wildlife population viability under land management alternatives from an environmental impact statement. Forest Ecology & Management 153: 29-42.

(23) Xu J, Johnson MP, Fischbeck PS, Small MJ, VanBriesen JM (2010) Integrating Location Models with Bayesian Analysis to Inform Decision Making. J Water Res Planning Manage, 136(2): 209-216.

(24) Stiber NS, Pantazidou M, Small MJ (1999) Expert System Methodology for Evaluating Reductive Dechlorination at TCE Sites. Environ. Sci. Technol., 33 (17): 3012–3020.

(25) Small MJ (2008) Methods for Assessing Uncertainty in Fundamental Assumptions and Associated Models for Cancer Risk Assessment. Risk Analysis, 28: 1289–1308.

(26) Stiber NA, Small MJ, Pantazidou M (2004) Site-specific updating and aggregation of Bayesian Belief Network models for multiple experts. Risk Analysis, 24(6): 1529-1538.

(27) Preuss K, Oldenburg C, Moridis G (1999) TOUGH2 User's Guide, Version 2.0. Tech. Rep. LBNL-43134, Lawrence Berkeley National Laboratory, Berkeley, CA.

(28) Yang Y, Small MJ, Ogretim EO, Gray DD, Bromhal GS, Smith DH, Strazisar B, Wells A (2007) Development a Bayesian Belief Network for Near-surface CO_2 - Statistical Methods For Integrating Near-surface CO_2 Migration Modeling With Monitoring Network Analysis, In Sixth Annual Conference on Carbon Capture & Sequestration, http://www.netl.doe.gov/publications/proceedings/07/carbon-seq/data/papers/p2_127.pdf

(29) Yang Y, Small MJ, Bromhal GS, Strazisar BR, Wells AW (2010a) Probabilistic Design of a Near-Surface CO_2 Leak Detection System. Unpublished manuscript (in preparation for the submission to Environ. Sci. Technol.)

(30) Oldenburg, C.M., Pruess, K., Benson, S.M., 2001. Process modeling of CO2 injection into natural gas reservoirs for carbon sequestration and enhanced gas recovery. Energy Fuels 15, 293–298.

(31) Oldenburg CM, Unger AJA (2004) Coupled vadose zone and atmospheric surface-layer transport of carbon dioxide from geologic carbon sequestration sites. Vadose Zone Journal 3:848-857.

(32) Lewicki JL, Hilley GE, Fischer ML, Pan L, Oldenburg CM, Dobeck L, Spangler L (2009) Eddy covariance observations of surface leakage during shallow subsurface CO_2 releases. Journal of Geophysical Research - Atmospheres, 114, D12302.

(33) Spangler LH, Dobeck LM, Repasky KS, Nehrir AR, Humphries SD, Barr JL, Keith CJ, Shaw JA, Rouse JH, Cunningham AB, et al. (2010). A shallow subsurface controlled release facility in Bozeman, Montana, USA, for testing near surface CO2 detection techniques and transport models. Environ. Earth Sci. 60 (2): 227-239.

(34) Wells A, Strazisar B, Diehl J, Veloski G (2010) Atmospheric tracer monitoring and surface plume development at the ZERT pilot test in Bozeman, Montana, USA, Environ. Earth Sci. 60 (2): 299-305.

(35) Yang Y, Small MJ, Junker BW, Bromhal GS, Strazisar BR, Wells AW (2010b) Bayesian hierarchical models for soil CO_2 flux and leak detection at geologic sequestration sites, Environ. Earth Sci. (in review).

(36) Wells A (2008) Atmospheric and soil-gas monitoring for surface leakage at the Michigan Basin CO2 Pilot Test Site in Ostego Co. Michigan using a Perfluorocarbon tracer. Technical paper. National Energy and Technology Laboratory. Unpublished manuscript.

(37) Brantley, S. L., and K. W. Koepenick (1995) Measured carbon dioxide emissions from Oldoinyo Lengai and the skewed distribution of passive volcanic fluxes, Geology, 23, 933–936.

(38) Schorlemmer D, Wiemer S, Wyss M (2005) Variations in earthquake-size distribution across different stress regimes. Nature, 437: 539-542.

(39) Norsys Software Corp. (1998) Netica Bayesian Belief Network Software. Acquired from http://www.norsys.com/.

(40) Wells AW, Diehl JR, Grant Bromhal GS, Strazisar BR, Wilson TH, White CM (2007) The use of tracers to assess leakage from the sequestration of CO2 in a depleted oil reservoir, New Mexico, USA. Applied Geochemistry, 22(5): 996-1016.

(41) Kim H, Yea SK, Ro CU, Lee CB, Jang M, Lee G, Yoo E, Han JS (2002) Determination of atmospheric Perfluorocarbon background concentrations of fL/L range at the Western coastal area of Korea, Bulletin-Korean Chemical Society, 23(2): 301-308.

(42) Nodop K, Connolly R, Girardi F (1998) The field campaigns of the European tracer experiment (ETEX): overview and results. Atmospheric, 32(24): 4095-4108.

Chapter 5: Conclusions and Future Research Directions

5.1   Summary and Conclusions

Bayesian methods for characterizing the natural background conditions of the monitoring techniques for leak detection

Bayesian hierarchical models have been successfully developed and applied to predict soil CO_2 respiration rates as a function of temperature at nine AmeriFlux sites. The hierarchical approach allows determination of a global parameter distribution for the set of sites, the sharing of information across sites, and site-specific parameter estimates for each. The prediction intervals from the predictive distributions provide a first basis for determining critical values of measured CO_2 fluxes (conditioned on temperature) for leak detection. Among the four selected soil respiration models, the square root-quadratic model has the best performance in fitting the site data and providing reasonable prediction intervals, which is a desirable feature for a model that may be applied for general use in leak detection applications. For the ZERT site, a simpler square root-linear relationship, a special case of square root-quadratic model, was found to provide the best fit for these data, and a Bayesian nonhierarchical square root-linear model is used for estimating the prediction intervals for leak detection.

The general method illustrated for characterizing soil CO_2 flux is also applied to PFC tracer monitoring at the ZERT site, using a simple Bayesian hierarchical normal model across the four test sites. Similarly, the critical value is estimated from the upper bound of the prediction intervals to determine when a measurement is unlike the

background concentrations. When measurements are available across multiple sites, Bayesian hierarchical models provide a basis for pooling this information, thereby reducing the overall uncertainty, while still maintaining site-specific model estimates.

Probability of Leak Detection for a Near-Surface CO₂ Monitoring System

The application on the soil CO_2 flux measurement at the idealized ZERT site shows nonlinear, non-monotonic relationships of network performance with soil permeability and network density. In general, dense monitoring networks (with ~10-20 meters between monitors) are required to ensure a moderate to high probability of leak detection. These effects are likely to be even more pronounced when the method is applied to actual site conditions with potential releases from deep formations; complex non-homogeneous site geology; facilitated transport through fissures, wells, and zones of high permeability; and spatial variation in pre-injection soil respiration rates. Similar results are found for PFC tracer monitoring with less dense networks (with ~50-20m meters between monitors) required for achieving the same probability of leak detection. For the PFC tracer, permeability only matters for the less dense networks.

As such, surface soil CO_2 flux measurement is unlikely to be feasible as a stand-alone technology for leak detection. Rather, it will most likely be applied in high risk locations, such as areas around wells and features, during the injection and post-injection period. As now recognized, a mix of complementary technologies targeting signals from potential leaks at different locations and in different ways will be needed to allow for practical and affordable designs that achieve high levels of assurance.

The methods presented here for integrating site characterization, site modeling, and monitoring device and network specification, to compute the detection probabilities of a network for each monitoring technique are generally applicable. Application to actual sites will require more detailed site characterization data and modeling tools for estimating the relationships between leakage events and monitoring results, and adaptation of the methodology will be required to address these complexities.

Bayesian Belief Network for Combining Sequestration Site Leak Detection Monitoring Results from Near-Surface CO_2 Fluxes and PFC Tracer Concentrations

A general and applicable framework of the BBN for CO_2 leak detection deployed at a site is presented with an illustration of the use of the two monitoring techniques for the idealized ZERT site. The results show that PFC monitoring has better performance in detecting a leak compared to soil CO_2 flux measurement for the same monitoring density and site conditions. Considering the pros and cons of the two monitoring techniques, soil CO_2 flux measurement is recommended for regions where large size leaks might occur, such as the area around wells and features, because of its quick feedback. PFC tracer monitoring is more flexible with regard to the location of monitors due to its sensitivity to small sized leaks.

Moreover, the BBN can be used to calculate the probability of leak detection for an acceptable leakage rate in order to optimize a monitoring network design or to select the monitoring techniques deployed at a site. In the illustrative analysis, a d=20m or less PFC tracer network alone is sufficient for detecting almost all sizes of leaks. For the leakge rate catetory 10^{-4} to 10^{-3} kg/s and the target probability of 95% detection, options

for the mix of the two technologies include: the mix of a d=50m network for PFC tracer

and a d=10m network for soil CO_2 flux in the case of high permeability; and the mix of a

d=50m network for PFC tracer and a d=20m network for soil CO_2 flux in the case of

median permeability. For low permeability, a d=100m PFC tracer network alone or a

d=20m network for soil CO_2 flux is sufficient. Considering the pros and cons of the two

monitoring techniques, soil CO_2 flux measurement is recommended for regions where the

large size leaks might occur, such as the area around wells and features. PFC tracer

monitoring is more flexible with regard to the location of monitors due to its sensitivity to

small sized leaks. The analysis of the set of idealized monitoring scenarios also gives a

general idea about the number of monitors needed for a monitoring network design and

shows the trade-offs between two monitoring methods.   Besides detection ability

presented in this research, the determination of the optimized network design usually

involves other factors such as the cost of monitoring, labor and technology availability,

which must be considered in the real decision making process.

5.2   Recommendations for Future Research

While building the BBN for CO_2 leak detection, some challenges and questions

have arisen, especially in regard to the consideration of actual site conditions and the best

use of each monitoring technique. We suggest the following directions which are worth

investigating in the future.

- The CO_2 soil flux and tracer models can be applied to evaluate monitoring
  network designs at an actual site, considering non-uniform/non-isotropic leak
  occurrence probability and subsurface CO_2 transport. Application to actual sites
  will require more detailed site characterization data and modeling tools, and
  adaptation of the methodology will be required to address these complexities. For
  example, methods will be needed to account for partial (imperfect) knowledge of
  more-likely leak locations such as wells and features and the need for denser
  monitoring coverage at or near these portions of the site. Therefore, leakage
  simulation scenarios close to the real site conditions, considering all possible
  leakage pathways, are needed. After the leakage simulations are made, the
  optimized monitoring network design for a technology can be evaluated based on
  the probability of leak detection.
- More monitoring technologies can be added to the BBN for a more fully
  integrated assessment of CO_2 leak detection in the application stage. The key
  challenge of adding a new monitoring technique into the BBN is the ability to
  relate the monitoring results to the size of a possible leak. It is equivalent to
  answering the question: what the possible size of a leak given the observation?
  Besides the CO_2 soil flux and PFC tracer technologies, other monitoring methods,
  such as groundwater chemistry and carbon isotopes, can be included in the BBN
  in the future.
- The joint deployment of technologies targeting both deep and near-surface
  leakage signals can be considered. The methods proposed here for computing
  detection probabilities are generally applicable, and related tests and the

112

simulations for deep saline aquifer storage have been performed by several

research groups (*1-10*). Therefore, it is feasible and practical to develop joint

assessments for the monitoring technologies applied in deep reservoirs and the

shallow near-surface area.

- The BBN can be expanded into a decision support system with the addition of

  other elements reflecting important operational, economic, and social concerns.

  For example, the use of a BBN to optimize the network design for an acceptable

  leakage rate can be linked to the cost associated with the monitoring technique

  considered.

- The time required for sampling and analysis is also another interesting factor

  discovered here besides the geological monitoring network designs. How the

  frequency of a monitoring technology affects the effective period for the

  probability of leak detection is worth investigating in the future.

Reference

(1) Bachu, S. and Adams, J. J. (2002) Sequestration of CO_2 in geological media in response to climate change: capacity of deep saline aquifers to sequester CO_2 in solution, Energy Conversion and Management 44(20), 3151–3175.

(2) Izgec, O., Demiral, B., Bertin, H., Akin, S. (2008) CO_2 injection into sline carbonate aquifer formations I: laboratory investigation. Transp. Porous Med. 72(1): 1-24.

(3) Izgec, O., Demiral, B., Bertin, H., Akin, S. (2008) CO_2 injection into saline carbonate aquifer formations II: comparison of numerical simulations to experiments Transport Porous Media. 72(1): 57-74.

(4) Jan M. Nordbotten, Dmitri Kavetski, Michael A. (2009) Celia and Stefan Bachu. Injection and storage of CO_2 in deep saline aquifers: Analytical solution for CO_2 plume evolution during injection. Environ. Sci. Technol, 43 (3): 743-749

(5) Kumar, A., R. Ozah, M. Noh, G. A. Pope, S. Bryant, K. Sepehrnoori, and L. W. Lake (2005), Reservoir simulation of CO_2 storage in deep saline aquifers, Soc. Pet. Eng. J., 10(3): 336– 348.

(6) Lagneau, V., Pipart, A., Catalette, H. (2005) Reactive transport modelling of CO_2 sequestration in deep saline aquifers. Oil Gas Sci. Technol. Revue De L Institut Francais Du Petrole 60(2): 231–247.

(7) Nordbotten, J.M., M.A. Celia, S. Bachu, and H.K. Dahle. (2005) Semi-analytical solution for CO_2 leakage through an abandoned well. Environmental Science and Tecnhology, Environ. Sci. Technol., 2005, 39 (2), pp 602–611

(8) Pruess, K., T. Xu, J. Apps, and J. Garcia (2003), Numerical modeling of aquifer disposal of CO2, Soc. Pet. Eng. J., 8(1), 49–60.

(9) Wellman, T. P., R. B. Grigg, B. J. McPherson, R. K. Svec, and P. C. Lichtner (2003), The evaluation of CO_2 – brine-rock interaction with laboratory flow test and reactive transport modeling, in SPE/DOE International Symposium on Oilfield Chemistry, Houston, Texas, (SPE 80228).

(10) Xu, T.F., Apps, J.A., Pruess, K.: Numerical simulation of CO_2 disposal by mineral trapping in deep aquifers. (2004) Appl. Geochem. 19(6), 917–936.

Appendix A: Interpretation of Parameter Estimates for the Four Soil Temperature-CO$_2$ Respiration Rate Models (see Table 2.2 in main text)

For the simple Q$_{10}$ model parameter estimates presented in Table 2.2, the median of parameter a at each site varies from -1.07 to 1.88, with the only positive value (1.88) estimated for the IOM site. In contrast, the median estimates of all parameter b values are positive, ranging from 0.04 to 0.16, except for the one for the IOM site, which has a value of -0.1. The Q$_{10}$ model is monotonic with temperature, sloping upward when b is positive and downward when b is negative. All sites except IOM yield an upward sloping curve. The large sample size associated with the IOM site and the relative respiration rates between sites with differing ranges of soil temperature result in a similarly downward sloping relationship for the pooled estimate, with a positive a value and a negative b value. The remaining models all allow for a non-monotonic relationship between soil temperature and CO$_2$ flux, providing greater flexibility for capturing a more realistic range of temperature effects both within and between sites.

The log-quadratic model includes an additional parameter for the quadratic term. The Bayesian hierarchical parameter estimation yields a median value of the parameter a ranging across sites from -1.88 to 1.27, with the median of parameter b ranging from -0.03 to 0.23. Once again, the IOM site yields parameter estimates with opposite signs compared to the other sites. The credible intervals indicate that most parameters are statistically significant for the model fit except for the parameter a at the UMB site and the parameters b and c at the JUN site. The parameters of the Bayesian pooled model agree with those parameters estimated for the Bayesian hierarchical model at most sites.

Compared to the parameter c of the hierarchical model, the parameter c of the pooled model is lower, indicating a greater degree of curvature in the pooled model relationship.

The square root-quadratic model likewise has three parameters. The Bayesian hierarchical estimates yield positive median values of parameter a, ranging from 0.37 to 1.56, positive median values of parameter b, ranging from 0.014 to 0.11, and negative parameter values for c, ranging from -0.007 to -0.001. However, the parameter c is statistically insignificant for the HAR, JUN, MEO, UMB and WDN sites, suggesting that adding curvature to the model for the square root transformed data is not necessary at most sites. The estimated parameters of the Bayesian pooled model agree well with those of the Bayesian hierarchical model. Like the log-quadratic model, the parameter c of the pooled model is lower than estimated for the hierarchical model, reflecting the larger concavity in the pooled model needed to capture variations across all sites.

For the modified Davidson model, the parameter estimates exhibit a higher degree of variation than for the other three models, in part due to the greater complexity of the model. The median value of parameter a at each site ranges from -6.44 to 62.14, and all parameter a estimates are statistically significant. The median values of parameter b range from 0.376 to -168.9, with the group 1 sites (HAR, THA and UMB) yielding similar, low negative values for b. The parameter b is not statistically significant for the JUN and WDN sites, indicating that there is no enhanced curvature due to temperature change at these sites. The parameters estimated from the pooled model are very close to the parameters of the illustrative model proposed by Davidson et al. (2006) which represents a general prediction for soil respiration.

116

Below are the correlation coefficient matrix tables of the parameters of the four soil temperature-CO_2 respiration rate models.

Table A. 1   The Correlation Coefficient Matrix of the Parameters of the Four Soil Temperature-CO$_2$ Respiration Rate Models Applied to the AmeriFlux Site Data

A. Simple Q$_{10}$ (log-linear) Model

Q$_{10}$	a(HAR)	a(HOW)	a(IOM)	a(JUN)	a(MEO)	a(MEY)	a(THA)	a(UMB)	a(WDN)	b(HAR)	b(HOW)	b(IOM)	b(JUN)	b(MEO)	b(MEY)	b(THA)	b(UMB)	b(WDN)
a(HAR)	1.000	0.023	0.008	0.009	0.009	-0.001	-0.005	0.020	-0.039	-0.927	-0.015	-0.001	-0.010	-0.008	0.000	0.004	-0.017	0.030
a(HOW)	0.023	1.000	0.017	0.000	0.009	-0.021	-0.025	-0.015	-0.020	-0.013	-0.849	-0.013	-0.006	-0.008	0.017	0.027	0.015	0.020
a(IOM)	0.008	0.017	1.000	-0.003	-0.010	0.005	0.016	0.009	0.007	-0.001	-0.023	-0.917	0.006	0.000	-0.011	0.000	-0.012	-0.009
a(JUN)	0.009	0.000	-0.003	1.000	0.012	0.027	-0.006	-0.011	0.002	-0.002	-0.001	0.008	-0.946	-0.008	-0.022	0.001	0.008	0.009
a(MEO)	0.009	0.009	-0.010	0.012	1.000	0.000	0.005	0.001	0.015	-0.006	-0.005	0.011	-0.008	-0.916	0.003	0.004	0.007	-0.016
a(MEY)	-0.001	-0.021	0.005	0.027	0.000	1.000	-0.004	-0.006	0.017	-0.006	0.021	-0.001	-0.019	0.002	-0.939	0.006	0.000	-0.017
a(THA)	-0.005	-0.025	0.016	-0.006	0.005	-0.004	1.000	0.010	0.015	0.011	0.020	-0.012	0.007	-0.008	0.007	-0.844	-0.012	-0.013
a(UMB)	0.020	-0.015	0.009	-0.011	0.001	-0.006	0.010	1.000	-0.016	-0.014	0.015	-0.004	0.009	-0.001	0.010	-0.013	-0.907	0.020
a(WDN)	-0.039	-0.020	0.007	0.002	0.015	0.017	0.015	-0.016	1.000	0.036	0.011	-0.002	0.001	-0.022	-0.011	-0.024	0.014	-0.952
b(HAR)	-0.927	-0.013	-0.001	-0.002	-0.006	-0.006	0.011	-0.014	0.036	1.000	0.007	-0.004	0.005	0.005	0.004	-0.007	0.013	-0.026
b(HOW)	-0.015	-0.849	-0.023	-0.001	-0.005	0.021	0.020	0.015	0.011	0.007	1.000	0.020	0.008	0.007	-0.024	-0.022	-0.011	-0.010
b(IOM)	-0.001	-0.013	-0.917	0.008	0.011	-0.001	-0.012	-0.004	-0.002	-0.004	0.020	1.000	-0.009	-0.001	0.005	-0.002	0.007	0.005
b(JUN)	-0.010	-0.006	0.006	-0.946	-0.008	-0.019	0.007	0.009	0.001	0.005	0.008	-0.009	1.000	0.005	0.015	-0.004	-0.005	-0.012
b(MEO)	-0.008	-0.008	0.000	-0.008	-0.916	0.002	-0.008	-0.001	-0.022	0.005	0.007	-0.001	0.005	1.000	-0.005	-0.001	-0.003	0.021
b(MEY)	0.000	0.017	-0.011	-0.022	0.003	-0.939	0.007	0.010	-0.011	0.004	-0.024	0.005	0.015	-0.005	1.000	-0.011	-0.004	0.013
b(THA)	0.004	0.027	0.000	0.001	0.004	0.006	-0.844	-0.013	-0.024	-0.007	-0.022	-0.002	-0.004	-0.001	-0.011	1.000	0.009	0.026
b(UMB)	-0.017	0.015	-0.012	0.008	0.007	0.000	-0.012	-0.907	0.014	0.013	-0.011	0.007	-0.005	-0.003	-0.004	0.009	1.000	-0.018
b(WDN)	0.030	0.020	-0.009	0.009	-0.016	-0.017	-0.013	0.020	-0.952	-0.026	-0.010	0.005	-0.012	0.021	0.013	0.026	-0.018	1.000

B. Log-quadratic model

LQ	a(HAR)	a(HOW)	a(IOM)	a(JUN)	a(MEO)	a(MEY)	a(THA)	a(UMB)	a(WDN)	b(HAR)	b(HOW)	b(IOM)	b(JUN)	b(MEO)	b(MEY)	b(THA)	b(UMB)	b(WDN)
a(HAR)	1.000	0.102	-0.020	0.039	-0.039	-0.056	0.155	0.119	-0.002	-0.836	-0.205	0.017	-0.031	0.031	0.050	-0.220	-0.148	-0.048
a(HOW)	0.102	1.000	-0.048	-0.134	0.012	-0.135	0.181	0.063	0.073	-0.175	-0.728	0.054	0.157	-0.023	0.148	-0.272	-0.080	-0.138
a(IOM)	-0.020	-0.048	1.000	0.010	0.113	0.038	-0.114	-0.038	-0.030	0.042	0.110	-0.963	-0.026	-0.124	-0.033	0.164	0.063	0.051
a(JUN)	0.039	-0.134	0.010	1.000	0.023	0.137	-0.199	-0.024	-0.065	-0.040	0.224	-0.009	-0.958	-0.021	-0.151	0.270	0.030	0.142
a(MEO)	-0.039	0.012	0.113	0.023	1.000	0.087	0.020	0.059	0.002	0.031	-0.048	-0.120	-0.020	-0.926	-0.087	-0.027	-0.051	-0.025

a(MEY)	-0.056	-0.135	0.038	0.137	0.087	1.000	-0.067	0.042	-0.055	0.082	0.229	-0.042	-0.149	-0.105	-0.930	0.125	-0.041	0.105
a(THA)	0.155	0.181	-0.114	-0.199	0.020	-0.067	1.000	0.019	0.086	-0.192	-0.293	0.117	0.219	-0.019	0.073	-0.785	-0.041	-0.164
a(UMB)	0.119	0.063	-0.038	-0.024	0.059	0.042	0.019	1.000	0.125	-0.158	-0.109	0.030	0.020	-0.072	-0.047	-0.041	-0.802	-0.157
a(WDN)	-0.002	0.073	-0.030	-0.065	0.002	-0.055	0.086	0.125	1.000	-0.038	-0.138	0.029	0.072	-0.003	0.055	-0.130	-0.177	-0.832
b(HAR)	-0.836	-0.175	0.042	-0.040	0.031	0.082	-0.192	-0.158	-0.038	1.000	0.314	-0.044	0.025	-0.021	-0.077	0.295	0.201	0.093
b(HOW)	-0.205	-0.728	0.110	0.224	-0.048	0.229	-0.293	-0.109	-0.138	0.314	1.000	-0.120	-0.262	0.057	-0.252	0.449	0.151	0.242
b(IOM)	0.017	0.054	-0.963	-0.009	-0.120	-0.042	0.117	0.030	0.029	-0.044	-0.120	1.000	0.024	0.131	0.038	-0.169	-0.056	-0.059
b(JUN)	-0.031	0.157	-0.026	-0.958	-0.020	-0.149	0.219	0.020	0.072	0.025	-0.262	0.024	1.000	0.019	0.166	-0.305	-0.027	-0.153
b(MEO)	0.031	-0.023	-0.124	-0.021	-0.926	-0.105	-0.019	-0.072	-0.003	-0.021	0.057	0.131	0.019	1.000	0.105	0.027	0.065	0.025
b(MEY)	0.050	0.148	-0.033	-0.151	-0.087	-0.930	0.073	-0.047	0.055	-0.077	-0.252	0.038	0.166	0.105	1.000	-0.131	0.045	-0.111
b(THA)	-0.220	-0.272	0.164	0.270	-0.027	0.125	-0.785	-0.041	-0.130	0.295	0.449	-0.169	-0.305	0.027	-0.131	1.000	0.072	0.250
b(UMB)	-0.148	-0.080	0.063	0.030	-0.051	-0.041	-0.041	-0.802	-0.177	0.201	0.151	-0.056	-0.027	0.065	0.045	0.072	1.000	0.230
b(WDN)	-0.048	-0.138	0.051	0.142	-0.025	0.105	-0.164	-0.157	-0.832	0.093	0.242	-0.059	-0.153	0.025	-0.111	0.250	0.230	1.000
c(HAR)	0.651	0.190	-0.049	0.033	-0.024	-0.088	0.187	0.159	0.057	-0.951	-0.333	0.053	-0.015	0.013	0.085	-0.298	-0.205	-0.107
c(HOW)	0.216	0.553	-0.122	-0.229	0.055	-0.237	0.298	0.112	0.145	-0.327	-0.960	0.133	0.268	-0.064	0.260	-0.462	-0.155	-0.252
c(IOM)	-0.014	-0.057	0.913	0.009	0.118	0.043	-0.116	-0.021	-0.026	0.044	0.122	-0.986	-0.023	-0.130	-0.040	0.166	0.048	0.060
c(JUN)	0.025	-0.163	0.035	0.897	0.017	0.150	-0.222	-0.018	-0.074	-0.015	0.276	-0.033	-0.983	-0.018	-0.169	0.315	0.025	0.154
c(MEO)	-0.026	0.029	0.121	0.018	0.829	0.113	0.016	0.078	0.002	0.016	-0.059	-0.129	-0.018	-0.971	-0.112	-0.025	-0.073	-0.022
c(MEY)	-0.041	-0.143	0.025	0.149	0.080	0.826	-0.073	0.047	-0.053	0.066	0.248	-0.029	-0.165	-0.096	-0.971	0.127	-0.047	0.109
c(THA)	0.225	0.282	-0.162	-0.268	0.025	-0.139	0.626	0.045	0.134	-0.309	-0.469	0.167	0.307	-0.027	0.145	-0.960	-0.077	-0.260
c(UMB)	0.142	0.078	-0.067	-0.029	0.042	0.032	0.052	0.579	0.177	-0.194	-0.151	0.062	0.026	-0.056	-0.038	-0.083	-0.937	-0.235
c(WDN)	0.073	0.158	-0.056	-0.171	0.035	-0.123	0.193	0.150	0.548	-0.115	-0.273	0.071	0.183	-0.036	0.131	-0.292	-0.226	-0.907

LQ (cont.)	c(HAR)	c(HOW)	c(IOM)	c(JUN)	c(MEO)	c(MEY)	c(THA)	c(UMB)	c(WDN)
a(HAR)	0.651	0.216	-0.014	0.025	-0.026	-0.041	0.225	0.142	0.073
a(HOW)	0.190	0.553	-0.057	-0.163	0.029	-0.143	0.282	0.078	0.158
a(IOM)	-0.049	-0.122	0.913	0.035	0.121	0.025	-0.162	-0.067	-0.056
a(JUN)	0.033	-0.229	0.009	0.897	0.018	0.149	-0.268	-0.029	-0.171
a(MEO)	-0.024	0.055	0.118	0.017	0.829	0.080	0.025	0.042	0.035
a(MEY)	-0.088	-0.237	0.043	0.150	0.113	0.826	-0.139	0.032	-0.123
a(THA)	0.187	0.298	-0.116	-0.222	0.016	-0.073	0.626	0.052	0.193
a(UMB)	0.159	0.112	-0.021	-0.018	0.078	0.047	0.045	0.579	0.150

a(WDN)	0.057	0.145	-0.026	-0.074	0.002	-0.053	0.134	0.177	0.548
b(HAR)	-0.951	-0.327	0.044	-0.015	0.016	0.066	-0.309	-0.194	-0.115
b(HOW)	-0.333	-0.960	0.122	0.276	-0.059	0.248	-0.469	-0.151	-0.273
b(IOM)	0.053	0.133	-0.986	-0.033	-0.129	-0.029	0.167	0.062	0.071
b(JUN)	-0.015	0.268	-0.023	-0.983	-0.018	-0.165	0.307	0.026	0.183
b(MEO)	0.013	-0.064	-0.130	-0.018	-0.971	-0.096	-0.027	-0.056	-0.036
b(MEY)	0.085	0.260	-0.040	-0.169	-0.112	-0.971	0.145	-0.038	0.131
b(THA)	-0.298	-0.462	0.166	0.315	-0.025	0.127	-0.960	-0.083	-0.292
b(UMB)	-0.205	-0.155	0.048	0.025	-0.073	-0.047	-0.077	-0.937	-0.226
b(WDN)	-0.107	-0.252	0.060	0.154	-0.022	0.109	-0.260	-0.235	-0.907
c(HAR)	1.000	0.346	-0.054	0.004	-0.008	-0.076	0.316	0.198	0.124
c(HOW)	0.346	1.000	-0.134	-0.282	0.065	-0.256	0.484	0.156	0.284
c(IOM)	-0.054	-0.134	1.000	0.032	0.128	0.032	-0.164	-0.056	-0.075
c(JUN)	0.004	-0.282	0.032	1.000	0.017	0.169	-0.318	-0.025	-0.183
c(MEO)	-0.008	0.065	0.128	0.017	1.000	0.103	0.026	0.063	0.033
c(MEY)	-0.076	-0.256	0.032	0.169	0.103	1.000	-0.140	0.042	-0.130
c(THA)	0.316	0.484	-0.164	-0.318	0.026	-0.140	1.000	0.087	0.305
c(UMB)	0.198	0.156	-0.056	-0.025	0.063	0.042	0.087	1.000	0.234
c(WDN)	0.124	0.284	-0.075	-0.183	0.033	-0.130	0.305	0.234	1.000

C. Modified Davidson model

MD	a(HAR)	a(HOW)	a(IOM)	a(JUN)	a(MEO)	a(MEY)	a(THA)	a(UMB)	a(WDN)	b(HAR)	b(HOW)	b(IOM)	b(JUN)	b(MEO)	b(MEY)	b(THA)	b(UMB)	b(WDN)
a(HAR)	1.000	-0.034	-0.006	0.039	0.101	-0.070	-0.438	0.563	0.080	-0.995	0.034	0.006	-0.042	-0.101	0.071	-0.556	-0.571	-0.078
a(HOW)	-0.034	1.000	0.015	-0.055	-0.024	-0.091	0.014	-0.042	-0.026	0.035	-0.996	-0.012	0.048	0.024	0.091	0.022	0.045	0.025
a(IOM)	-0.006	0.015	1.000	0.002	-0.012	0.012	-0.027	-0.015	-0.003	0.005	-0.016	-0.456	0.002	0.012	-0.012	-0.023	0.014	0.002
a(JUN)	0.039	-0.055	0.002	1.000	0.372	0.262	-0.014	0.034	0.274	-0.041	0.053	0.015	-0.953	-0.370	-0.262	-0.038	-0.039	-0.272
a(MEO)	0.101	-0.024	-0.012	0.372	1.000	0.239	-0.058	0.114	0.570	-0.100	0.022	0.018	-0.370	-0.997	-0.239	-0.080	-0.115	-0.573
a(MEY)	-0.070	-0.091	0.012	0.262	0.239	1.000	0.005	-0.043	0.276	0.068	0.090	-0.007	-0.248	-0.238	-0.995	-0.003	0.043	-0.275
a(THA)	-0.438	0.014	-0.027	-0.014	-0.058	0.005	1.000	-0.414	-0.040	0.438	-0.015	0.028	0.021	0.059	-0.006	0.746	0.417	0.040
a(UMB)	0.563	-0.042	-0.015	0.034	0.114	-0.043	-0.414	1.000	0.100	-0.567	0.043	0.010	-0.039	-0.114	0.044	-0.547	-0.980	-0.098
a(WDN)	0.080	-0.026	-0.003	0.274	0.570	0.276	-0.040	0.100	1.000	-0.081	0.025	0.021	-0.270	-0.572	-0.278	-0.058	-0.104	-0.992
b(HAR)	-0.995	0.035	0.005	-0.041	-0.100	0.068	0.438	-0.567	-0.081	1.000	-0.035	-0.007	0.045	0.100	-0.069	0.559	0.575	0.078

b(HOW)	0.034	-0.996	-0.016	0.053	0.022	0.090	-0.015	0.043	0.025	-0.035	1.000	0.013	-0.046	-0.022	-0.091	-0.023	-0.046	-0.024
b(IOM)	0.006	-0.012	-0.456	0.015	0.018	-0.007	0.028	0.010	0.021	-0.007	0.013	1.000	-0.015	-0.019	0.008	0.018	-0.009	-0.018
b(JUN)	-0.042	0.048	0.002	-0.953	-0.370	-0.248	0.021	-0.039	-0.270	0.045	-0.046	-0.015	1.000	0.368	0.248	0.044	0.044	0.268
b(MEO)	-0.101	0.024	0.012	-0.370	-0.997	-0.238	0.059	-0.114	-0.572	0.100	-0.022	-0.019	0.368	1.000	0.238	0.081	0.115	0.574
b(MEY)	0.071	0.091	-0.012	-0.262	-0.239	-0.995	-0.006	0.044	-0.278	-0.069	-0.091	0.008	0.248	0.238	1.000	0.003	-0.044	0.276
b(THA)	-0.556	0.022	-0.023	-0.038	-0.080	-0.003	0.746	-0.547	-0.058	0.559	-0.023	0.018	0.044	0.081	0.003	1.000	0.557	0.058
b(UMB)	-0.571	0.045	0.014	-0.039	-0.115	0.043	0.417	-0.980	-0.104	0.575	-0.046	-0.009	0.044	0.115	-0.044	0.557	1.000	0.103
b(WDN)	-0.078	0.025	0.002	-0.272	-0.573	-0.275	0.040	-0.098	-0.992	0.078	-0.024	-0.018	0.268	0.574	0.276	0.058	0.103	1.000

D. Square root-quadratic model

SQ	a(HAR)	a(HOW)	a(IOM)	a(JUN)	a(MEO)	a(MEY)	a(THA)	a(UMB)	a(WDN)	b(HAR)	b(HOW)	b(IOM)	b(JUN)	b(MEO)	b(MEY)	b(THA)	b(UMB)	b(WDN)
a(HAR)	1.000	0.012	-0.147	0.202	0.166	0.130	0.095	0.216	0.010	-0.853	-0.050	0.159	-0.232	-0.195	-0.139	-0.200	-0.299	-0.008
a(HOW)	0.012	1.000	-0.018	-0.001	0.040	-0.017	0.010	-0.003	0.048	-0.020	-0.677	0.013	0.005	-0.040	0.017	-0.029	-0.037	-0.071
a(IOM)	-0.147	-0.018	1.000	-0.090	-0.092	-0.104	0.018	-0.118	0.073	0.198	-0.016	-0.958	0.099	0.108	0.095	-0.042	0.178	-0.119
a(JUN)	0.202	-0.001	-0.090	1.000	0.287	0.204	0.069	0.153	0.118	-0.264	-0.020	0.093	-0.921	-0.319	-0.217	-0.108	-0.217	-0.144
a(MEO)	0.166	0.040	-0.092	0.287	1.000	0.198	0.011	0.127	0.123	-0.215	-0.110	0.102	-0.316	-0.921	-0.221	-0.063	-0.197	-0.161
a(MEY)	0.130	-0.017	-0.104	0.204	0.198	1.000	0.006	0.155	0.056	-0.165	-0.044	0.112	-0.232	-0.227	-0.928	-0.047	-0.211	-0.084
a(THA)	0.095	0.010	0.018	0.069	0.011	0.006	1.000	0.062	0.065	-0.124	-0.061	-0.026	-0.085	-0.023	-0.009	-0.716	-0.076	-0.073
a(UMB)	0.216	-0.003	-0.118	0.153	0.127	0.155	0.062	1.000	0.074	-0.248	-0.029	0.124	-0.180	-0.146	-0.161	-0.080	-0.776	-0.093
a(WDN)	0.010	0.048	0.073	0.118	0.123	0.056	0.065	0.074	1.000	-0.020	-0.100	-0.076	-0.147	-0.138	-0.056	-0.083	-0.103	-0.827
b(HAR)	-0.853	-0.020	0.198	-0.264	-0.215	-0.165	-0.124	-0.248	-0.020	1.000	0.063	-0.216	0.304	0.259	0.180	0.243	0.373	0.019
b(HOW)	-0.050	-0.677	-0.016	-0.020	-0.110	-0.044	-0.061	-0.029	-0.100	0.063	1.000	0.023	0.018	0.124	0.042	0.111	0.076	0.151
b(IOM)	0.159	0.013	-0.958	0.093	0.102	0.112	-0.026	0.124	-0.076	-0.216	0.023	1.000	-0.104	-0.120	-0.102	0.044	-0.194	0.128
b(JUN)	-0.232	0.005	0.099	-0.921	-0.316	-0.232	-0.085	-0.180	-0.147	0.304	0.018	-0.104	1.000	0.348	0.248	0.129	0.261	0.182
b(MEO)	-0.195	-0.040	0.108	-0.319	-0.921	-0.227	-0.023	-0.146	-0.138	0.259	0.124	-0.120	0.348	1.000	0.248	0.084	0.228	0.178
b(MEY)	-0.139	0.017	0.095	-0.217	-0.221	-0.928	-0.009	-0.161	-0.056	0.180	0.042	-0.102	0.248	0.248	1.000	0.058	0.223	0.087
b(THA)	-0.200	-0.029	-0.042	-0.108	-0.063	-0.047	-0.716	-0.080	-0.083	0.243	0.111	0.044	0.129	0.084	0.058	1.000	0.124	0.113
b(UMB)	-0.299	-0.037	0.178	-0.217	-0.197	-0.211	-0.076	-0.776	-0.103	0.373	0.076	-0.194	0.261	0.228	0.223	0.124	1.000	0.139
b(WDN)	-0.008	-0.071	-0.119	-0.144	-0.161	-0.084	-0.073	-0.093	-0.827	0.019	0.151	0.128	0.182	0.178	0.087	0.113	0.139	1.000
c(HAR)	0.687	0.024	-0.202	0.268	0.222	0.166	0.127	0.236	0.024	-0.957	-0.064	0.221	-0.309	-0.266	-0.181	-0.240	-0.370	-0.023
c(HOW)	0.060	0.389	0.036	0.024	0.117	0.068	0.078	0.040	0.102	-0.073	-0.911	-0.042	-0.025	-0.135	-0.067	-0.130	-0.079	-0.157
c(IOM)	-0.161	-0.010	0.900	-0.092	-0.105	-0.113	0.030	-0.124	0.074	0.219	-0.027	-0.983	0.104	0.123	0.103	-0.044	0.197	-0.127

c(JUN)	0.235	-0.008	-0.097	0.800	0.311	0.232	0.089	0.184	0.154	-0.307	-0.014	0.104	-0.965	-0.340	-0.249	-0.134	-0.271	-0.192
c(MEO)	0.202	0.038	-0.108	0.318	0.813	0.228	0.031	0.149	0.135	-0.270	-0.125	0.121	-0.344	-0.968	-0.247	-0.092	-0.233	-0.173
c(MEY)	0.136	-0.016	-0.081	0.210	0.220	0.818	0.010	0.151	0.054	-0.179	-0.038	0.087	-0.243	-0.243	-0.968	-0.063	-0.213	-0.085
c(THA)	0.220	0.030	0.044	0.114	0.082	0.069	0.426	0.083	0.076	-0.260	-0.116	-0.043	-0.134	-0.105	-0.082	-0.897	-0.134	-0.111
c(UMB)	0.294	0.049	-0.176	0.217	0.204	0.208	0.073	0.531	0.104	-0.379	-0.087	0.195	-0.264	-0.236	-0.219	-0.127	-0.928	-0.142
c(WDN)	0.004	0.080	0.130	0.126	0.148	0.088	0.063	0.085	0.465	-0.013	-0.158	-0.142	-0.161	-0.161	-0.091	-0.108	-0.132	-0.862

SQ (cont.)	c(HAR)	c(HOW)	c(IOM)	c(JUN)	c(MEO)	c(MEY)	c(THA)	c(UMB)	c(WDN)
a(HAR)	0.687	0.060	-0.161	0.235	0.202	0.136	0.220	0.294	0.004
a(HOW)	0.024	0.389	-0.010	-0.008	0.038	-0.016	0.030	0.049	0.080
a(IOM)	-0.202	0.036	0.900	-0.097	-0.108	-0.081	0.044	-0.176	0.130
a(JUN)	0.268	0.024	-0.092	0.800	0.318	0.210	0.114	0.217	0.126
a(MEO)	0.222	0.117	-0.105	0.311	0.813	0.220	0.082	0.204	0.148
a(MEY)	0.166	0.068	-0.113	0.232	0.228	0.818	0.069	0.208	0.088
a(THA)	0.127	0.078	0.030	0.089	0.031	0.010	0.426	0.073	0.063
a(UMB)	0.236	0.040	-0.124	0.184	0.149	0.151	0.083	0.531	0.085
a(WDN)	0.024	0.102	0.074	0.154	0.135	0.054	0.076	0.104	0.465
b(HAR)	-0.957	-0.073	0.219	-0.307	-0.270	-0.179	-0.260	-0.379	-0.013
b(HOW)	-0.064	-0.911	-0.027	-0.014	-0.125	-0.038	-0.116	-0.087	-0.158
b(IOM)	0.221	-0.042	-0.983	0.104	0.121	0.087	-0.043	0.195	-0.142
b(JUN)	-0.309	-0.025	0.104	-0.965	-0.344	-0.243	-0.134	-0.264	-0.161
b(MEO)	-0.266	-0.135	0.123	-0.340	-0.968	-0.243	-0.105	-0.236	-0.161
b(MEY)	-0.181	-0.067	0.103	-0.249	-0.247	-0.968	-0.082	-0.219	-0.091
b(THA)	-0.240	-0.130	-0.044	-0.134	-0.092	-0.063	-0.897	-0.127	-0.108
b(UMB)	-0.370	-0.079	0.197	-0.271	-0.233	-0.213	-0.134	-0.928	-0.132
b(WDN)	-0.023	-0.157	-0.127	-0.192	-0.173	-0.085	-0.111	-0.142	-0.862
c(HAR)	1.000	0.073	-0.225	0.311	0.277	0.180	0.255	0.380	0.016
c(HOW)	0.073	1.000	0.045	0.024	0.140	0.062	0.133	0.088	0.164
c(IOM)	-0.225	0.045	1.000	-0.106	-0.125	-0.087	0.039	-0.200	0.143
c(JUN)	0.311	0.024	-0.106	1.000	0.335	0.244	0.139	0.276	0.172
c(MEO)	0.277	0.140	-0.125	0.335	1.000	0.240	0.113	0.240	0.156
c(MEY)	0.180	0.062	-0.087	0.244	0.240	1.000	0.086	0.210	0.089

c(THA)	0.255	0.133	0.039	0.139	0.113	0.086	1.000	0.137	0.110
c(UMB)	0.380	0.088	-0.200	0.276	0.240	0.210	0.137	1.000	0.135
c(WDN)	0.016	0.164	0.143	0.172	0.156	0.089	0.110	0.135	1.000

Appendix B: Model Selection Procedure for ZERT Site Soil CO_2 Flux vs. Temperature Relationship

The following four models were fit to the soil temperature vs. CO_2 flux data for

the ZERT site, based on the research by Yang et. al (*1*):

Simple Q_{10} (log-linear) model: $\ln[CO_2 \text{ flux}] = a + bT + \varepsilon$

Log-quadratic model: $\ln[CO_2 \text{ flux}] = a + bT + cT^2 + \varepsilon$

Square root-linear model: $[CO_2 \text{ flux}]^{1/2} = a + bT + \varepsilon$

Square root-quadratic model: $[CO_2 \text{ flux}]^{1/2} = a + bT + cT^2 + \varepsilon$

Model selection was made by comparing the mean square error (MSE) and the deviance

information criterion (DIC) for each. MSE is a commonly used method for model

selection, and the DIC is specifically developed for Bayesian model selection to account

for the tradeoff between model complexity (number of parameters) and goodness of fit

(*2,3*). Like for the MSE, lower values of the DIC are preferred. The MSE and DIC of

each model are shown in Table B.1 below, and the parameter distributions are

summarized in Table B.2. As can been seen in Table B.1, the square root-linear model

has the best model fit, with the lowest values of MSE and DIC. In fact the square root-

linear model is a particular case of the square root-quadratic model, which was found by

Yang et. al (*1*) to provide the best fit across nine Ameriflux sites. In this application to

the ZERT site, the quadratic term is not statistically significant (see Table B.2). While the

MSE and DIC values of the square root-quadratic model are similar to those of the square

root-linear model, the lowest values for both measures are achieved with the square root-

linear model, and this less-complex model is thus selected for our subsequent analysis.

Table B. 1 Computed Mean Square Error (MSE) and Deviance Information Criterion (DIC) for Four Models of Soil Respiration. Lower values of the MSE indicate a closer goodness of fit of the model to the data. The DIC further accounts for model complexity by penalizing models with more parameters. For both the MSE and the DIC, the model with the lowest value is preferred (value shown in bold).

	Model			
Metric	Simple Q_{10}	Log-quadratic	Square root-linear	Square root-quadratic
MSE	5.82	5.75	**5.36**	5.39
DIC	210.7	212.7	**172.8**	174.8

Table B. 2 Summary of Markov Chain Monte Carlo Parameter Estimates for Four Model Fits Tested for ZERT Site

Simple Q_{10} (log-linear) Model: $\ln[CO_2 \text{ flux}] = a + bT + \varepsilon$

	mean	Sd	2.50%	25%	50%	75%	97.50%
A	-0.7537	0.2647	-1.2710	-0.9310	-0.7549	-0.5760	-0.2361
B	0.0945	0.0116	0.0718	0.0866	0.0945	0.1023	0.1174
σ_ε	0.6558	0.0462	0.5710	0.6238	0.6536	0.6845	0.7521

Log-quadratic Model: $\ln[CO_2 \text{ flux}] = a + bT + cT^2 + \varepsilon$

	mean	Sd	2.50%	25%	50%	75%	97.50%
A	-0.9644	1.4030	-3.7249	-1.9230	-0.9683	-0.0203	1.7881
B	0.1147	0.1336	-0.1426	0.0258	0.1149	0.2054	0.3778
C	-0.0005	0.0030	-0.0064	-0.0025	-0.0004	0.0015	0.0053
σ_ε	0.6577	0.0469	0.5735	0.6250	0.6553	0.6874	0.7558

Square root-Linear Model: $[CO_2 \text{ flux}]^{1/2} = a + bT + \varepsilon$

	mean	Sd	2.50%	25%	50%	75%	97.50%
A	0.2076	0.2200	-0.2195	0.0564	0.2100	0.3571	0.6350
B	0.0855	0.0097	0.0668	0.0790	0.0855	0.0920	0.1047
σ_ε	0.5470	0.0388	0.4781	0.5202	0.5447	0.5718	0.6292

Square root-quadratic Model: $[CO_2 \text{ flux}]^{1/2} = a + bT + cT^2 + \varepsilon$

	mean	Sd	2.50%	25%	50%	75%	97.50%
A	0.3160	1.1879	-2.0226	-0.4775	0.3087	1.1093	2.6403
B	0.0748	0.1133	-0.1493	-0.0006	0.0760	0.1511	0.2968
C	0.0002	0.0026	-0.0047	-0.0015	0.0003	0.0020	0.0053
σ_ε	0.5502	0.0394	0.4798	0.5229	0.5481	0.5751	0.6344

Reference

(1) Yang, Y.; Small, M. J.; Junker, B. W.; Bromhal, G. S.; Strazisar B. R.; Wells A.W
Bayesian hierarchical models for soil CO_2 flux and leak detection at geologic
sequestration sites. *Environ. Earth Sci*. (in review).

(2) Spiegelhalter, D. J.; Best, N. G.; Carlin, B. P.; van der Linde, A. Bayesian measures
of model complexity and fit. *J Roy Stat Soc Ser. B*. **2002**, 64, 583–639

(3) Gelman, A.; Carlin, J. B.; Stern, H. S.; Rubin, D. B. *Bayesian Data Analysis*; 2nd
edn. Chapman & Hall/CRC Press: Boca Raton, FL, 2003.

Appendix C: Cross Validation of Kriging Method for Interpolating CO_2 Seepage Rate Predictions

To validate the accuracy of the 2-D kriging prediction for unmodeled values of permeability and leakage rate, Figure C1 shows the same results as Figure 3.2, but with the TOUGH2 output withheld (from the spline fitting and 2D kriging routines) for each of the five leakage rates for which a curve is predicted (predictions are shown for the five intermediate cases, L2 – L6). For example, when fitting the response surface for case L3, only the TOUGH2 outputs for cases L1, L2, and L4 – L7 are used. Figure C.2 shows similar cross validation results for varying permeability (Figure C.2 has the same TOUGH2 results as Figure 3.3, but with the spline-kriging interpolation conducted with each curve's TOUGH2 results withheld). The cross-validations in Figures C.1 and C.2 indicate a good correspondence between the TOUGH2 simulation results and the values estimated by the combined spline-kriging interpolation method.
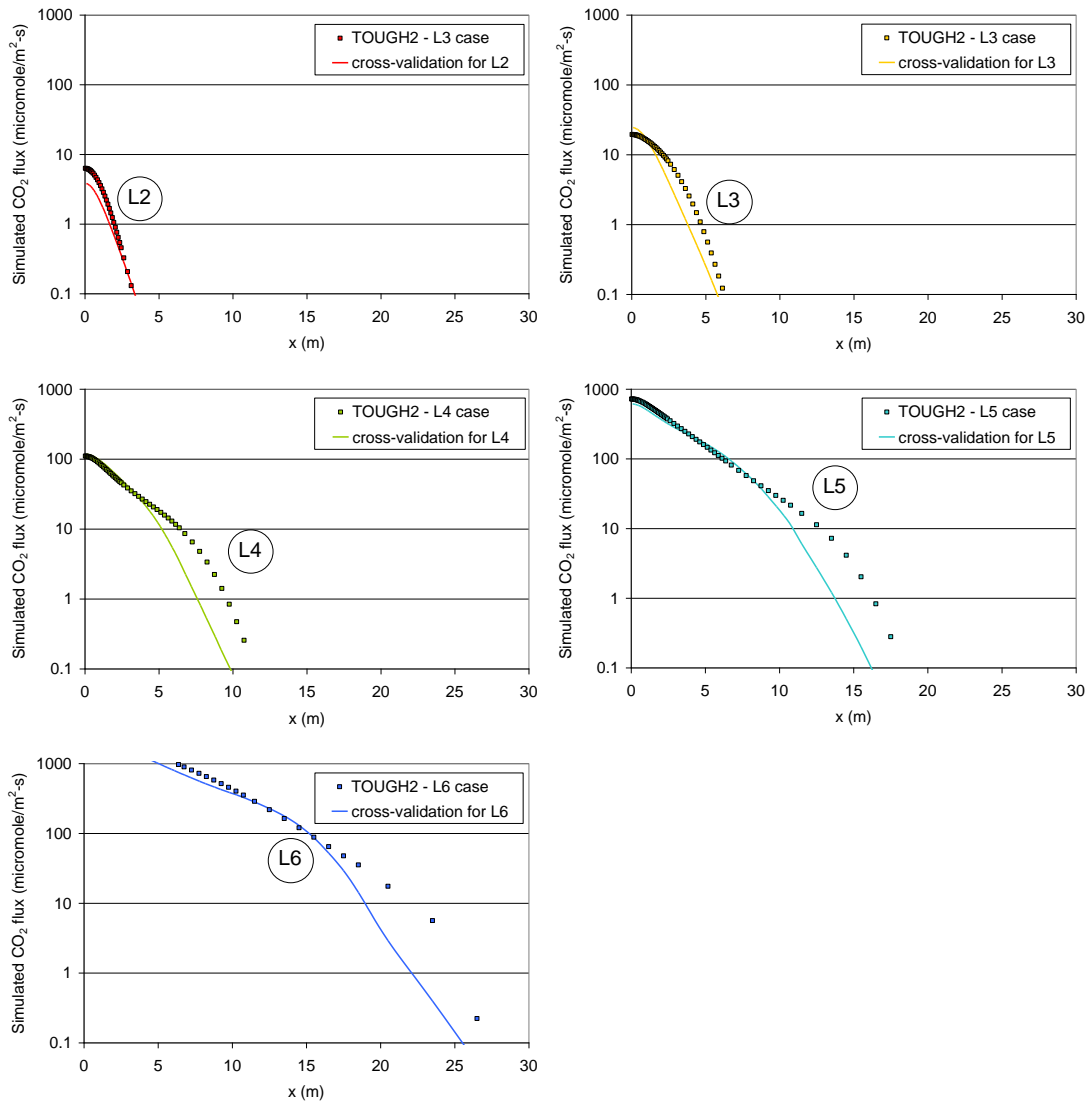
Figure C. 1   Cross-validation of the combined spline-kriging method for TOUGH2 simulated CO$_2$ seepage rates for different leakage rates, ranging from L2=1.93 x 10^{-6} kg/s to L6 = 1.93 x 10^{-2} kg/s, by factors of 10. For all cases, permeability = 1 Darcy, vadose zone thickness = 1.35m. Points are TOUGH2 simulation results, and solid lines are the predictions made by the spline-kriging method.
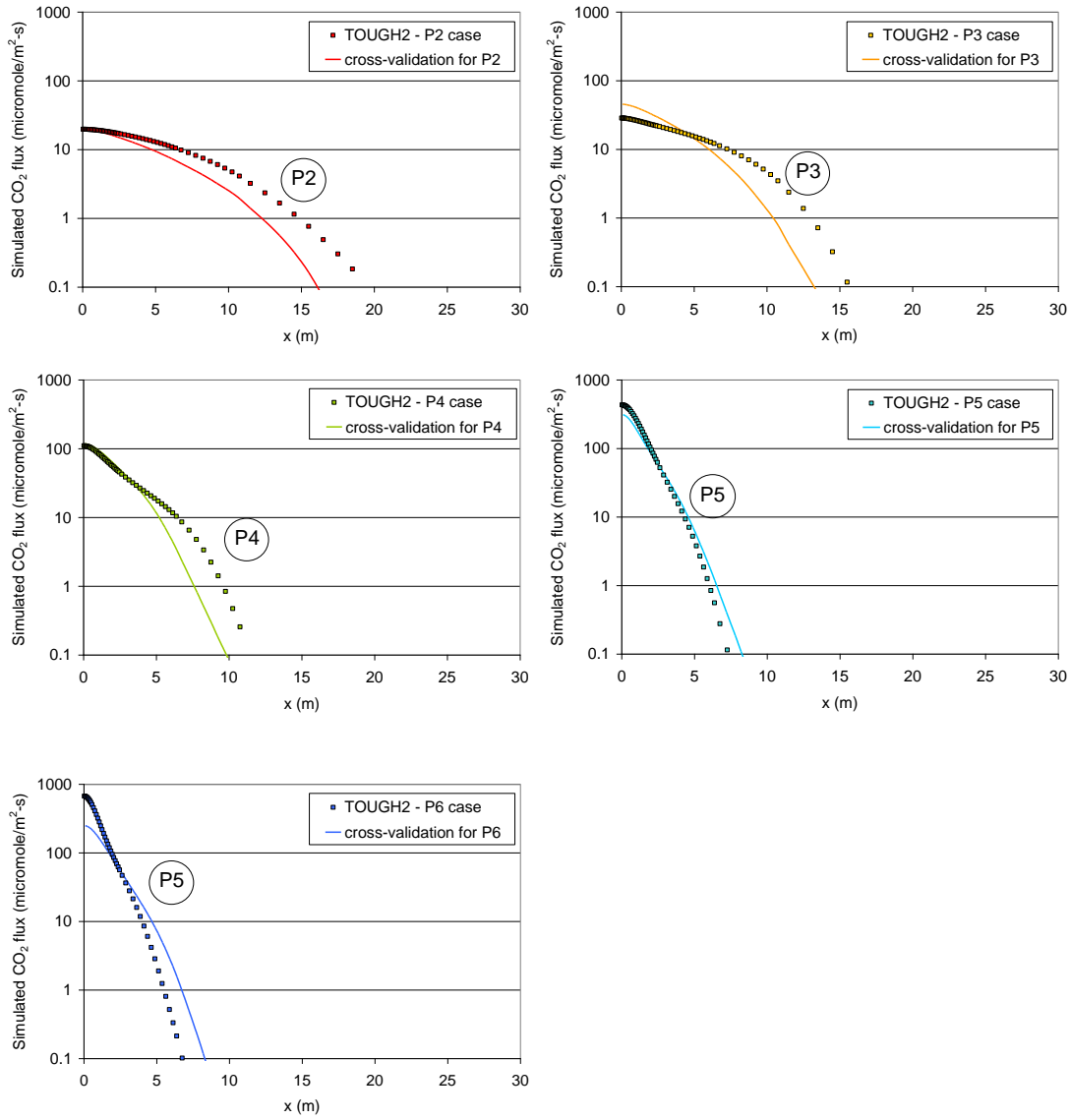
Figure C. 2   Cross-validation of the combined spline-kriging method for TOUGH2 simulated CO_2 seepage rates for different soil permeability, ranging from P2=0.01 Darcy to P6=100 Darcy, by factors of 10. For all cases, leakage rate = 1.93 x 10^{-4} kg/s, vadose zone thickness = 1.35m. Points are TOUGH2 simulation results, and solid lines are the predictions made by the spline-kriging method.

130

Appendix D: TOUGH2 Simulations of PMCH Seepage Flux for Different Leakage Rates and Permeabilities

The Figure D.1 and D.2 below present the results of simulated PMCH seepage flux by TOUGH2 (*1*) for different leakage rates and permeabilities. The simulation scenarios for the associated CO_2 leakage rates (L1-L7) and permeabilities (P1-P7) are described in Chapter 4, section *4.2.2*, and the leakage event is simulated for 10 days.
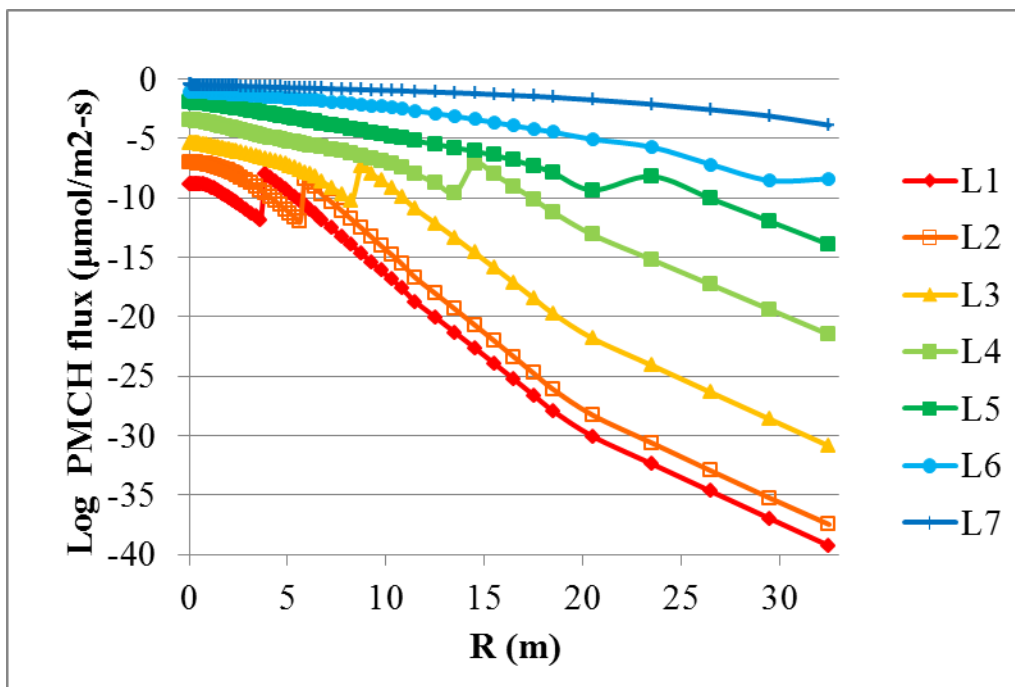
Figure D. 1   Simulated PMCH seepage rates along with CO_2 injection for different CO_2 leakage rates, ranging from L1 = 1.93 x 10^{-7} kg/s to L7 = 1.93 x 10^{-1} kg/s, by factors of 10. For all cases, permeability = 1 Darcy, vadose zone thickness = 1.35m.
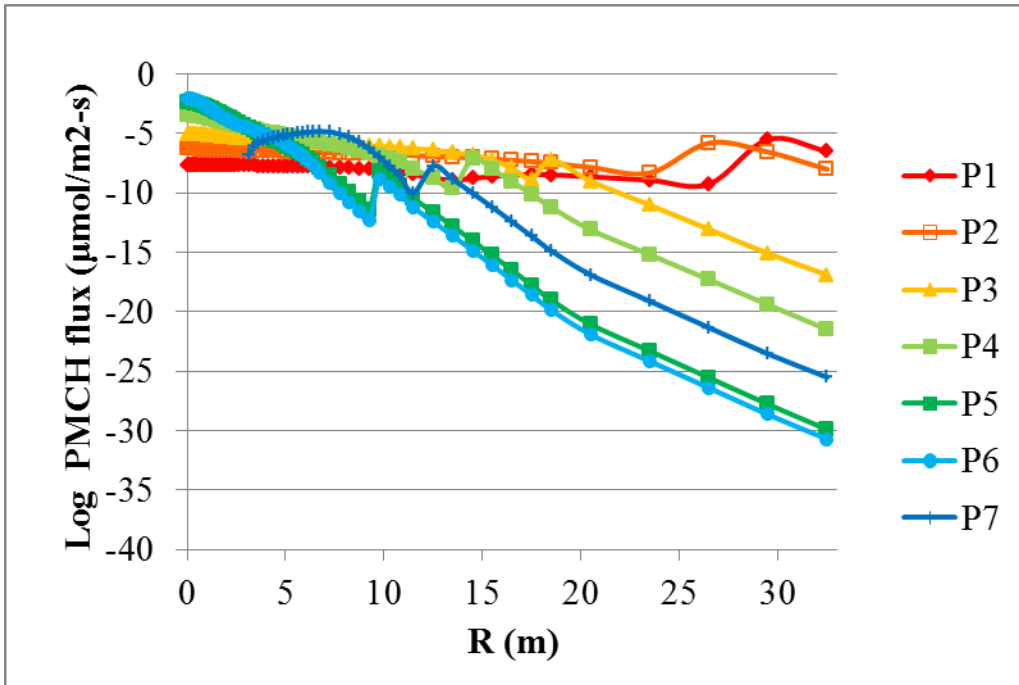
Figure D. 2   Simulated PMCH seepage rates along with CO_2 injection for different soil permeability, ranging from P1 = 0.001 Darcy to P7=1000 Darcy, by factors of 10. For all cases, CO_2 leakage rate = 1.93 x 10^{-4} kg/s, vadose zone thickness = 1.35m.

Reference
(1) Pruess, K., Oldenburg, C.M., Moridis, G., 1999. TOUGH2 User's Guide, version 2.0. Report LBNL-43134, Lawrence Berkeley National Laboratory, Berkeley, CA, USA.

Appendix E: The Simulation Summary of the Bayesian Hierarchical Modeling of Background PMCH Concentrations

Bayesian approach allows model inferences to be shared across sites and yields both global and subunit-specific parameter estimates. A simple normal model is applied here. The model structure for the Bayesian hierarchical model of the PMCH concentration is given by $Y_{ij} \sim N(\mu_j, \sigma_y^2)$, where y_{ij} is the ith observation of PMCH concentrations at site j; μ_j is the mean (or prediction) of the observed PMCH concentrations at each site; and σ_y is the variance representing the variability that occurs over time or from point to point.

The second level of the Bayesian hierarchical model is implemented by assuming a multivariate normal distribution for μ_j: $\mu_j \sim N(a_j, \sigma_a^2)$, where a_j and σ_a^2 are the hyperparameters.

In our study, the background PMCH concentration are obtained from four sites in 2007: the ZERT(ZH) site in Montana, during the ZERT Horizontal Pipe Injection (Strazisar et al. 2009), the Lower Michigan Basin (LMB) site near Gaylord, Michigan (Wells, 2008), the San Juan Basin (SJB) site in New Mexico, and the Pines parking lot at NETL Pittsburgh (PN), Pennsylvania. All observations are obtained in the summer and fall of 2007. Table E.1 below shows the summary of the data from the four sites. The Bayesian hierarchical model is a simple normal model with the mean for each site and a variance across site is used, though the mean of PMCH might be modeled with year since PMCH is cumulative in the atmosphere (*1*). In this study, all observations are from the same year so the year is not considered as a predictor variable. The model can be refined

in the future when more data are available. Table B2 below summarizes the simulations

for the Bayesian hierarchical model of the PMCH concentration.

Table E. 1   Summary of PMCH Concentration at the Four Sites, 2007

Site	sample size	mean	sd	min	median	max
LMB	3	4.33	0.58	4.00	4.00	5.00
SBJ	26	6.41	3.26	0.33	6.33	14.60
ZH	7	14.69	8.93	1.50	17.00	28.30
PN	10	9.37	0.78	7.67	9.33	10.30

Table E. 2   Summary of Markov Chain Monte Carlo Estimates for Bayesian Hierarchical Modeling of Background PMCH Concentrations

Site	mean	sd	2.50%	**50%**	97.50%
LMB	5.2	2.4	0.4	5.3	10.0
SBJ	6.5	0.9	4.9	6.5	8.2
ZH	14.0	1.7	10.6	14.1	17.3
PN	9.3	1.3	6.6	9.3	11.8
mu.a	8.7	6.3	-4.0	8.7	20.4
sigma.y	4.4	0.5	3.6	4.3	5.6
sigma.a	8.8	8.7	1.9	6.1	33.5

pD=6.4 and DIC = 271 (using the rule, pD = var(deviance)/2)
DIC is an estimate of expected predictive error (lower deviance is better).

Reference
(1) Watson TB, Wilke R, Dietz RN, Heiser J, Kalb P (2007) The Atmospheric
    Background of Perfluorocarbon Compounds Used as Tracers. *Environ. Sci. Technol.*,
    41 (20): 6909–6913.

Appendix F: Relationships between Simulated CO_2 Flux and PMCH Flux

The relationships between simulated CO_2 flux and PMCH flux are presented in Figure F.1 and F.2 below. Figure F.1 represent all 17 simulated cases. In Figure F.1, the extreme case of the largest leakage rate and the largest permeability shows a very different pattern compared to the other 16 cases. Therefore, Figure F.2 only shows the relationships between simulated CO_2 flux and PMCH flux for the 16 cases.
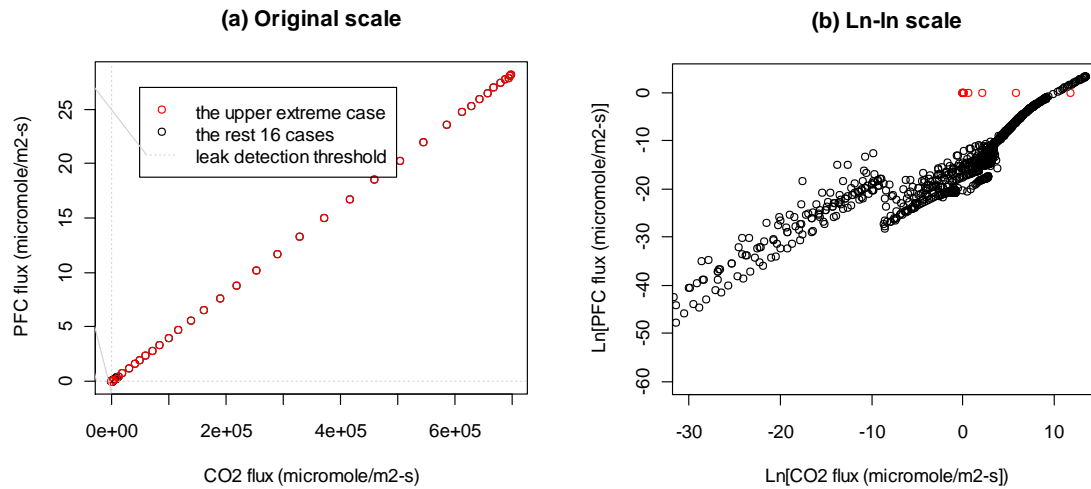
Figure F. 1   The relationships between the simulated PMCH seepage flux and the simulated CO_2 seepage for all 17 cases

(a) Original scale

(b) Ln-ln scale
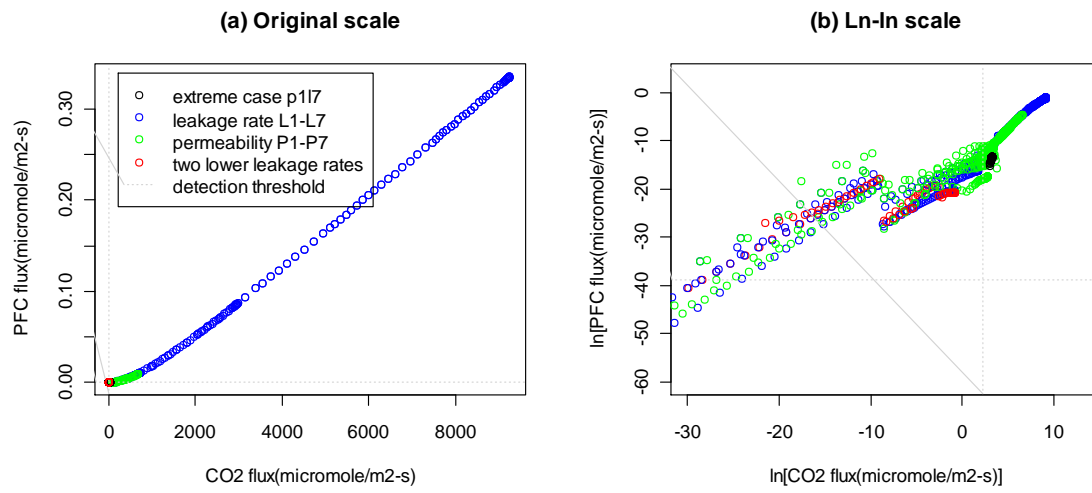
**Figure F. 2   The relationships between the simulated PMCH seepage flux and the simulated CO$_2$ seepage for the 16 cases**

Appendix G: Conditional Probability Table in the BBN Model

Table G.1 below shows the conditional probability tables for the soil CO_2 flux and the

PFC tracer in the BBN model for the idealized ZERT site.

Table G. 1   Conditional Probability Tables for Soil CO_2 Flux Measurement and PFC Tracer Monitoring

Monitoring density	Permeability (D)	Leakage rate (kg/s)	Soil CO_2 flux measurement		PFC tracer monitoring	
			Below critical value	Above critical value	Like background	Above background
100m	high	0 to 1e-6	94.4	5.6	99.5	0.5
100m	high	1e-6 to 1e-5	92.56	7.44	99.5	0.5
100m	high	1e-5 to 1e-4	90.18	9.82	99.42	0.58
100m	high	1e-4 to 0.001	84.1	15.9	98.71	1.29
100m	high	0.001 to 0.01	44.89	55.11	96.87	3.13
100m	high	0.01 to 0.1	2.52	97.48	93.98	6.02
100m	high	0.1 to 1	0.13	99.87	92.03	7.97
100m	median	0 to 1e-6	94.53	5.47	99.5	0.5
100m	median	1e-6 to 1e-5	92.12	7.88	99.5	0.5
100m	median	1e-5 to 1e-4	87.79	12.21	99.27	0.73
100m	median	1e-4 to 0.001	72.15	27.85	96.56	3.44
100m	median	0.001 to 0.01	0	100	91.38	8.62
100m	median	0.01 to 0.1	0	100	77.82	22.18
100m	median	0.1 to 1	0	100	0	100
100m	low	0 to 1e-6	93.75	6.25	99.5	0.5
100m	low	1e-6 to 1e-5	87.93	12.07	99.5	0.5
100m	low	1e-5 to 1e-4	27.6	72.4	99.5	0.5
100m	low	1e-4 to 0.001	0	100	92.11	7.89
100m	low	0.001 to 0.01	0	100	85.48	14.52
100m	low	0.01 to 0.1	0	100	67.03	32.97
100m	low	0.1 to 1	0	100	0	100
50m	high	0 to 1e-6	81.38	18.62	99.5	0.5
50m	high	1e-6 to 1e-5	73.23	26.77	99.48	0.52
50m	high	1e-5 to 1e-4	62.59	37.41	98.03	1.97
50m	high	1e-4 to 0.001	39.62	60.38	95.33	4.67
50m	high	0.001 to 0.01	6.18	93.82	91.03	8.97
50m	high	0.01 to 0.1	0.16	99.84	79.96	20.04
50m	high	0.1 to 1	0.01	99.99	69.65	30.35
50m	median	0 to 1e-6	81.35	18.65	99.5	0.5
50m	median	1e-6 to 1e-5	69.53	30.47	99.35	0.65

50m	median	1e-5 to 1e-4	50.4	49.6	97.26	2.74
50m	median	1e-4 to 0.001	9.02	90.98	90.3	9.7
50m	median	0.001 to 0.01	0.01	99.99	67.64	32.36
50m	median	0.01 to 0.1	0	100	18.78	81.22
50m	median	0.1 to 1	0	100	0	100
50m	low	0 to 1e-6	78.36	21.64	99.5	0.5
50m	low	1e-6 to 1e-5	53.65	46.35	99.5	0.5
50m	low	1e-5 to 1e-4	2.44	97.56	98.66	1.34
50m	low	1e-4 to 0.001	0	100	69.96	30.04
50m	low	0.001 to 0.01	0	100	42.52	57.48
50m	low	0.01 to 0.1	0	100	4.16	95.84
50m	low	0.1 to 1	0	100	0	100
20m	high	0 to 1e-6	6.88	93.12	99.5	0.5
20m	high	1e-6 to 1e-5	0.91	99.09	98.66	1.34
20m	high	1e-5 to 1e-4	0.03	99.97	89.73	10.27
20m	high	1e-4 to 0.001	0	100	73.73	26.27
20m	high	0.001 to 0.01	0	100	43.12	56.88
20m	high	0.01 to 0.1	0	100	1.98	98.02
20m	high	0.1 to 1	0	100	0	100
20m	median	0 to 1e-6	6.91	93.09	99.5	0.5
20m	median	1e-6 to 1e-5	0.39	99.61	97.85	2.15
20m	median	1e-5 to 1e-4	0	100	83.9	16.1
20m	median	1e-4 to 0.001	0	100	36.39	63.61
20m	median	0.001 to 0.01	0	100	0	100
20m	median	0.01 to 0.1	0	100	0	100
20m	median	0.1 to 1	0	100	0	100
20m	low	0 to 1e-6	4.27	95.73	99.5	0.5
20m	low	1e-6 to 1e-5	0.03	99.97	99.5	0.5
20m	low	1e-5 to 1e-4	0	100	93.38	6.62
20m	low	1e-4 to 0.001	0	100	0	100
20m	low	0.001 to 0.01	0	100	0	100
20m	low	0.01 to 0.1	0	100	0	100
20m	low	0.1 to 1	0	100	0	100
10m	high	0 to 1e-6	0.1	99.9	99.5	0.5
10m	high	1e-6 to 1e-5	0.09	99.91	96.32	3.68
10m	high	1e-5 to 1e-4	0.05	99.95	63.69	36.31
10m	high	1e-4 to 0.001	0	100	10.09	89.91
10m	high	0.001 to 0.01	0	100	0.1	99.9
10m	high	0.01 to 0.1	0	100	0.1	99.9
10m	high	0.1 to 1	0	100	0.1	99.9
10m	median	0 to 1e-6	0.1	99.9	99.5	0.5
10m	median	1e-6 to 1e-5	0.08	99.92	93.53	6.47
10m	median	1e-5 to 1e-4	0	100	42.78	57.22

10m	median	1e-4 to 0.001	0	100	0.1	99.9
10m	median	0.001 to 0.01	0	100	0.09	99.91
10m	median	0.01 to 0.1	0	100	0	100
10m	median	0.1 to 1	0	100	0	100
10m	low	0 to 1e-6	0.1	99.9	99.5	0.5
10m	low	1e-6 to 1e-5	0.02	99.98	99.44	0.56
10m	low	1e-5 to 1e-4	0	100	78	22
10m	low	1e-4 to 0.001	0	100	0	100
10m	low	0.001 to 0.01	0	100	0	100
10m	low	0.01 to 0.1	0	100	0	100
10m	low	0.1 to 1	0	100	0	100